2015

Analysis of non-stationary power quality waveforms using iterative empirical mode decomposition methods and SAX algorithm

Mohammad Jasa Afroni
University of Wollongong

UNIVERSITY OF WOLLONGONG

School of Electrical, Computer and Telecommunication Engineering

Analysis of Non-Stationary Power Quality Waveforms Using Iterative Empirical Mode Decomposition Methods and SAX Algorithm

Mohammad Jasa Afroni

This thesis is presented as part of the requirements for the

Award of the Degree of the Doctor of Philosophy

University of Wollongong

September, 2015

CERTIFICATION

I, Mohammad Jasa Afroni, declare that this thesis, submitted in partial fulfillment of the requirements for the award of Ph.D, in the School of Electrical, Telecommunications and Computer Engineering, University of Wollongong, is wholly my own work unless otherwise referenced or acknowledge. The document has not been submitted for qualification at any other academic institution.

Mohammad Jasa Afroni

2 September 2015

ABSTRACT

The nonstationary nature of power-quality (PQ) waveforms requires a tool that can accurately analyze and visually identify the instants of transitions. One of the recently reported tools available to analyze nonstationary complex waveforms with a very good time resolution is the Hilbert Huang Transform (HHT) which consists of two steps - the Empirical Mode Decomposition (EMD) and the Hilbert Transform (HT). The EMD process decomposes the signal into Intrinsic Mode Functions (IMFs), each of which represents the identified signal component. Once the IMFs are obtained, the HT can then be applied to find the instantaneous amplitude, frequency and phase of each IMF.

However, HHT has difficulty in resolving waveforms containing components with close frequencies with a ratio of less than two, and similar to other waveform classification techniques, it has difficulty in resolving the instants of sudden changes in the waveform. To overcome the problem with components containing close frequencies, a novel Iterative Hilbert Huang transform (IHHT) is proposed in this thesis. The problem in identifying instants of sudden changes in the waveform is resolved by proposing the use of Symbolic Aggregate ApproXimation (SAX) method. SAX converts the signal into symbols that can be utilized by a pattern detector algorithm to identify the boundaries of the stationary signals within a nonstationary signal. Results from IHHT and SAX method to analyze and visually identify simulated and measured nonstationary PQ waveforms will be provided and discussed. The proposed method is particularly useful when investigating the behavior of the harmonic components of a particular PQ waveform of interest in a given interval of time, following a data-mining search of a large database of PQ events. It can be used to both identify, and later isolate unique signatures within a provider's distribution system.

The Hilbert Huang Transform (HHT) can also decompose noisy Power Quality (PQ) waveforms, however, when the noise level becomes relatively high, the EMD process may generate mixed IMFs which give inaccurate results when the HT is applied to the IMFs. To resolve the mode mixing issue, an improved EMD method, referred to as the Ensemble Empirical Mode Decomposition (EEMD), is then used. Results from the decomposition process of the signals demonstrate the ability of the EEMD method in resolving mode-mixing issues resulting from the presence of noise.

However, the EEMD method may not produce accurate instantaneous amplitude values of the detected IMFs and hence the Iterative EEMD (IEEMD) method is proposed in this thesis together with the SAX (Symbolic Aggregate approXimation) based pattern detector algorithm, to determine the boundaries of the segments in the non-stationary signal. Results from simulated signals show that the proposed methods are effective in decomposing noisy non-stationary signal.

The Iterative HHT and the Iterative EEMD methods have also been tested with real single and three phase signals from measurement using Dranetz PQ analyzer and from Pqube cloud storage of PQ events. The decomposition results have shown the accuracy of the Iterative HHT over the standard / traditional HHT for less noisy signals. However, for more noisy signals, the EMD process will fail to identify the correct frequency of the signal components due to the mode mixing issue and therefore the standard HHT as well as the iterative HHT can not decompose the signal accurately. The EEMD method can resolve the mode mixing issue in the decomposition process of the more noisy signal. However, the MSE of the reconstructed signal to the original is still high and therefore, the proposed Iterative EEMD is used to decompose the signals and it is found that the accuracy of the IEEMD is better than the traditional EEMD method.

ACKNOWLEDGEMENTS

I would like to express my sincere gratitude to my supervisor, Prof. Danny Soetanto, for his guidance and encouragement throughout the duration of my study and the work of this thesis. Danny has forced me to ‘understand what is really going on’ with each method I employ. His attention to detail is remarkable and quite helpful.

I also wish to thank my co supervisor Dr. David Stirling for guiding me in my study and the writing of the thesis.

I am very grateful to the Ministry of Education, Directorate General of Higher Education (DIKTI) Indonesia, for providing me a Ph.D scholarship with sufficient financial support for me.

I would also like to extend my gratitude to the technical staff of the School of Electrical, Computer and Telecommunication Engineering (SECTE), particularly Sean Elphick and Vic Smith for their constant hard work and the pleasant manner in which they provided solutions to many problems that surfaced during the research.

Special thanks to the students at SECTE, in particular Jan E Alam, Chao Sun, Nishad Mendis and Hamid Reza Ghasemabadi for all the support and exchange of knowledge in a very friendly environment.

No list of acknowledgements would be complete without thanking my wife Hariroh Hannan who has supported me in every way possible. Especially I would like to acknowledge her patience as I have worked to complete my thesis.

I would also like to thank my children Fayyad, Salsa and Yusuf who has been patiently spent their time in the home country while I was away for my study.

I also wish to thank my parents and other family members for their unwavering, never-ending support, inspiration and encouragement in pursuing my education.

Finally, thanks to every friend or family member who has not been mentioned here, but who have all contributed to making my life easier, more enjoyable and valuable.

TABLE OF CONTENTS

LIST OF FIGURES

LIST OF TABLES

LIST OF ABBREVIATIONS

DFT	Discrete Fourier Transform
EEMD	Ensemble Empirical Mode Decomposition
EMD	Empirical Mode Decomposition
ESPRIT	Estimation of Signal Parameters via Rotational Invariance Techniques
FFT	Fast Fourier Transform
HHT	Hilbert Huang Transform
IEEMD	Iterative Ensemble Empirical Mode Decomposition
IHHT	Iterative Hilbert Huang Transform
IMF	Intrinsic Mode Function
MSE	Mean Square Error
MUSIC	MUltiple SIgnal Classification
PAA	Piecewise Aggregate Approximation
PQ	Power Quality
SAX	Symbolic Aggregate approXimation
WT	Wavelet Transform

CHAPTER 1 INTRODUCTION

1.1. Problem statements and background

The growth of the usage of power electronics equipment at the customer side, such as computers and consumer electronics, right through to adjustable-speed drives has become the source of Power Quality (PQ) pollution which will create poor PQ environment. At the same time, the use of sensitive electrical equipment controlled by power electronics or microprocessor is rapidly increasing. When there is no balance of the PQ environment with the immunity characteristics of the sensitive equipment, many PQ problems may occur which may lead to reduced reliability and expensive outages at the customer side [1].

In a competitive electricity market, electricity utilities are required to guarantee the operation of the customer's equipment by providing a high quality power supply in order to satisfy their customer. To meet both utility and customer requirements, continuous monitoring of PQ waveforms is essential.

Most of PQ waveforms are non-stationary and noisy in nature which requires a tool that can accurately analyse and visually identify the components of various PQ events. Fourier Transform (FT) is a simple and computationally efficient algorithm which has dominated the data analysis work since it was first discovered. However, there are some crucial limitations of the Fourier spectral analysis: the data must be strictly stationary and the system must be linear; otherwise, erroneous resulting spectrum will be obtained [2]. Since most PQ events are usually non-stationary, the Short-Time Fourier Transform (STFT) has been developed to analyze such signals. A windowing technique is used by the STFT method to concentrate the FT on a smaller area of the entire signal [3]. However, the width of the window needs to be fixed prior to carrying out the analysis. Therefore, the resolution of the STFT method is fixed, which may not produce accurate result when the signal being analyzed contains various frequencies.

Wavelet Transform (WT) uses flexible windowing function which is shifted and scaled version of the mother wavelet. Therefore, Wavelet analysis can give good time resolution for high-frequency events, and good frequency resolution for low-frequency events. However, once the mother function has been chosen, it will have to be used to analyze all of the data, which may require a different choice of mother

wavelet because of the non-stationary nature of the signal. The WT is therefore not adaptive to analyze the on-stationary PQ waveforms [2].

A couple of parametric methods such as Prony analysis, Multiple Signal Classification (MUSIC) and Estimation of Signal Parameters via Rotational Invariance Techniques (ESPRIT) have also been used for PQ signal analysis. The parametric methods estimate the signal parameters (such as amplitude, frequency and phase) by fitting the signal being analyzed to the model used in the method. It is reported that parametric methods are very accurate to estimate the signals parameters [4]. However, the methods assume that the number of sinusoids in the signal are known prior to the analysis which may not be possible for most practical cases [4].

One of the recently reported tools available to analyse non-stationary complex waveforms with a very good time resolution is the Hilbert Huang Transform (HHT) which consists of two distinct processes. First the signal to be analyzed is decomposed using the Empirical Mode Decomposition (EMD) process into Intrinsic Mode Functions (IMFs) that have meaningful instantaneous frequencies, amplitudes and phases of the signal components being analyzed [5]. Second, The Hilbert Transform is then applied to each IMF giving the instantaneous amplitude, frequency and phase versus time. HHT method does not require any assumption before the analysis and hence it can be considered as an adaptive method. However, it has been reported [6], [7], that the HHT has difficulties in decomposing harmonic signals containing close frequencies that occasionally results in IMFs with mixed frequencies. Mixed IMFs generally produce incorrect result from the Hilbert Transform and therefore they are not desirable. The IMFs with mixed frequencies are also found, when the signal being analyzed by the EMD process contain relatively significant noise level [8].

The EMD process estimates the local average of the waveform being analyzed by identifying the maxima and minima points of the waveform which are then connected by using cubic spline interpolation to build the maxima and minima envelopes. The local average is approximated from the mean of these envelopes. However, since the points to be interpolated are not sufficiently available at both ends of the waveform, the end effect phenomenon generally appears in the resulted IMF, which is another issue with the EMD method [2].

1.2. Thesis objectives and methodology

The aim of this thesis is to develop a methodical approach using the original and the extended Hilbert Huang Transform, Ensemble Empirical Mode Decomposition and SAX boundary detector to decompose non-stationary PQ signals that contain close frequency components and noise. The decomposition result can assist data analysts or utility engineers to analyse the monitored data. Such approach will also allow the utility engineers to gain more information into the occurrence of PQ events that may damage electrical equipment.

Although various researchers have endeavoured to address mode mixing problem resulted from the EMD process of signals containing close frequencies, none has exploited the mixed IMF resulting from the original EMD process. The new concept proposed in this thesis is based on utilising certain IMFs (which may be mixed) produced by the original EMD, that contain correct mean value of instantaneous frequencies, and subtracting these from the original signal. The HHT process is then repeated in an iterative mode (so that all signal components are decomposed accurately), in contrast to subtracting all IMFs obtained from a typical HHT process at once. The proposed technique which is referred to as the Iterative HHT, modifies the IMFs to sinusoidal representations by using the mean values of amplitude, frequency and phase obtained from the Hilbert Transform of the IMFs. Therefore, the end effect issue is avoided by using such technique.

Ensemble EMD (EEMD) which has been proposed by Wu [9], is a variant of EMD where an ensemble of white noise-added signals is created from the original data. The EMD is applied to each of these signals to produce an ensemble of IMFs which are then averaged to obtain the final IMF. EEMD has been recently reported to help in solving some of the issues with mode mixing [9] resulting from the EMD process of noisy signals [8]. However, the results from the EEMD method has been found to produce inaccurate amplitude values of the components since the averaging process of the mixed IMFs may produce final identified amplitudes which are less than the actual values. This inaccuracy indicates that part of the signal components remain unidentified by the decomposition process [8]. Therefore, a similar iterative technique to the HHT improvement is proposed in this thesis to obtain the remaining signal component in the residue. The sinusoidal representations of the IMFs are also used in the Iterative EEMD method to avoid the end effect issue.

Both the Iterative HHT and Iterative EEMD use EMD algorithm as the main method to perform the decomposition process. The EMD process is employed in an iterative fashion to improve the accuracy of the decomposition process of the proposed methods. These methods are therefore referred to as the Iterative EMD techniques in the thesis.

To analyze non-stationary signals, Symbolic Aggregate ApproXimation (SAX) algorithm is used in the thesis to obtain a symbolic representation of the signal which is then used by a boundary detector algorithm to identify the instant of changes of the signal. The identified instant of changes are then used to segment the signal to a sequence of stationary signals The decomposition methods are then applied to decompose the signal of the associated segment.

In summary, the objectives of the thesis are as follows:

1. To investigate the application of HHT techniques to decompose PQ events.
2. To extend the HHT technique to remove mode mixing issues when used to decompose PQ events containing closely related frequencies.
3. To investigate the application of the EEMD technique in decomposing noisy PQ events.
4. To adapt the EEMD technique to mitigate mode mixing issues when used to decompose more noisy PQ events
5. To develop a signal pre-processing method by using a SAX-based boundary detector to identify the boundaries of non-stationary signals so that the decomposition method can be used for the analysis of non-stationary signals.

1.3. Thesis outline

The outline of the thesis is as follows. Chapter 2 will provide the literature review. Chapter 3 will introduce the HHT method and discuss the issue in implementing HHT. Chapter 4 will describe several techniques from the literature to improve the HHT method in resolving the mode mixing problem caused by signals having close frequency components. A new method using an iterative process will also be proposed to improve the original HHT in decomposing such signals. Chapter 5 will present a signal pre-processing technique to identify the boundaries of the non-stationary signal by translating the signal to a lower dimensional representation using SAX algorithm and applying a boundary detector to the symbolic representation of the original data. Chapter 6 will describe the traditional Ensemble Empirical Mode

Decomposition (EEMD) and propose the Iterative Ensemble Empirical Mode Decomposition (IEEMD) to improve its accuracy. Chapter 7 will provide the results of the application of the decomposition methods to measured signals. A summary of the thesis and a discussion of future work are contained in Chapter 8.

1.4. Summary of original contributions

The following methods are the original contributions of the research.

1. The development of the Iterative Hilbert Huang Transform.
2. The development of the Iterative Ensemble Empirical Mode Decomposition.
3. The development of SAX-based boundary detector to identify the instant of changes of the non-stationary signal.

1.5. Thesis related publications

The following publications have been the result of the research presented in the thesis:

Journal papers

AFRONI, M. J., SUTANTO, D. & STIRLING, D. 2013 "Analysis of Non-Stationary Power Quality Waveforms Using Iterative Hilbert Huang Transform and SAX Algorithm" *IEEE Transactions on Power Delivery* 28**,** 2134 - 2144.

Conference and presentation

AFRONI, M. J., SUTANTO, D. & STIRLING, D. "SAX-based decomposition of non-stationary Power Quality waveforms". *In:* Harmonics and Quality of Power (ICHQP), 2012 IEEE 15th International Conference on, 2012. IEEE, 829-834.

AFRONI, M. J., & SUTANTO, D. "The Hilbert Huang Transform for decomposition of Power Quality waveforms,". *In Power Engineering Conference (AUPEC), 2014 Australasian Universities*, 2014, pp. 1-6.

CHAPTER 2 LITERATURE REVIEW

2.1. Introduction

PQ disturbances due to the usage of power electronics equipment may cause harmful effect such as malfunction or failure to sensitive power electronic and microprocessor controlled equipments. To get the consumers satisfaction, the electric utilities need to maintain good PQ supply in such a competitive electricity market nowadays. Therefore, PQ monitoring and PQ troubleshooting are becoming more important to the electric utilities to ensure a high level of service [10].

This chapter initially describes the increasing PQ problems and why PQ monitoring is needed. A review of the techniques that have been used to analyse PQ data obtained from such monitoring system is then presented. The basics of signal processing techniques such as Fourier Transform (FT), Discrete Fourier Transform (DFT), Short Term Fourier Transform (STFT), Wavelet Transform (WT), Prony Algorithm, Multiple Signal Classification (MUSIC), and Estimation of Signal Parameters via Rotational Invariance Techniques (ESPRIT) which can be used to analyze PQ events are discussed. Finally the use of Hilbert Huang Transform is presented. The advantage and limitation of each technique is discussed.

2.2. Power Quality Problems

The increasing use of power electronics equipment has polluted the power system with harmful PQ disturbances such as harmonics input current which consist not only a power frequency component, which can be 50 Hz or 60Hz, but also harmonic components which may cause overheating of induction motors and transformers [10]. Other PQ events such as over-voltage, under-voltage, sag and swell has also been reported to significantly contribute to the pollution of the PQ environment [10], [11]. When there is no balance of PQ environment with the immunity characteristics of the equipment, PQ disturbances may cause malfunction or damage to the electrical equipment which lead to reduced reliability and expensive outages [1].

For a deeper understanding of PQ issues, it is important to understand the basics of PQ [12]. PQ has been defined as "a set of electrical boundaries that allow equipment to function in its intended manner without significant loss of performance or life expectancy" [13] and "any power problems manifested in voltage, current or

frequency deviation that result in failure or mal-operation of customer equipment," [14]. Therefore, to have sufficient understanding of PQ, it is necessary to study the deviation of the load current, the supply voltage, or the frequency waveforms from the pure sinusoidal waveforms [12]. Chowdhury reported that voltage disturbances (such as voltage sags) can result in malfunction of equipment that can cost approximately 20 billion dollars annually in the United States [15].

There are three general types of PQ disturbances that may be experienced by a power system, as follows [11]:

a) Frequency events.
b) Voltage events.
c) Waveform events.

The above events will be described in more details in the following subsections.

2.2.1. Frequency events

The frequency of power system is usually determined by the rotational speed of generators in the power station. The stability of the power system interconnection and the efforts made to maintain the frequency within the required limits make frequency deviations beyond the acceptable range to be a very rare phenomenon [16]. Therefore, this type of event will not be discussed further in the thesis.

2.2.2. Voltage events

In Australia, the supply voltage is normally held in the range +10% and -6% at the customer's point of connection which is considered as the normal PQ range [17]. If the supply voltage rises much higher than the rated voltage (over-voltage) or decreases lower than the rated voltage (under-voltage), PQ problems may occur. For example, over-voltage causes overstressed motor insulation while under-voltage may cause motor overheating which can lead to loss of life [11].

Voltage variations can be divided into the following categories [11]:

a) Long term variations of duration more than 1 minute. These are called over-voltage (if greater than 110% of nominal voltage) or under-voltage (if less than 90% of nominal voltage).

b) Short term variations lasting less than 1 minute. These are called swell (voltage greater than 110% of nominal) or sag (voltage between 10% and 90% of nominal). These are illustrated in Figure 2.2.2.1(a).

c) Voltage unbalance where the voltage of each phase conductor is different to other phases as shown in Figure 2.2.2.1(b).

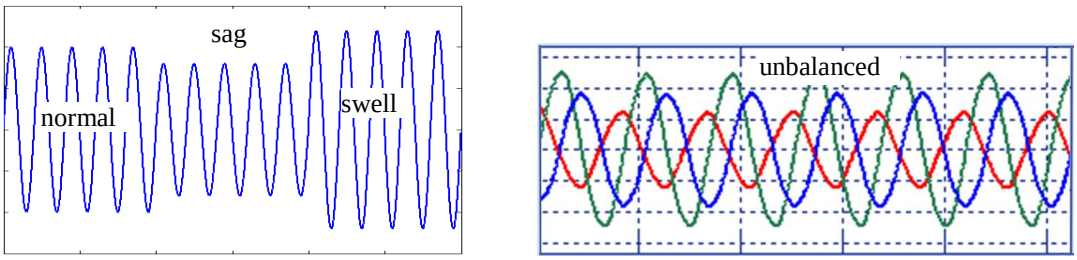

a) b)

Figure 2.2.2.1. (a)Voltage sag and swell (b) Voltage unbalance.

d) Voltage fluctuations is continuous or random fluctuations in the amplitude of the supply voltage that can be observed as light flicker as shown by Figure 2.2.2.2.

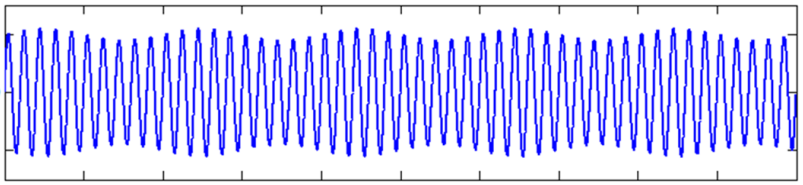

Figure 2.2.2.2. Voltage fluctuations

e) Voltage Interruption is a complete lost of the supply voltage. The voltage interruption waveform is shown in Figure 2.2.2.3.

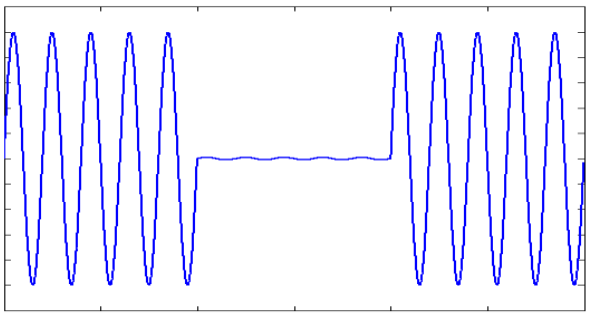

Figure 2.2.2.3. Voltage interruption

2.2.3. Waveform Events

These events cause the normally sinusoidal waveform of the mains voltage or current to be distorted. The following is a classification of the waveform events:

a) Harmonics are integer multiples of the mains frequency superimposed on to the fundamental 50 Hz or 60 Hz mains frequency [18]. The main cause of the harmonics are non-linear loads such as switched power supplies in computers, arc welding machines and arc furnaces. The effect of harmonics is shown in Figure 2.2.3.1. Each cycle is still identical to the other even though the waveform is distorted.

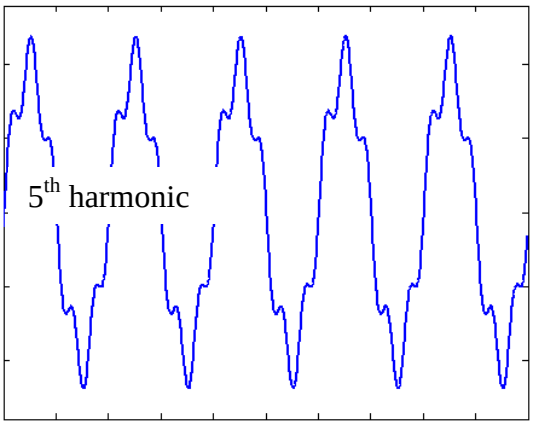

Figure 2.2.3.1. Harmonic.

b) Inter-harmonics are non-integer multiples of the mains frequency superimposed on to the fundamental 50 Hz or 60 Hz mains frequency [18]. The presence of the interharmonic causes the neighbouring cycles non–identical [11], as shown in Figure 2.2.3.2.

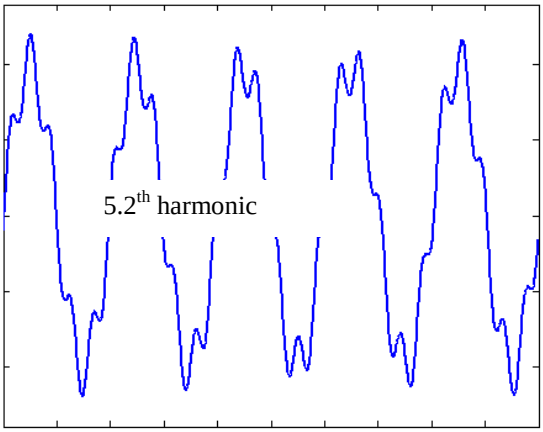

Figure 2.2.3.2. Inter-harmonic

c) Notching is defined as a recurring PQ disturbance due to the normal operation of 3-phase electronic switching devices such as AC to DC converters. When current is commutated from one phase to another, a momentary short circuit between two phases will occur which can be seen as the notching event in the waveform. This is illustrated in Figure 2.2.3.3 and is present on many consecutive cycles.

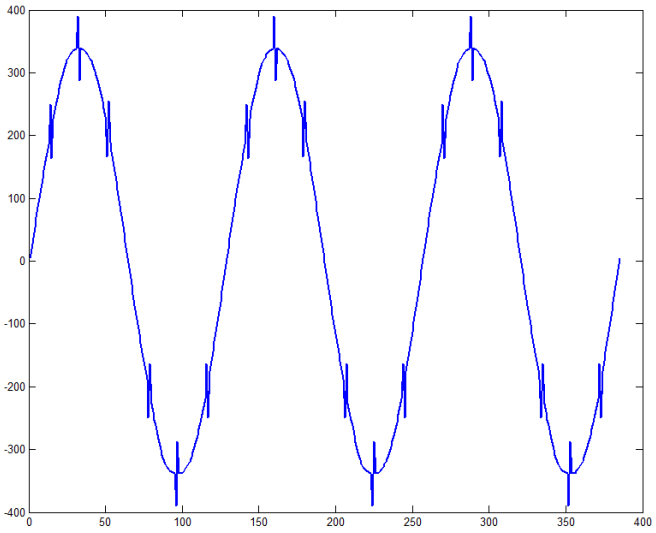

Figure 2.2.3.3. Notching.

d) Transients are commonly large, momentary changes in voltage or current that occurs over a short period of time. This time interval is usually described as less than one half cycle of the main voltage. Transients are caused primarily by lightning strikes or switching operations on the network. These events are shown in Figure 2.2.3.4.

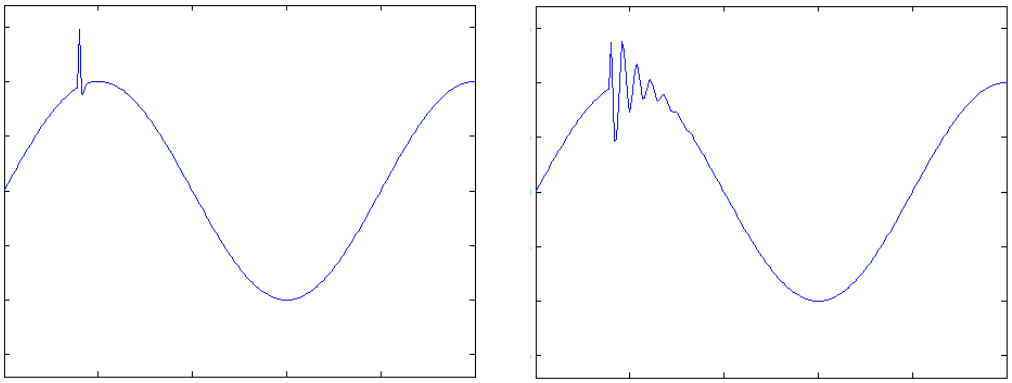

a) b)

Figure 2.2.3.4. Typical transients, (a) From lightning (b) From system switching

e) Noise is a disturbance with low amplitude and wide frequency distribution up to about 200,000 Hz [11]. A waveform distorted by noise is shown in Figure 2.2.3.5. This event may be caused from both inside and outside the facility, such as electromagnetic interference (from currents in conductor) or radio frequency interference (from radio systems radiating signals). The noise can also be caused by normal equipment operations, poor maintenance, or powerful electric disruptions [19].

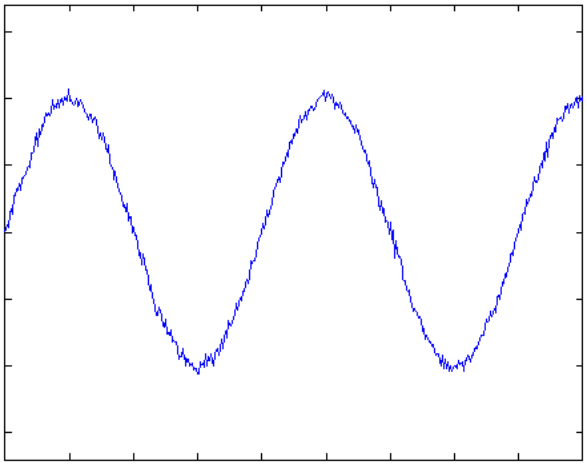

Figure 2.2.3.5. A waveform with noise content.

To quantify PQ variations, a set of parameters has been provided by the International Electrotechnical Commission (IEC), which classify PQ disturbances to several categories such as transients, voltage sags (dips), voltage surges (swells), voltage flicker, voltage unbalance, forced interruptions, harmonics, inter-harmonics, and frequency variation. A detail list of various PQ disturbances are shown in Table 2.1 based on the IEEE 1159-1995 and IEC 61000 classification method [20].

Table 2.1. PQ Disturbances

(source: IEEE, " Recommended practice for monitoring electric PQ", 1995 [20])

Categories	Typical Spectral content	Typical duration	Typical Voltage amplitude
1.0 Transients			
1.1 Impulsive			
1.1.1 Nanosecond	5-ns rise	< 50 ns	
1.1.2 Microsecond	1-μs rise	50 ns-1ms	
1.1.3 Millisecond	0.1-ms rise	> 1 ms	
1.2 Oscillatory			
1.2.1 Low freq.	< 5 kHz	0.3-50 ms	0-4 pu
1.2.2 Medium freq.	5-500 kHz	20 μs	0-8 pu
1.1.3 High freq.	0.5-5 Mhz	5 μs	0-4 pu
2.0 Short-duration variations			
2.1 Instantaneous			
2.1.1 Interruption		0.5-30 cycles	<0.1 pu
2.1.2 Sag (dip)		0.5-30 cycles	0.1-0.9 pu
2.1.3 Swell		0.5-30 cycles	1.1-1.8 pu
2.2 Momentary			
2.2.1 Interruption		30 cycles-3 s	<0.1 pu
2.2.2 Sag (dip)		30 cycles-3 s	0.1-0.9 pu
2.2.3 Swell		30 cycles-3 s	1.1-1.4 pu
2.3 Temporary			
2.3.1 Interruption		3 s-1 min	<0.1 pu
2.3.2 Sag (dip)		3 s-1 min	0.1-0.9 pu
2.3.3 Swell		3 s-1 min	1.1-1.2 pu
3.0 Long-duration variations			
3.1 Interruption, sustained		> 1 min	0.0 pu
3.2 Undervoltages		> 1 min	0.8-0.9 pu
3.3 Overvoltages		> 1 min	1.1-1.2 pu
4.0 Voltage unbalance		Steady state	0.5-2%
5.0 Waveform distortion			
5.1 dc offset		Steady state	0-0.1%
5.2 Harmonics	0-100th harmonic	Steady state	0-20%
5.3 Interharmonics	0-6 kHz	Steady state	0-2%
5.4 Notching		Steady state	
5.5 Noise	Broadband	Steady state	0-1%
6.0 Voltage fluctuations	< 25 Hz	Intermittent	0.1-7%
7.0 Power frequency variations		< 10 s	

2.3. Effects of PQ Disturbances

Some of the effects of the PQ disturbances such as voltage events and waveform events are listed in Table 2.2 and Table 2.3 respectively [11].

Table 2.2. Typical Effects of voltage Events.
(source: APQRC Technical Note No. 1, Understanding PQ [11])

Disturbance	Effect
Over-voltage	Overstress insulation
Under-voltage	Excessive motor current
Unbalance	Motor heating
Neutral-ground voltage	Digital device malfunction
Interruption	Complete shutdown
Sag	Variable speed drive & computer trip – out
Swell	Overstress insulation
Fluctuations	Light flicker

Table 2.3. Typical Effects of Waveform Events.
(source: APQRC Technical Note No. 1, Understanding PQ [11])

Disturbance	Effect
Harmonic	Motor, Transformer & neutral conductor overheating, instrumentation malfunction.
Notching	Zero – crossover device malfunction
Transients	Electronic device failure or malfunction; drive trip-out
Noise	Fast running clocks, zero crossover device malfunction

2.4. Existing PQ Monitoring Systems

In order to measure and identify PQ problems, a lot of PQ measuring equipments are now used in the electric power systems [12], such as:

a. ***Harmonic analysers or harmonic meters*** are instruments used to measure the amplitudes, frequencies and phases of the harmonic components of PQ waveforms. In addition, the devices can also estimate the harmonics distortion by calculating the Total Harmonic Distortion (THD) index.
b. ***Transient-disturbance analysers*** are devices used to capture, store, and present short-duration, sub-cycle power system disturbances.
c. ***Oscilloscope*** is a PQ measuring instrument used to observe and visualize electric signal in the form of two-dimensional plot of the waveform vs. time. A

modern digital oscilloscope may analyse the signal directly to identify its properties such as the frequency, amplitude and distortion.

d. ***PQ analysers*** are advanced electronic test instruments that are equipped with several tools to measure, monitor and analyse PQ events. The devices generally have the ability like the oscilloscope as well as the harmonic analyser and also have extra features such as communication ports and storage memory to save the recorded waveforms.

2.5. Methods of PQ signal Decomposition

The data collected by the PQ instruments is generally further analysed to extract the features and information from the measured signals [4]. Certain analysis methods such as decomposition techniques are consequently required to identify the frequencies, amplitudes and phases of the components contained in the waveform. Details of these methods are further described in the following subsections.

2.5.1. Fourier Transform (FT).

Fourier analysis assumes that a signal *v(t)* is composed from a series of sinusoidal waveforms of various frequencies, known as Fourier series. Using the assumption, a signal which is usually defined in time domain can be transformed to frequency domain by utilizing Fourier Transform. Fourier analysis is found to be extremely useful for many signals, since frequency content of the signal is really essential [21]. A Fourier series of a periodic signal *v(t)* is given by (2-1).

$$v(t) = \frac{a_0}{2} + \sum_{n=1}^{\infty} (a_n \cos n\omega t + b_n \sin n\omega t) \tag{2-1}$$

Where:

a_n and b_n are the Fourier coefficients

n = sinusoid (wave) number

$\omega = 2\pi f = \frac{2\pi}{T}$

T = period of the signal

The expression in (2-1) can be written in a general form as given by (2-2)

$$v(t) = \sum_{n=-\infty}^{\infty} c_n e^{\frac{2n\pi it}{T}}$$

(2-2)

Where :

c_n = Fourier coefficients

The coefficient *c* can be represented as a function of $\omega = \frac{2n\pi}{T}$ as given by (2-3):

$$c_n = \frac{1}{T}\int_{\frac{-T}{2}}^{\frac{T}{2}} v(t)e^{\frac{2n\pi it}{T}}dt$$

(2-3)

If *T* is large, ω is small and therefore $c(\omega)$ becomes a continuous function. The relation in (2-2) can then be expressed as given by (2-4):

$$v(t) = \sum_{n=-\infty}^{\infty} \frac{1}{T}\int_{\frac{-T}{2}}^{\frac{T}{2}} v(t)e^{\frac{2n\pi it}{T}}dt\, e^{\frac{2n\pi it}{T}}$$

(2-4)

Further, when we let $T \rightarrow \infty$, the expression in (2-4) can be written as given by (2-5)

$$v(t) = \frac{1}{2\pi}\int_{-\infty}^{\infty}\left(\int_{-\infty}^{\infty} v(t)e^{-i\omega t}dt\right)e^{i\omega t}d\omega$$

(2-5)

The inside integral (in the bracket) is denoted by $V(\omega)$, which is the Fourier Transform of $v(t)$.

Fourier spectral analysis works well to analyse signals, however, there are some crucial limitations of the Fourier spectral analysis, the data must be strictly periodic or stationary and the system must be linear. Otherwise, erroneous resulting spectrum will be obtained [2].

Furthermore, a serious drawback of the spectral analysis is that the method transforms a signal to the frequency domain which does not have the time information any more. When a signal is transformed to the Fourier spectrum, it is not possible to identify the time instant when a particular event occurs [22].

2.5.2. Discrete Fourier Transform (DFT) and Fast Fourier Transform (FFT)

In order to perform the computation of the Fourier spectrum for a signal using a digital system, the signal needs to be represented in the sample form which is then quantized to obtain the spectrum at a discrete number of frequencies. An

approximation to the Fourier spectrum of a signal at frequencies $k/(NT_s), k = 0,1,.,N-1$ can be provided by the following sum [12]:

$$V[k] = \sum_{p=0}^{N-1} v_p e^{-i2\pi pk/N} \qquad k = 0,1, \ldots . N-1 \tag{2-6}$$

where T_s is the sampling period, $v_0, v_1, v_2, \ldots, v_{N-1}$ are N discrete values of the signal sampled uniformly at sampling period T_s. The above expression is referred to as the Discrete Fourier transform (DFT) of the sequence (v_n). However, the original form of the DFT is not efficient for applying a Fourier Transform digitally. Therefore, a faster algorithm was further developed which is referred to as the Fast Fourier Transform (FFT) to compute the DFT of the sequence (v_n). The FFT factorizes the DFT matrix into a product of sparse (mostly zero) factors. Therefore, the complexity of the DFT computation which is $O(n^2)$ can be reduced significantly to $O\ (n\ log\ n)$ by using the FFT algorithm. [23].

According to Bollen and Gu [4], among the existing signal analysis methods, DFT is the simplest one to implement while FFT algorithm has made the DFT more computationally efficient.

By using the DFT algorithm, the decomposition process of a signal can be performed by identifying the frequency of the signal components from the peaks of the Fourier spectrum given by (2-6). Once the frequency of a signal component is obtained, the amplitude of the signal component $v(n)$ can be calculated from the absolute value $A = \sqrt{Im\big(V(f)\big)^2 + Re(V(f))^2}$, while the initial phase angle can be estimated by a relation given by (2-7).

$$\theta = \tan^{-1} \frac{Im(V(f))}{Re(V(f))} \tag{2-7}$$

2.5.3. Short Term Fourier Transform (STFT)

Whilst the FFT performs very well when dealing with stationary periodic signals, it is not suitable for non-stationary signals, whose frequency, amplitude or phase vary over time – as FFT essentially assumes the signal is stationary. In order to enable the FFT algorithm work for non-stationary waveforms, a further modification was developed which is referred to as the Short Term Fourier Transform (STFT). This transform utilises a windowing technique which moves the window along the

time axis (from the beginning to the end of the signal) in order to evaluate the FFT of a smaller area of the whole signal [24]. This process results in a two-dimensional representation of the signal, both in time and frequency. The STFT of a signal *x(t)* by using windowing function *w(t)* can be expressed as follows :

$$STFTx(t,f) = \int_t [x(t).w^*(t-\tau)].e^{-j2\pi ft}dt \quad (2\text{-}8)$$

The result of (2-8) provides the frequency response as well as the occurrence of that frequency in time. Various window function such as Hanning window or Blackman window [24], [25] can be used to do the analysis. The width of the window function determines if there is an adequate time resolution (the points in time where the frequencies change) or a sufficient frequency resolution (where the frequency components that are close together can be separated). A narrow window provides enhanced time resolution but with reduced frequency resolution, while a wide window provides improved frequency resolution but reduced (poorer) time resolution. Once a suitable window size is determined, it is used for all the frequencies contained in the whole signal. However, to determine either frequency or the time more accurately, a windowing technique using variable window size is required [26].

2.5.4. Wavelet Transform (WT)

Unlike the Fourier Transform, the Wavelet Transform uses a different approach by multiplying the original signal over its interval by the scaled and shifted representation of a mother wavelet, defined as “wavelets” [27], [28], [29].

In contrast to the STFT which uses fixed window width, wavelet transform uses a windowing technique with variable window size. Therefore, it is possible to select either a long time window to obtain more precise information of low frequency signal or shorter window for high frequency signal analysis [21]. With this flexible windowing technique, the wavelet transform is able to analyse a localized area of a larger signal known as the local analysis.

The wavelet transform of a signal *h(t)* is provided by

$$C(a,b) = |a|^{-1/2} \int_{-\infty}^{\infty} h(t) w^* \left(\frac{t-b}{a}\right) dt \tag{2-9}$$

Where :

a = scale factor

b = translation factor

w = window function

Continuous Wavelet Transform (CWT) implements the expression in (2-9) to obtain a representation of many wavelet coefficients C which is a function of scale factor (or dilation) *a* and position (or translation) *b.* The value of wavelet coefficients indicate how closely correlated the wavelet is with a localized section of the signal being analyzed. Therefore, when the frequency of *w(t)* is the same as the frequency of the signal component, the value of *C(a, b)* is large, otherwise it is small [30]. By calculating the wavelet coefficients for each wavelet segment, a time-scale function represents the wavelets correlation to the signal is obtained [31].

The decomposition process of a signal is performed by using a filter bank consisting of high pass and low pass filters which separates the signal to high frequency and low frequency components. A multilevel filter banks can decompose the signal to its components. Once the signal has been decomposed using the filter bank, the non-zero time-domain components are then analysed using CWT.

The frequency of the signal component associated to the transform coefficients *C(a,b)* are given by f_0/a, where f_0 is the frequency of *w(t).* To estimate the amplitude and phase angle of the signal components, an exponential mother wavelet obtained by the truncation of the exponential function, $w(t) = e^{(j\omega_0 t)}$ can be used. The amplitude of the n^{th} signal component is given by $\sqrt{a}|C(a,b)|_n/T$. The phase angle of the component can be obtained from the relation given by (2-10) [30].

$$\theta_n = \tan^{-1} \frac{Im(C(a,b))}{Re(C(a,b))} \tag{2-10}$$

The appropriate choice of the mother wavelet can enable the detection and localization of various disturbances [32],[33]. However, the accuracy of PQ signal decomposition is significantly affected by the choice of the wavelet family and the mother wavelet [27], [34]. Once a mother wavelet function is chosen it will have to

be used to analyse all the data, however, because of the non-stationary nature of the signal, a different choice of mother wavelet may be required. The wavelet transform therefore cannot become adaptive to the analysis of non-stationary PQ waveforms.

2.5.5. Prony Algorithm

While Fourier analysis considers that a signal is composed from a series of undamped complex exponential, Prony method models the signal as a linear combination of damped complex exponentials [35].

For a signal $\hat{y}(t)$, the investigated model can be approximated by L damped complex exponential functions, as given by (2-11) :

$$\hat{y}(t) = \sum_{i=1}^{L} A_i e^{\sigma_i t} \cos(2\pi f_i t + \Phi_i) \tag{2-11}$$

where L is the total number of damped exponential components; A_i is the amplitude; σ_k is the damping factor; f_i is the frequency; t is the sampling period and Φ_i is the initial phase.

For the sake of mathematical convenience, the cosine function is converted to the exponential representation by using Euler's theorem as given by (2-12):

$$\cos(2\pi f_i t + \Phi_i) = \frac{e^{j(2\pi f_i t + \Phi_i)} + e^{-j(2\pi f_i t + \Phi_i)}}{2} = \frac{e^{j2\pi f_i t} e^{j\Phi_i}}{2} + \frac{e^{-j2\pi f_i t} e^{-j\Phi_i}}{2} \tag{2-12}$$

let $t=kT$ (where T is the sampling period), the sampled representation of $\hat{y}(t)$ can be expressed as [35]:

$$\hat{y}[k] = \sum_{i=1}^{L} C_i \mu_i^k \tag{2-13}$$

where

$$C_i = \frac{A_i}{2} e^{j\Phi_i} \tag{2-14}$$

$$\mu_i = e^{(\sigma_i + j2\pi f_i)T} \tag{2-15}$$

The Prony analysis performs the decomposition process by computing C_i and μ_i in the following steps [36], :

Step 1: Solve a Linear Prediction Model (LPM) of *y[k]*, by assuming the current value of *y[k]* equals to a weighted combination of its previous values *y(k - i), i = 1,2,…,L* as given by (2-16).

$$y[k] = a_1 y[k-1] + a_2 y[k-2] + ... + a_L y[k-L] \quad (2\text{-}16)$$

if *y[k]* is computed at *k=L*, (2-16) can be expressed by:

$$y[L] = a_1 y[L-1] + a_2 y[L-2] + ... + a_L y[0] \quad (2\text{-}17)$$

y[k] can then be expressed in matrix form for various values of *k* as given in (2-18):

$$\begin{bmatrix} y[L] \\ y[L+1] \\ .. \\ . \\ . \\ y[N-1] \end{bmatrix} = \begin{bmatrix} y[L-1] & y[L-2] & .. & .. & y[0] \\ y[L] & y[L-1] & .. & .. & y[1] \\ y[L+1] & y[L] & .. & .. & y[2] \\ .. & .. & .. & .. & .. \\ y[N-2] & y[N-3] & .. & .. & y[N-L-1] \end{bmatrix} \begin{bmatrix} a_1 \\ a_2 \\ a_3 \\ .. \\ a_L \end{bmatrix} \quad (2\text{-}18)$$

where:

$$d = \begin{bmatrix} y[L] \\ y[L+1] \\ .. \\ . \\ . \\ y[N-1] \end{bmatrix}, D = \begin{bmatrix} y[L-1] & y[L-2] & .. & .. & y[0] \\ y[L] & y[L-1] & .. & .. & y[1] \\ y[L+1] & y[L] & .. & .. & y[2] \\ .. & .. & .. & .. & .. \\ y[N-2] & y[N-3] & .. & .. & y[N-L-1] \end{bmatrix} \text{ and } a = \begin{bmatrix} a_1 \\ a_2 \\ a_3 \\ .. \\ a_L \end{bmatrix}.$$

Vector *a* (the linear prediction coefficients) can be estimated by Assuming N > 2L and solving the over-determined least square problem. A Matlab code can be used to calculate vector *a* as given by (2-19):

$$a = pinv(D)*d \quad (2\text{-}19)$$

where *pinv* function calculates the pseudo inverse of D

Step 2: The key of Prony method is that the coefficients obtained from the LPM is related to the characteristic polynomial as given by (2-20). The value of linear prediction coefficients can be used to form the characteristic polynomial whose roots can then be calculated [37].

$$\mu^L - a_1\mu^{L-1} - \ldots . - a_{L-1}\mu - a_L = (\mu - \hat{\mu}_1)(\mu - \hat{\mu}_2) \ldots . (\mu - \hat{\mu}_L) \quad (2\text{-}20)$$

Step 3: estimate the exponential amplitude and phase of the sinusoid by solving the original set of linear equations.

$$\begin{bmatrix} y[0] \\ y[1] \\ \cdots \\ \cdots \\ y[N-1] \end{bmatrix} = \begin{bmatrix} 1 & 1 & \ldots & 1 \\ \hat{\mu}_1^1 & \hat{\mu}_2^1 & \ldots & \hat{\mu}_L^1 \\ \hat{\mu}_1^2 & \hat{\mu}_2^2 & \ldots & \hat{\mu}_L^2 \\ \cdots & \cdots & \cdots & \cdots \\ \hat{\mu}_1^{N-1} & \hat{\mu}_2^{N-1} & \ldots & \hat{\mu}_L^{N-1} \end{bmatrix} \begin{bmatrix} C_1 \\ C_2 \\ \cdots \\ \cdots \\ C_L \end{bmatrix} \tag{2-21}$$

$$\text{or } Y=UC \tag{2-22}$$

where :

$$Y = \begin{bmatrix} y[0] \\ y[1] \\ \cdots \\ \cdots \\ y[N-1] \end{bmatrix}, U = \begin{bmatrix} 1 & 1 & \ldots & 1 \\ \hat{\mu}_1^1 & \hat{\mu}_2^1 & \ldots & \hat{\mu}_L^1 \\ \hat{\mu}_1^2 & \hat{\mu}_2^2 & \ldots & \hat{\mu}_L^2 \\ \cdots & \cdots & \cdots & \cdots \\ \hat{\mu}_1^{N-1} & \hat{\mu}_2^{N-1} & \ldots & \hat{\mu}_L^{N-1} \end{bmatrix}, C = \begin{bmatrix} C_1 \\ C_2 \\ \cdots \\ \cdots \\ C_L \end{bmatrix}$$

Coefficients C_i can be calculated by solving equations in (2-22). A Matlab code can be used for C_i calculation as follows:

$$C = pinv(U)*Y \tag{2-23}$$

As C_i and $\hat{\mu}_i$ for $i=1,2...L$ (where L = the number of signal components) are now known, the amplitude, frequency, phase and damping coefficient of each component can be computed using (2-14) and (2-15).

Prony method is best used when the components of the signal have damped exponential characteristic. When the signal is undamped, the value of σ_i will be 0. The problem of Prony algorithm is that the number of components *(L)* of the signal model given in (2-11) must first be known to fit the model to the signal being analyzed. If the actual number of components is not equal to *L*, erroneous result will be obtained.

2.5.6. Multiple Signal Classification (MUSIC) [4]

The MUSIC method models signal *v(n)* of length *L* as *K* sinusoidal components in noise given in (2-24).

$$v(n) = s(n) + w(n) = \sum_{k=1}^{K} a_k \cos(n\omega_k + \Phi_k) + w(n)$$

(2-24)

where *s(n)* is the clean signal (without noise), *w(n)* is the noise, K is the total number of sinusoidal components, a_k is the amplitude, ϕ_k is the initial phase angle and ω_k is the sinusoidal frequency.

An exponential expression which is equivalent to the model in (2-24) and referred to as the harmonic model is given in (2-25).

$$v(n) = \sum_{k=1}^{K} \underline{A}_k e^{jn\omega_k} + \omega(n) \tag{2-25}$$

where $\underline{A}_k = |A_k|e^{j\phi k}$ is the complex amplitude of the k^{th}-sinusoidal signal component.

The MUSIC method uses the exponential model given in (2-25) and assumes that the number of sinusoidals K is known. The decomposition process is performed to estimate the unknown frequencies, amplitudes and phase angle of each sinusoids in the model by employing noise subspace.

The autocorrelation matrix $\mathbf{R}_v$ of *v(n)* can be estimated from the signal data as given in (2-26).

$$\hat{\mathbf{R}}_v = \frac{1}{N}\mathbf{V}^H\mathbf{V} \tag{2-26}$$

Let the length of the data sequence *v(n)* is $L = N + M - 1$ and the size of $\mathbf{R}_v$ is $M \times M$. The superscript $(.)^H$ denotes the Hermitian operator (to obtain the transpose and complex conjugate of the matrix). *V* is the data matrix of size $N \times M$ and is described by

$$\mathbf{V} = \begin{bmatrix} \mathbf{v}^T(0) \\ \mathbf{v}^T(1) \\ \vdots \\ \mathbf{v}^T(N-1) \end{bmatrix}^T = \begin{bmatrix} v(0) & v(1) & \cdots & v(M-1) \\ v(1) & v(2) & \cdots & v(M) \\ \vdots & \vdots & \ddots & \vdots \\ v(N-1) & v(N) & \cdots & v(N+M-2) \end{bmatrix} \tag{2-27}$$

Since *v(n)* consist of the clean signal *s(n)* and noise *w(n)* as shown in (2-24), the autocorrelation matrix of *v(n)* $\hat{\boldsymbol{R}}_{\boldsymbol{v}}$ also consist of the autocorrelation matrices of clean signal $\boldsymbol{R}_s$ and noise $\boldsymbol{R}_w$. Substituting (2-25) in (2-26) yields

$$\hat{\mathbf{R}}_v = \mathbf{R}_s + \mathbf{R}_w = \mathbf{EPE}^{\mathrm{H}} + \sigma_w^2\mathbf{I} \tag{2-28}$$

Where **E** and **P** are defined as given by (2-29):

$$\mathbf{E} = \begin{bmatrix} \mathbf{e}_1 & \mathbf{e}_2 & \cdots & \mathbf{e}_K \end{bmatrix} \qquad \mathbf{P} = \mathrm{diag}\{|\underline{A}_1|^2|\underline{A}_2|^2\cdots|\underline{A}_K|^2\} \tag{2-29}$$

and

$$\mathbf{e}_l = \begin{bmatrix} 1 & e^{j\omega_l} & e^{j2\omega_l} & \cdots & e^{j(M-1)\omega_l} \end{bmatrix}^{\mathrm{T}} \qquad l = 1, 2, \ldots, K \tag{2-30}$$

$\boldsymbol{e}_l$ are the eigenvectors of $\boldsymbol{R}_s$

If $\boldsymbol{R}_v$ is assumed as full rank M, the eigenvalues of $\boldsymbol{R}_v$ (arranged in decreasing order) are $\lambda_1 \geq \lambda_2 \geq \ldots \geq \lambda_M$, and the associated eigenvectors are $s_1, s_2, \ldots\ldots s_M$, their relationship can be expressed by

$$\hat{\mathbf{R}}_v\mathbf{s}_i = \lambda_i\mathbf{s}_i \qquad i = 1, 2, \ldots, M \tag{2-31}$$

The eigenvectors $\boldsymbol{s}_i$ consist of K eigenvectors associated to the K largest eigenvalues of the signal subspace and M – K eigenvectors corresponding to the noise subspace. The sinusoid frequencies ω_k are estimated by using the noise subspace in the MUSIC pseudospectrum formula as given by (2-32) :

$$P_{\mathrm{music}}(e^{j\omega}) = \frac{1}{\sum_{i=K+1}^{M} |\mathbf{e}^{\mathrm{H}}\mathbf{s}_i|^2} \tag{2-32}$$

Where $\boldsymbol{s}_i$,$(i = K+1, \ldots, M)$ are the noise eigenvectors which are orthogonal to the clean signal eigenvector $\boldsymbol{e}_l = [1\ e^{j\omega}\ e^{j2\omega}\ldots\ldots e^{j(M-1)\omega}]^T$. Therefore, when the frequency of the pseudospectrum equals to any one of the frequencies related to the signal eigenvectors, the denominator has zero values and its reciprocals are infinite which are represented by the peaks of the pseudospectrum.

The frequencies of the signal components $\omega_k = 2\pi f_k$, $k = 1, 2, \ldots, K$, in (2-24) are obtained from the frequency locations associated to the K highest peaks in the pseudospectrum $P_{music}(e^{j\omega})$. Once ω_k are known, the amplitude of signal components are then estimated by solving the following equations :

$$\sum_{k=1}^{K} P_k|\boldsymbol{e}_k^H\boldsymbol{S}_i| = \lambda_i - \hat{\sigma}_w^2 \qquad i = 1,2,\ldots,K \tag{2-33}$$

Since $\boldsymbol{e}_k^H\boldsymbol{S}_i = \boldsymbol{S}_i(e^{j\omega_k}) = \sum_{m=0}^{M-1}\boldsymbol{s}_i(m)e^{-jm\omega_k}$, (2-33) can be expressed as

$$\begin{bmatrix} |S_1(e^{j\omega_1})|^2 & |S_1(e^{j\omega_2})|^2 & \cdots & |S_1(e^{j\omega_K})|^2 \\ |S_2(e^{j\omega_1})|^2 & |S_2(e^{j\omega_2})|^2 & \cdots & |S_2(e^{j\omega_K})|^2 \\ \vdots & \vdots & \ddots & \vdots \\ |S_K(e^{j\omega_1})|^2 & |S_K(e^{j\omega_2})|^2 & \cdots & |S_K(e^{j\omega_K})|^2 \end{bmatrix} \begin{bmatrix} P_1 \\ P_2 \\ \vdots \\ P_K \end{bmatrix} = \begin{bmatrix} \lambda_1 - \hat{\sigma}_w^2 \\ \lambda_2 - \hat{\sigma}_w^2 \\ \vdots \\ \lambda_K - \hat{\sigma}_w^2 \end{bmatrix} \quad (2\text{-}34)$$

By solving (2-34), the harmonic power P_k, $k = 1, 2, \ldots, K$ are obtained. The amplitude of the kth harmonic is then calculated from the following relation $V_k = \sqrt{2P_k}$.

Similar to Prony algorithm, the number of sinusoids K needs to be known before the decomposition process. The usage of an incorrect value of K in the method may produce error in the decomposition result.

2.5.7. Estimation of Signal Parameters via Rotational Invariance Techniques (ESPRIT)

Similar to MUSIC algorithm, the ESPRIT method also models signal *v(n)* of length L as K sinusoidal components in noise given in (2-35).

$$v(n) = s(n) + w(n) = \sum_{k=1}^{K} a_k \cos(n\omega_k + \phi_k) + w(n) \quad (2\text{-}35)$$

Let *v(n)* consists of M samples as given in (2-36)

$$\begin{bmatrix} v(n) \\ v(n+1) \\ \vdots \\ v(n+M-1) \end{bmatrix} = \sum_{k=1}^{K} \begin{bmatrix} s_k(n) \\ s_k(n+1) \\ \vdots \\ s_k(n+M-1) \end{bmatrix} + \begin{bmatrix} w(n) \\ w(n+1) \\ \vdots \\ w(n+M-1) \end{bmatrix} \quad (2\text{-}36)$$

For the sake of simplicity, the signal data is represented in the complex exponential form which consist of K harmonic components and therefore $s(n) = \sum_{k=1}^{K} S_k(n) = \sum_{k=1}^{K} \underline{A_k}\, e^{jn\omega k}$. The k^{th} harmonic component vector can be written as given in (2-37).

$$\mathbf{s}_k(n) = \begin{bmatrix} s_k(n) \\ s_k(n+1) \\ \vdots \\ s_k(n+M-1) \end{bmatrix} = \underline{A}_k e^{jn\omega_k} \begin{bmatrix} 1 \\ e^{j\omega_k} \\ \vdots \\ e^{j(M-1)\omega_k} \end{bmatrix} \quad (2\text{-}37)$$

By substituting (2-37) into (2-36), it follows that

$$\mathbf{v}(n) = \mathbf{E}\boldsymbol{\Phi}^{n}\underline{\mathbf{A}} + \mathbf{w}(n) \tag{2-38}$$

Where $\boldsymbol{\Phi}$ = diag$\{e^{j\omega 1}, e^{j\omega 2}, \ldots e^{j\omega k}\}$,

$\underline{\mathbf{A}} = [\underline{\mathbf{A}}_1, \underline{\mathbf{A}}_2, \ldots \underline{\mathbf{A}}_k]^{\mathrm{T}}$ and

$\mathbf{E}$ is defined as

$$\mathbf{E} = \begin{bmatrix} 1 & 1 & \cdots & 1 \\ e^{j\omega_1} & e^{j\omega_2} & \cdots & e^{j\omega_K} \\ \vdots & \vdots & \ddots & \vdots \\ e^{j(M-1)\omega_1} & e^{j(M-1)\omega_2} & \cdots & e^{j(M-1)\omega_K} \end{bmatrix} \tag{2-39}$$

In the exponential form, a time shifting of a signal sample is equivalent to a phase shifting of the data which can be represented by an associated rotation on the unit circle.

$$s(n+1) = \sum_{k=1}^{K} \underline{A}_k e^{j\omega_k(n+1)} = \sum_{k=1}^{K} s_k(n) e^{j\omega_k} \tag{2-40}$$

Let the signal *v(n)* in (2-38) is time shifted as given in (2-41)

$$\tilde{\mathbf{v}}(n) = \mathbf{v}(n+1) = [v(n+1) \quad v(n+2) \quad \cdots \quad v(n+M)]^{\mathrm{T}} \tag{2-41}$$

Since $v(n+1) = s(n+1) + w(n+1) = \tilde{s}_n + \tilde{w}_n$, the time time shifted signal can be represented as given in (2-42):

$$\tilde{\mathbf{v}}(n) = \mathbf{E}\boldsymbol{\Phi}^{n+1}\underline{\mathbf{A}} + \mathbf{w}(n+1) \tag{2-42}$$

Where $\boldsymbol{\Phi}$ is referred to as the rotation matrix.

The autocorrelation matrix of *v(n)* and its crosscorrelation matrix to the shifted version is given in (2-43):

$$\mathbf{R}_{\mathbf{v}} = E\{\mathbf{v}(n)\mathbf{v}^{\mathrm{H}}(n)\} \quad \mathbf{R}_{\mathbf{v}\tilde{\mathbf{v}}} = E\{\mathbf{v}(n)\tilde{\mathbf{v}}^{\mathrm{H}}(n)\} \tag{2-43}$$

Where H(.) and (E(.) denote the Hermitian operator and Expectation respectively. By including the clean signal *s(n)* and the noise component *w(n)*, the autocorrelation and crosscorrelation matrices can be written as

$$\begin{aligned} \mathbf{R}_{\mathbf{v}} &= \mathbf{E}\underline{\mathbf{A}}\underline{\mathbf{A}}^{\mathrm{H}}\mathbf{E}^{\mathrm{H}} + \sigma_w^2\mathbf{I} = \mathbf{R}_{\mathbf{s}} + \sigma_w^2\mathbf{I} \\ \mathbf{R}_{\mathbf{v}\tilde{\mathbf{v}}} &= \mathbf{E}\underline{\mathbf{A}}\underline{\mathbf{A}}^{\mathrm{H}}\boldsymbol{\Phi}^{\mathrm{H}}\mathbf{E}^{\mathrm{H}} + \sigma_w^2\mathbf{Q} = \mathbf{R}_{\mathbf{s}\tilde{\mathbf{s}}} + \sigma_w^2\mathbf{Q} \end{aligned} \tag{2-44}$$

Where

$$\mathbf{Q} = \begin{bmatrix} 0 & 0 & \cdots & 0 & 0 \\ 1 & 0 & \cdots & 0 & 0 \\ 0 & 1 & \cdots & 0 & 0 \\ \vdots & \vdots & \ddots & \vdots & \vdots \\ 0 & 0 & \cdots & 1 & 0 \end{bmatrix} \tag{2-45}$$

For the signal subspace, the generalized eigenvalue problem can be written as

$$\mathbf{R}_{\mathbf{s}}\mathbf{u}_i = \lambda_i \mathbf{R}_{\mathbf{s}\tilde{\mathbf{s}}}\mathbf{u}_i \qquad i = 1, \ldots, K \tag{2-46}$$

Where $\boldsymbol{u}_i$ is the eigenvector of $\boldsymbol{R}_s - \lambda_i \boldsymbol{R}_{\tilde{s}s}$. By substituting the expression in (2-44) into (2-46) the following relation is obtained :

$$\mathbf{E}\underline{\mathbf{A}}\mathbf{A}^{\mathrm{H}}\mathbf{E}^{\mathrm{H}}\mathbf{u}_i = \lambda_i \mathbf{E}\underline{\mathbf{A}}\mathbf{A}^{\mathrm{H}}\boldsymbol{\Phi}^{\mathrm{H}}\mathbf{E}^{\mathrm{H}}\mathbf{u}_i \qquad i = 1, 2, \ldots, K \tag{2-47}$$

The expression in (2-47) can also be written as

$$\mathbf{E}\underline{\mathbf{A}}\mathbf{A}^{\mathrm{H}}(\mathbf{I} - \lambda_i \boldsymbol{\Phi}^{\mathrm{H}})\mathbf{E}^{\mathrm{H}}\mathbf{u}_i = 0 \qquad i = 1, 2, \ldots, K \tag{2-48}$$

The decomposition process is performed by estimating the frequencies of sinusoid f_i from

$$\lambda_i = e^{j\omega_i} \qquad i = 1, 2, \ldots, K$$

where $\omega_i = 2\pi f_i$

Once ω_i are obtained, the amplitudes and powers of the harmonics can be estimated in the same way as used in MUSIC (Section 2.5.6).

Similar to other parametric methods such as Prony analysis and MUSIC algorithm, the total number of components of the signal to be decomposed by the ESPRIT algorithm needs to be determined prior to the analysis. Otherwise, inaccurate result will be obtained from the decomposition process.

2.5.8. Hilbert Huang Transform (HHT)

A recent adaptive method to decompose signals is the Hilbert Huang method (HHT), which is well suited for analysing stationary and non-stationary signals and thus is well suited method for PQ waveform decomposition. The Hilbert Huang Transform consists of two distinct processes. First, the Empirical Mode Decomposition (EMD) process is applied to decompose the signal being analysed to obtain the signal components represented in the Intrinsic Mode Functions (IMFs).

Second, the Hilbert Transform is performed to each IMF to obtain the instantaneous frequencies, amplitudes and phases [5].

The main advantage of the HHT technique over other PQ decomposition methods is the high time resolution. The intuitive visual information of the frequency, amplitude and phase of the signal components is also a valuable result of analysis using HHT method [38]. This method will be discussed in details in the next chapter.

2.6. Chapter summary

This chapter has defined the PQ problems, and discussed the classification of a variety of PQ disturbances and their effects to the equipment. To help identify PQ problems, PQ meters are required. The analysis of the data collected by the instruments is needed to decompose the signal for the PQ disturbance identification. Several methods to decompose non-stationary PQ waveforms have been described. In summary, the FFT is limited to stationary signals, STFT can be used for non-stationary signal analysis but it has a fixed resolution which depends on the chosen window size. The wavelet transform has better resolution than STFT, however it is not adaptive. The parametric methods such as Prony, MUSIC and ESPRIT algorithm require to know or assume the number of sinusoids in the signal being analyzed prior to the decomposition process, and hence these methods cannot be used to decompose unknown signals. The HHT technique is well suited for analysing stationary and non-stationary signals and requires no initial assumption of the signal and therefore it is adaptive to any unknown signals. The method is most suitable for decomposing non-stationary signals often found in PQ waveforms measured by associated meters. For this reason, this method has been chosen for use in this research and will be discussed in details in the next chapter.

CHAPTER 3 THE HILBERT HUANG TRANSFORM (HHT)

3.1 Introduction

This chapter describes the use of HHT in this research to decompose stationary and non-stationary signals in considerably high time resolution. A brief description of why the method is needed and the operation of the method are presented. The advantages and disadvantages of HHT when applied to decompose non-stationary, noisy and close frequencies PQ signals are discussed.

3.2 Why HHT?

Data analysis is an important part to extract the information from PQ signals measured by the associated meters. While the data might not be perfect, they represent the reality at hand. The main purposes of data analysis are to determine the parameters required to build a model and to confirm that a phenomenon is precisely represented by a built model [2].

Despite this, physical measurement data or numerical modelling data has a high probability of having the following issues, either the total range of data is not long enough, it is non-stationary, or represents nonlinear processes. Each problem can represent itself independent of other problems or in conjunction, but it is important to note that the first two listed above can be related to each other, as data that appears to be non-stationary can be a result of data that is shorter than the longest time scale of a stationary process. In regards to these problems, there is little we can do in terms of analysis [2].

Historically, the Fourier spectral type of data analysis gave us with a standard data analysis method to examine global energy-frequency distributions. The usage of the terminology 'spectrum' has come to be associated with the Fourier transformation method. Fourier analysis has been the primary method for data analysis since the first time it was introduced, and continues to be widely used for the analysis due to its intrinsic ability and simplicity.

Although it has been demonstrated by some researchers that Fourier transformation is valid in a range of general conditions, (for example, see Titchmarsh [39]), there are some key restrictions of this method. Firstly the system must be linear, and the data be precisely periodic or stationary. If this is not the case,

erroneous result can be obtained [2]. However, most of PQ signals are non-stationary, with data sets usually of finite duration and from often systems which are by design non-linear. Therefore, there is a limitation of applying Fourier Transform for PQ signal analysis. For example, according to International Electrotechnical Commission (IEC) standard, signals whose amplitudes vary with time cannot be described correctly by their harmonic components (obtained from the FFT spectrum) only. Therefore, a grouping method is suggested to resolve the issue of describing such signal [18].

HHT has been devised as a data analysis method with its basis on the Empirical Mode Decomposition (EMD) method, which extracts the components of the signal represented as a set of Intrinsic Mode Functions (IMFs) without the need of any assumption prior to the analysis. Basically, the decomposition identifies directly the instantaneous energy associated with various time scales to extract the IMFs which have well-behaved Hilbert transforms. The instantaneous frequency can then be calculated from the IMFs using the Hilbert Transform to localize any event by time and by frequency [2].

3.3 The Basic of HHT

As described in Section 3.2, the Hilbert Huang Transform consists of two distinct processes. First, the Empirical Mode Decomposition (EMD) process is applied to decompose the signal being analysed to obtain the signal components represented in the Intrinsic Mode Functions (IMFs). Once the IMFs are obtained, the Hilbert Transform process is then applied to each IMF to obtain the instantaneous frequencies amplitudes and phases [5]. In this research, the MATLAB code available online is used to perform the analysis using the standard HHT method [40].

3.3.1 Empirical Mode Decomposition (EMD)

EMD is designed to analyse oscillatory signals, but is not limited to describing these signals in terms of a sum of sinusoids as the Fourier method does. Changes in frequency or amplitude within an oscillatory period can be detected when EMD is paired with Hilbert Transform in a process called the Hilbert-Huang Transform (HHT). EMD is also not limited to stationary signals in that it adapts to changes in the signal. A number of studies have used EMD on physical problems including climate data, ocean waves, testing for structural damage, and image analysis. It is

reported that the EMD has extracted physically meaningful components in many of these applications [41].

Each IMF resulting from EMD process has to satisfy the following conditions [5].

(a) There is exactly one zero between any two consecutive local extremas.

(b) The “local mean” has to be zero

A signal that satisfies the IMF conditions allows for instantaneous frequency and amplitude to be clearly defined [6].

The IMFs are extracted through a sifting process in the EMD algorithm. Sifting is used to subtract away large-scale features of the signal consecutively until only fine-scale features are left. Once the sifting process is done, a signal *S(t)* is separated into the fine-scale oscillation *d(t)* which will become the first IMF and the residual *r(t)* which may replace the original signal to go through the next sifting process [6]. The process will be repeated in iterative fashion as long as the residue / signal to be processed have at least 3 extremas. When the residue / signal has less than 3 extremas indicating that the scale has become very large, the EMD process is then terminated. The last waveform remaining from the process is not an IMF but the trend of the original signal.

In the sifting process, it is necessary to have a local mean of the signal, which can be obtained by identifying the local maxima and minima of the signal. The maximum and minimum envelopes are then created using natural cubic splines connecting the respective local extrema. The mean of the two envelopes is used for the approximation of the local mean. [6]

A flowchart describing the algorithm of the EMD process is shown in Figure 3.3.1.1.

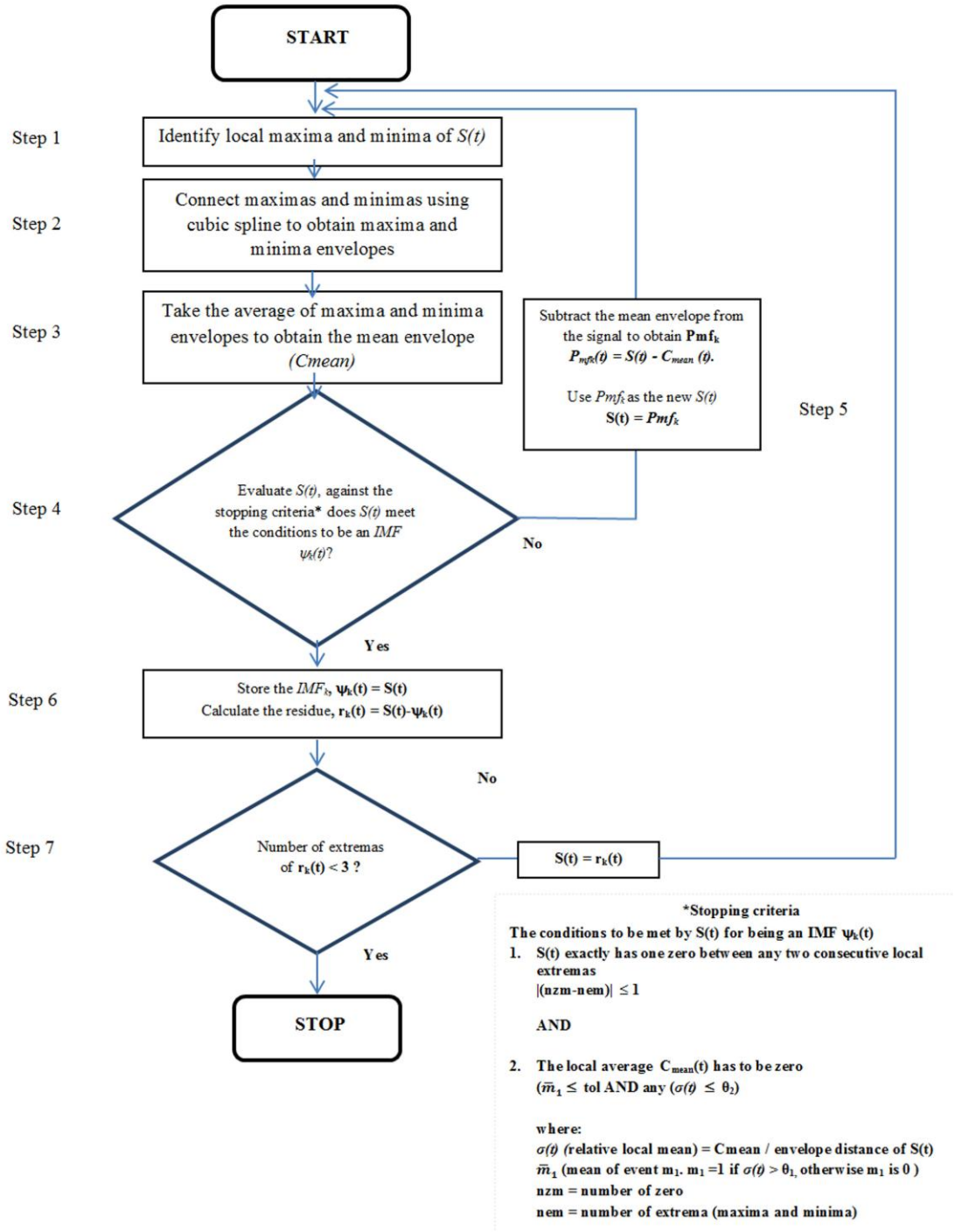

Figure 3.3.1.1 The Flowchart of EMD process

To demonstrate how the sifting process works to extract the IMF and how the stopping criteria is used to control the sifting process, consider a signal *S(t)* given in (3-1)

$$S(t) = \cos(2\pi\, 50t - 10^0) + 0.33\cos(2\pi\, 150t - 60^0) \quad (3\text{-}1)$$

The signal S(t) and its components are shown in Figure 3.3.1.2:

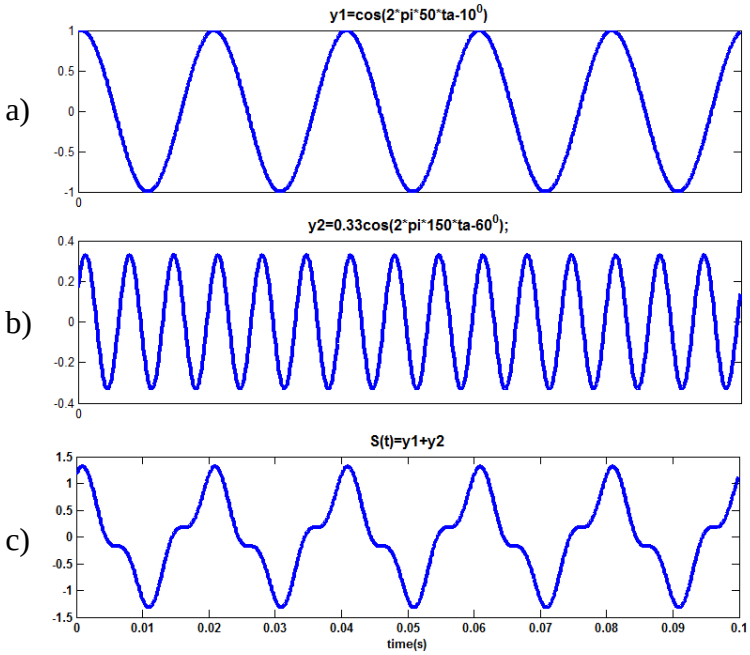

Figure 3.3.1.2: The components of signal S(t), (a) 50Hz component (b) 150 Hz component (c) The signal S(t)

The EMD process is then performed according to the flowchart shown in Figure 3.3.1.1 as follows :

Step 1: Identify the local maxima and minima of the signal S(t). Figure 3.3.1.3 shows the signal with identified maxima and minima at iteration 0.

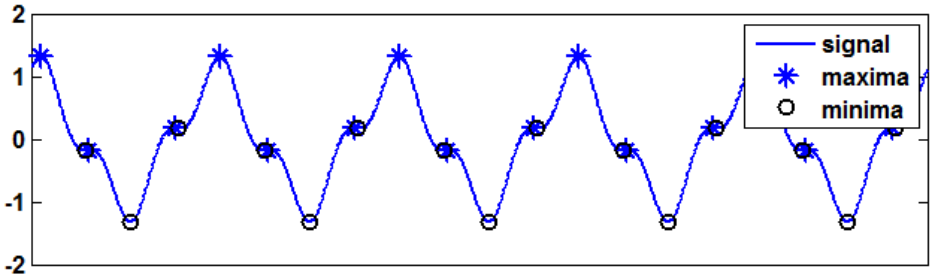

Figure 3.3.1.3 The signal with identified maxima and minima

Step 2. By using cubic spline interpolation, connect all of the maxima to obtain the maximum envelope $C_{max}(t)$ and connect all of the minima to obtain the minimum envelope $C_{min}(t)$. The signal with identified maximum and minimum envelopes is shown in Figure 3.3.1.4.

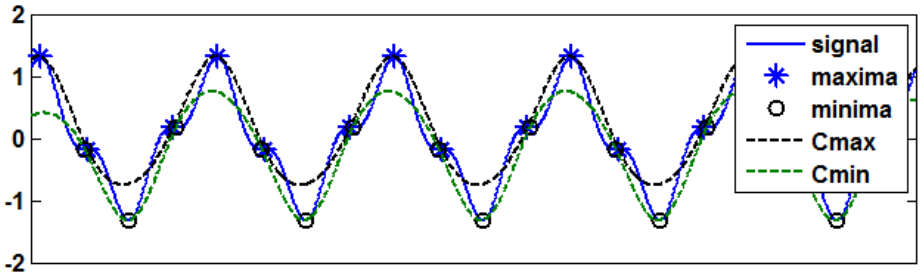

Figure 3.3.1.4. The signal with maximum and minimum envelopes

Step 3. Calculate the mean of the two envelopes as given by (3-2). The mean envelope is shown in Figure 3.3.1.5.

$$C_{mean}(t) = (C_{max}(t) + C_{min}(t))/2 \quad (3\text{-}2)$$

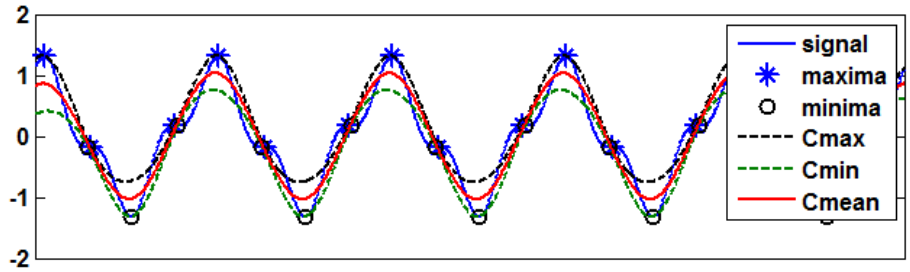

Figure 3.3.1.5 The signal with identified mean envelope

Step 4. Test whether *S(t)* qualifies against the requirements to be an IMF by checking its waveform. The first condition to be an IMF is that there is exactly one zero between any two consecutive local extrema or when the difference between the number of zero and the extrema is less or equal to 1. The waveform of *S(t)* in Figure 3.3.1.5 indicates that a zero always exists between each two consecutive local extrema which satisfies the first condition to be an IMF.

The $C_{mean}(t)$ waveform of *S(t)* shown in Figure 3.3.1.5 is then evaluated against the stopping criteria shown at the bottom part of the flowchart in Figure 3.3.1.1. $C_{mean}(t)$ waveform shown in Figure 3.3.1.5 indicates that its amplitude is still large at this stage (iteration 0). $C_{mean}(t)$ is then evaluated to identify how close it is to zero (which is the second condition to be an IMF). The evaluation is performed by using 3 thresholds (θ_1, θ_2 and tol) as proposed by Rilling [5]. Threshold θ_1 is designed to guarantee globally small fluctuations of $C_{mean}(t)$ while threshold θ_2 is used to take into account locally large excursions of

$C_{mean}(t)$ [4]. In this example, the default stopping criteria (θ_1 = 0.05, θ_2=0.5 and *tol* = 0.05) is used [5].

Some variables related to the thresholds which are referred to as envelope distance $a(t)$ and normalized local mean $\sigma(t)$ need to be calculated first as given by (3-3) and (3-4) :

The envelope distance of $S(t)$ denoted by $a(t)$ is given by

$$a(t) = (C_{max}(t) - C_{min}(t))/2 \tag{3-3}$$

Figure 3.3.1.6 shows the waveform of $a(t)$ superimposed on Figure 3.3.1.5.

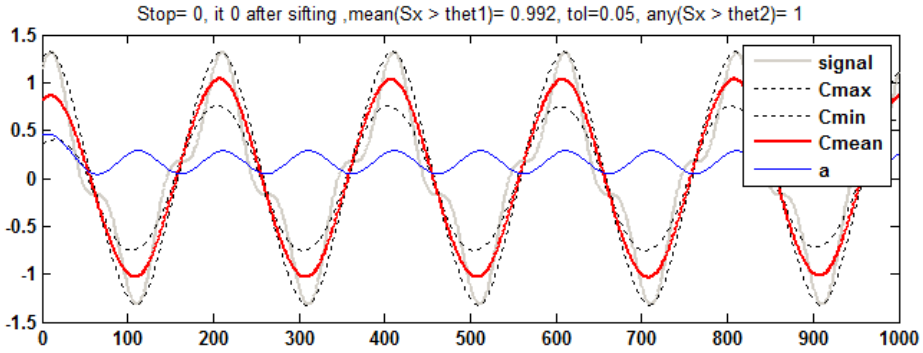

Figure 3.3.1.6 The waveform of $a(t)$ superimposed on Figure 3.3.1.5

A relative local mean $\sigma(t)$ is given by:

$$\sigma(t) = |C_{mean}(t)|/a(t) \tag{3-4}$$

Figure 3.3.1.7 shows the waveform of $\sigma(t)$ superimposed on Figure 3.3.1.6.

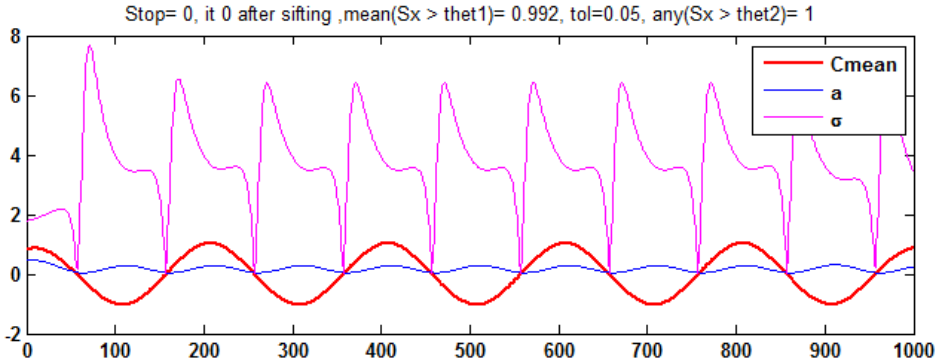

Figure 3.3.1.7 The waveform of $\sigma(t)$ superimposed on Figure 3.3.1.6

Figure 3.3.1.7 shows $C_{mean}(t)$, $a(t)$ and $\sigma(t)$ which will be used to evaluate the local mean. To guarantee a globally small fluctuation, $\sigma(t)$ is compared to θ_1 (specified as 0.05), whenever $\sigma(t) > \theta_1$, a variable denoted by m_1 is set to 1, otherwise m_1 is 0. A mean value of of m_1 denoted by $\overline{m}_1$

is then compared to a tolerance 'tol' (specified as 0.05), and if $\overline{m}_1$ exceeds tol, this indicates that the resulting $C_{mean}(t)$ does not meet the requirement of globally minimum small fluctuation. Only when $\overline{m}_1$ is below 'tol' then a globally small fluctuation is guaranteed. The criterion that takes into account locally large excursions is obtained by considering if there is any event where the value of $\sigma(t)$ is greater than a threshold θ_2 (specified as 0.5).

The sifting process is terminated once the difference between the number of zero and the extrema is less or equal to 1 AND when $\overline{m}_1$ is less than *tol* AND there is no point of $\sigma(t)$ greater than θ_2. The complete stopping criteria is shown in the relation given by (3-5).

Stop = $|(nzm\text{-}nem)| \leq 1$ AND ($\overline{m}_1 \leq tol$ AND any ($\sigma(t) \leq \theta_2$)) (3-5)

Figure 3.3.1.8 shows m_1 superimposed on Figure 3.3.1.7.

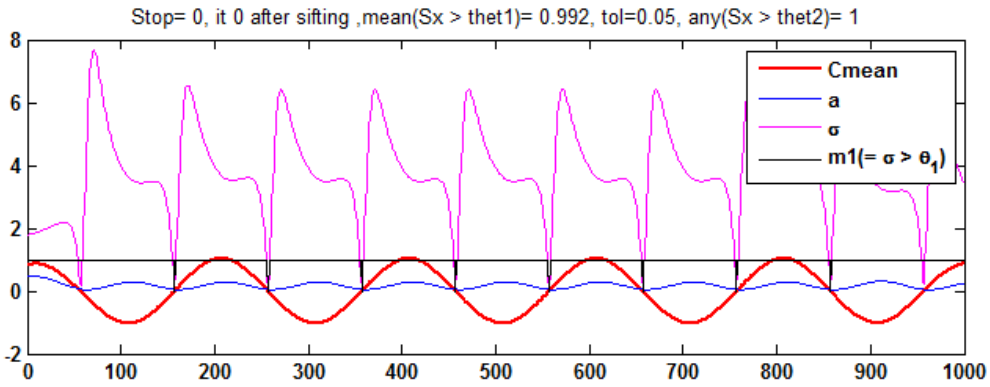

Figure 3.3.1.8 The waveform of m_1 superimposed on Figure 3.3.1.7.

Figure 3.3.1.8 shows $\overline{m}_1$ equals 0.992 which means that the globally minimum small fluctuation is not met, and therefore the next iterations are required. From Figure 3.3.1.8, it is obvious that most of the value of $\sigma(t)$ are greater than 0.5 and therefore the locally large excursions are identified which means that $S(t)$ does not satisfy the second condition to be an IMF.

Step 5. The original signal $S(t)$ is then subtracted by $C_{mean}(t)$ to obtain P_{mfk} which is then considered as the new $S(t)$ to be processed further through step 1 to step 4. Figure 3.3.1.9 shows the obtained P_{mfk} or the new $S(t)$ with the identified local mean.

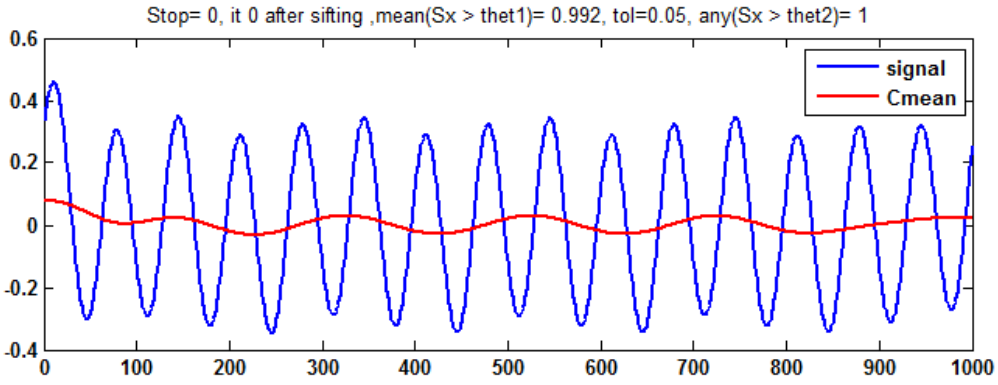

Figure 3.3.1.9 The new *S(t)* with the local mean

Figure 3.3.1.9 shows the new *S(t)* and the resulting $C_{mean}(t)$. As previously, *S(t)* has to be checked whether it is an IMF or not. Since a zero exists between each two consecutive local extremas, the first condition to be an IMF is satisfied by *S(t)*.

To check whether *S(t)* meets the the second condition to be an IMF, the closeness of $C_{mean}(t)$ to zero is then evaluated. First, *a(t)* and *σ(t)* are calculated and the default value of the thresholds are used to do the evaluation, as shown in Figure 3.3.1.10.

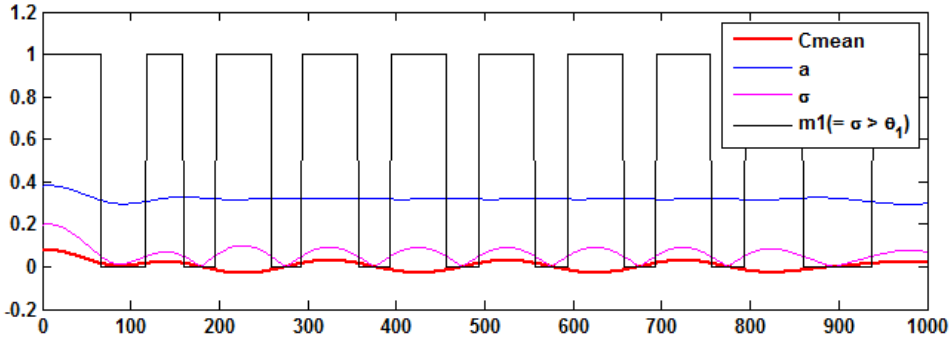

Figure 3.3.1.10 The evaluation of $C_{mean}(t)$

Figure 3.3.1.10 shows that *σ(t)* is now smaller than threshold θ_2 (0.5) which means that there is no more locally large excursion exist in $C_{mean}(t)$. The mean value of m_1 is now smaller and equal to 0.613. However, it is still greater than *tol* (0.05) and therefore a globally small fluctuation is not met. Since *S(t)* does not satisfy the second condition to be an IMF, more iterations are needed to obtain the IMF.

S(t) is again subtracted by $C_{mean}(t)$ to obtain P_{mfk} which is then considered as the new *S(t)* to be processed further through step 1 to step 4.

Figure 3.3.1.11 shows the obtained P_{mfk} or the new $S(t)$ with the identified local mean.

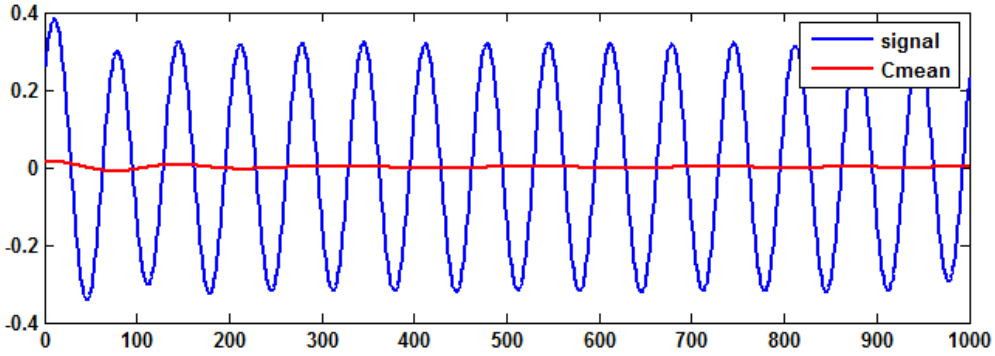

Figure 3.3.1.11 The new S(t) with the local mean

Figure 3.3.1.11 shows the new $S(t)$ with a less fluctuating $C_{mean}(t)$. As previously, $S(t)$ has to be checked whether it is an IMF or not. Since a zero exists between each two consecutive local extremas, the first condition to be an IMF is satisfied by $S(t)$.

To check whether $S(t)$ meets the second condition to be an IMF, the closeness of $C_{mean}(t)$ to zero is evaluated. First, $a(t)$ and $\sigma(t)$ are calculated and the default value of the thresholds are used to do the evaluation, as shown in Figure 3.3.1.12.

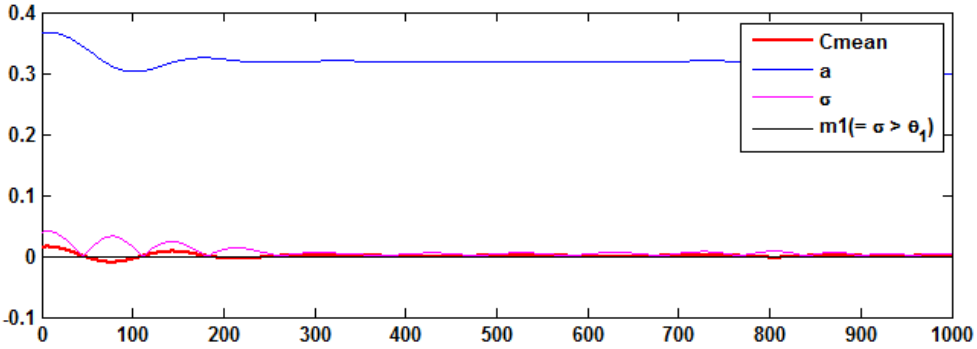

Figure 3.3.1.12 The evaluation of $C_{mean}(t)$

Figure 3.3.1.12 shows that $\sigma(t)$ is smaller than threshold $\theta_2(0.5)$ which means that there is no more locally large excursion exist in $C_{mean}(t)$. The value of $\bar{m}_1$ is now below 0.05 which means that a globally small fluctuation is met. At this stage, the second condition to be an IMF is satisfied by $S(t)$, therefore, no more iteration is required.

Step 6 Store $S(t)$ as an IMF and calculate the residue by subtracting the IMF from the original signal. Figure 3.3.1.13 shows the residue.

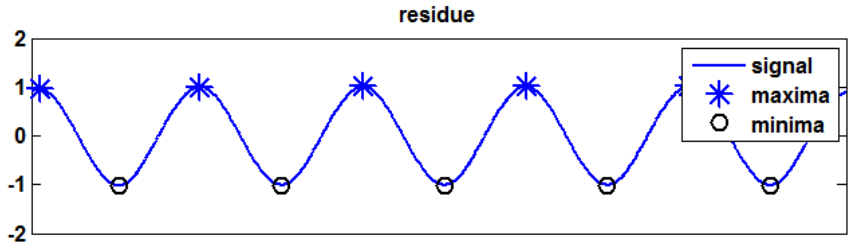

Figure 3.3.1.13. The first residue of the signal S(t)

Step 7: Test whether the number of local maxima or minima is less than three, if so terminate the EMD process, otherwise repeat steps 1 - 7 on the residue $r_k(t)$.

Since the number of local maxima and minima of the residue is more than three, as shown in Figure 3.3.1.13, the residue will then be considered as the new signal *S(t)* to be processed through step 1 to step 4. Figure 3.3.1.14 shows the new *S(t)* with the identified local $C_{mean}(t)$.

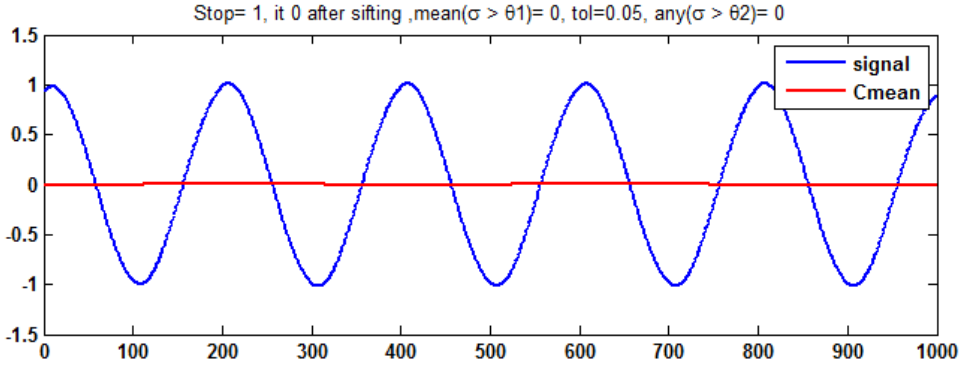

Figure 3.3.1.14. The new S(t) with the local mean

Figure 3.3.1.14 shows the new *S(t)* and the resulting $C_{mean}(t)$ waveform which indicates that its amplitude is very close to zero at this stage (iteration 0). The stopping criteria is then used to check the waveform against the second condition to be an IMF as shown in Figure 3.3.1.15.

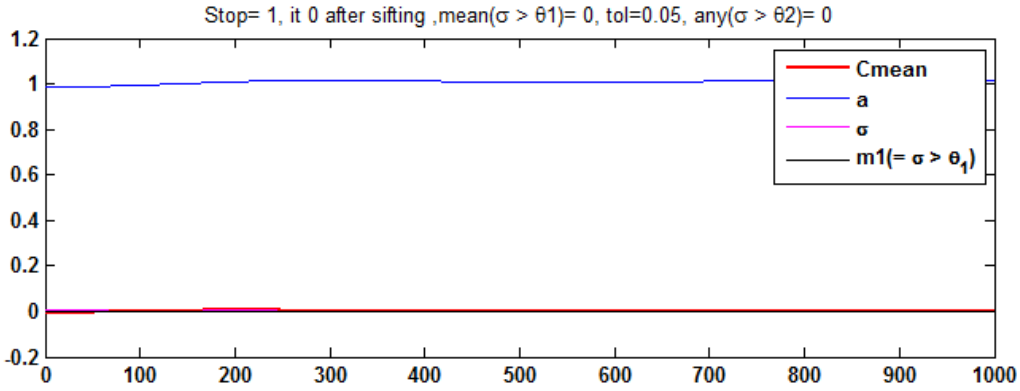

Figure 3.3.1.15 The evaluation of $C_{mean}(t)$

Figure 3.3.1.15 shows that $\sigma(t)$ is completely smaller than threshold $\theta_2(0.5)$ which means that there is no locally large excursion exist in $C_{mean}(t)$. Further, $C_{mean}(t)$ is now below θ_1 (0.05) all the time indicated by continuous zero value of m_1. Hence, $\overline{m}_1$ is now 0 which means that a globally small fluctuation is met. To this stage, the second condition to be an IMF is satisfied by $S(t)$, therefore, no more iteration is needed. $S(t)$ is considered as the next IMF, which is then stored as IMF_2.

The second residue $r_k(t)$ $(k=2)$ is then calculated by subtracting the IMF_2 from S(t). Figure 3.3.1.16 shows the second residue of the process.

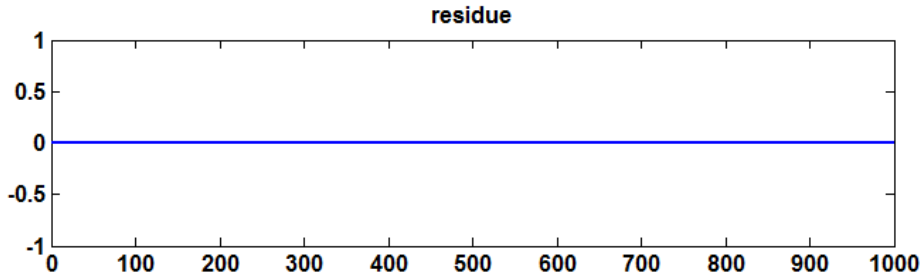

Figure 3.3.1.16. The second residue of the process

Figure 3.3.1.16 shows that the second residue does not have sufficient extrema number according to step 7 to continue the EMD process. Therefore, the process is terminated. The final result of the decomposition is shown in Figure 3.3.1.17.

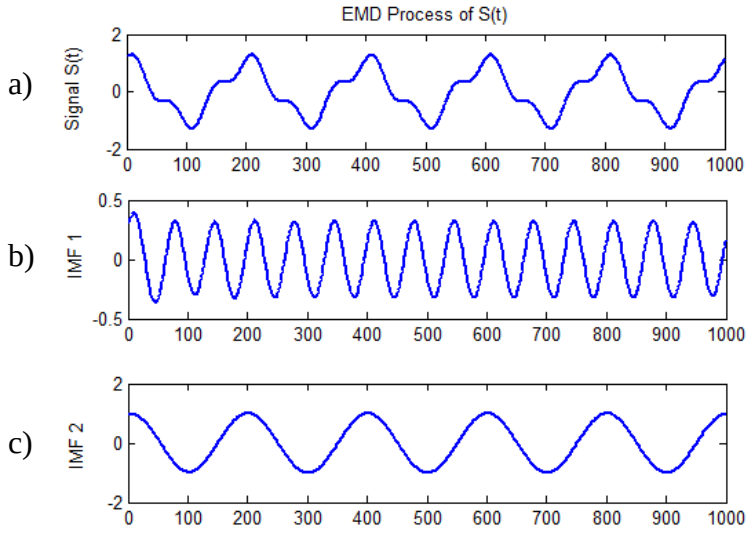

Figure 3.3.1.17: The Final result of Empirical Mode Decomposition process on S(t), (a) The signal S(t), (b) IMF_1 (150Hz), (c) IMF_2 (50Hz)

Figure 3.3.1.17 demonstrates how the EMD process has succesfully decomposed the original signal S(t) into its components represented in the IMFs. The IMFs in Figure 3.3.1.17 (b)-(c) show very similar waveforms to the original components shown in Figure 3.3.1.2(a)-(b). However, there are small differences at both ends of the IMFs which is attributed to the end effect problem of the IMFs. End effect phenomenon is caused by the limitation of cubic spline interpolation to estimate the maxima and minima envelopes due to insufficient number of extrema points to be interpolated at both ends of the waveform being analyzed.

3.3.2 Hilbert Transform (HT)

The Hilbert Transform (HT) [6], [42] of x(t) is defined as:

$$H[x(t)] = \frac{1}{\pi} P \int_{-\infty}^{\infty} \frac{x(\tau)}{t-\tau} d\tau \tag{3-6}$$

where: P is the Cauchy Principal Value integral

The Hilbert Transform of a real signal x_r is an analytic signal $x = x_r + i*x_i$ where x_r is the original data and the imaginary part $i*x_i$ is a version of x_r shifted by 90^0. The Hilbert transformed signal x has the same amplitude and frequency as the original data x_r with the phase angle depends on the phase angle of x_r. [43].

The analytic signal obtained from The Hilbert transform can be used to determine the instantaneous amplitude, frequency and phase of the original data. For

a pure sinusoid, the instantaneous amplitude, frequency and phase are constant. However, for the IMF which usually has the end effect issue, the instantaneous parameters are fluctuating as will be demonstrated in the following paragraphs.

The analytic signal $z(t)$ of a signal $x(t)$ is defined as:

$$z(t) = x(t) + H[x(t)] = x + jy = a(t)\, e^{j\theta(t)} \tag{3-7}$$

For a pure cosine signal $x(t) = A\cos(\omega t+\theta)$, the analytic signal contains its sine version :

$$z(t) = A\cos(\omega t+\theta) + j\, A\sin(\omega t+\theta) = A\, e^{j(\omega t+\theta)} \tag{3-8}$$

For example, a pure cosine signal is given by (3-9) :

$$S(t) = \cos(\omega t - 10^0) \tag{3-9}$$

where f =50 Hz and $\omega = 2\pi f$.

The Hilbert Transform of S(t) is shown in Figure 3.3.2.1. The instantaneous amplitude of S(t) can be calculated as follows [6], [42] :

$$a(t) = \sqrt{x^2 + y^2} \tag{3-10}$$

By applying (3-10) to S(t), the instantaneous amplitude is obtained and shown in Figure 3.3.2.2, which is a constant value of 1.0.

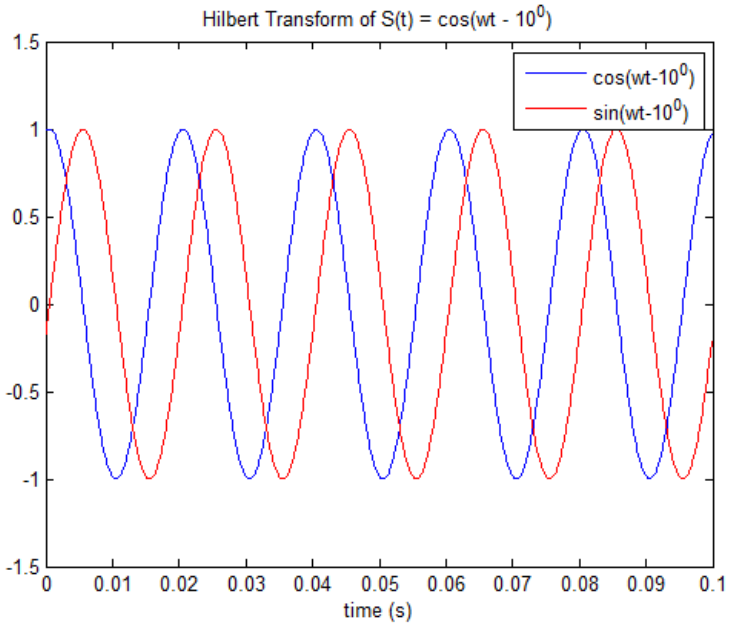

Figure 3.3.2.1 The Hilbert Transform of S(t).

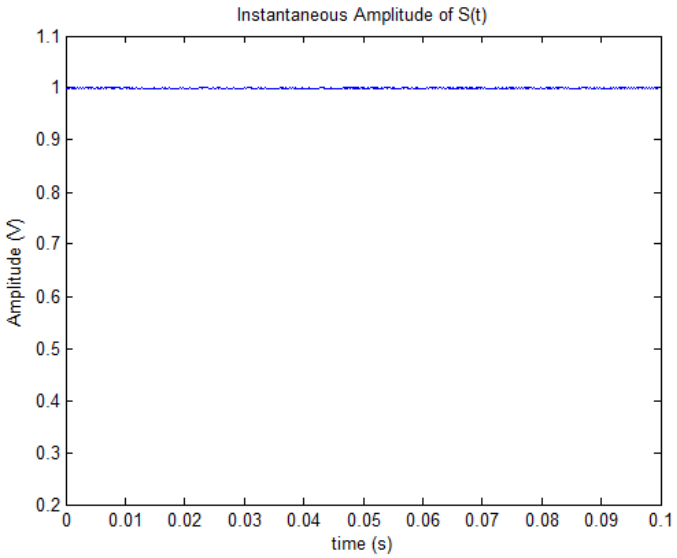

Figure 3.3.2.2 The instantaneous amplitude of *S(t)*.

The Hilbert Transform is then applied to IMF_2 of the signal *S(t)* shown in Figure 3.3.1.17(c) obtained from the of EMD process to calculate the analytic signal *z(t)* of the IMF shown in Figure 3.3.2.3.

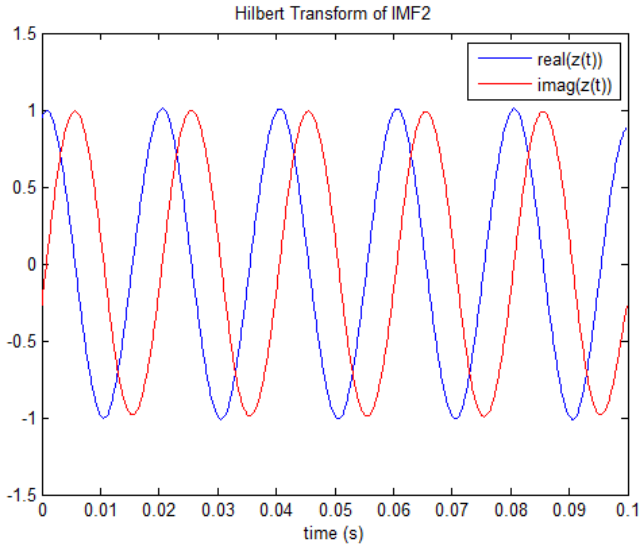

Figure 3.3.2.3 The analytic signal *z(t)* of IMF_2 obtained by the Hilbert Transform .

By using the relation in (3-10), the instantaneous amplitude of IMF_2 can be determined as shown in Figure 3.3.2.4. The calculated instantaneous amplitude in Figure 3.3.2.4 shows that the end effect due to the sifting process can affect the Hilbert transform of the IMF, and therefore the instantaneous amplitude is not constant all the time. To find the actual amplitude, the impact of the end effect should be avoided by taking the mean of the instantaneous amplitude from 10% -

90% of the data which result in the estimated amplitude 1.01p.u. The mean value of the instantaneous amplitude is shown by the red line in Figure 3.3.2.4.

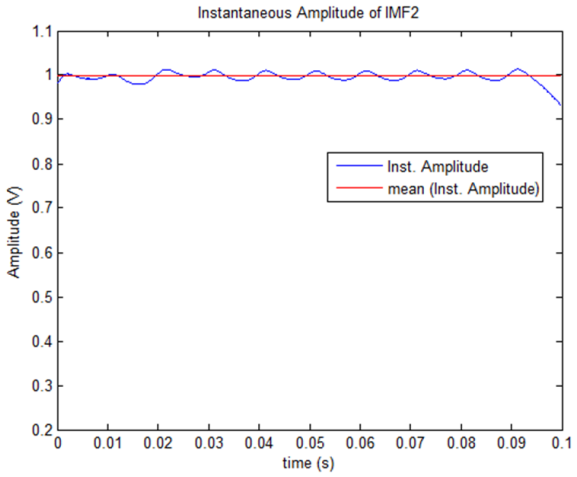

Figure 3.3.2.4: The instantaneous amplitude of IMF_2.

The instantaneous phase angle $\theta(t)$ can be calculated from the instantaneous x and y values of the signal as given in (3-11)

$$\theta(t) = \arctan\left(\frac{y}{x}\right) \tag{3-11}$$

Applying Equation (3-11) to the pure sinusoid signal S(t) will result in a saw tooth instantaneous phase signal shown in Figure 3.3.2.5, since $\theta(t) = (\omega t - 10^0)$:

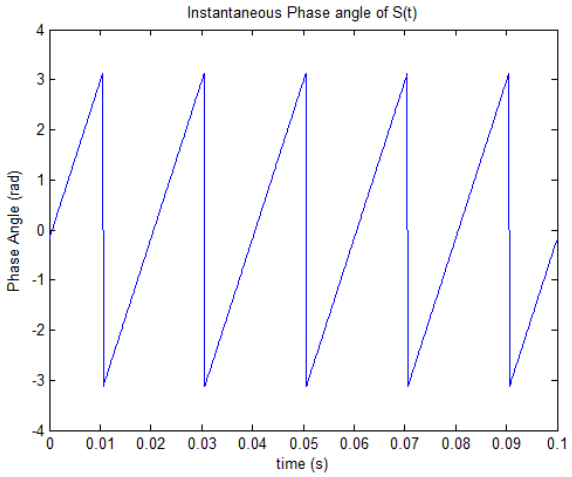

Figure 3.3.2.5 The instantaneous phase angle of S(t).

To obtain the actual instantaneous phase values, the result in Figure 3.3.2.5 needs to be subtracted by ωt (this can be done since the frequency f is known and equals to 50 Hz), as shown in Figure 3.3.2.6, showing that the instantaneous phase is constant and equals to -10^0 as expected.

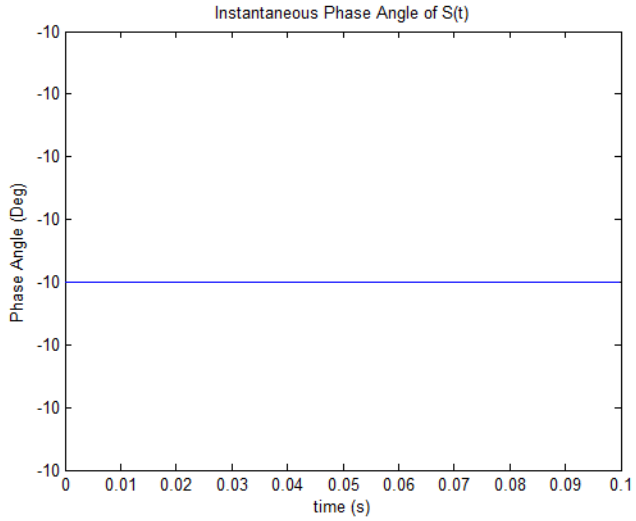

Figure 3.3.2.6 The instantaneous phase angle of *S(t)* after the subtraction.

However, for most general cases, the frequency ω is not known and hence it needs to be estimated by using the relation given in (3-12).

$$\omega(t) = \frac{d\theta}{dt} \tag{3-12}$$

and

$$f(t) = \omega(t)/(2\pi)$$

Once the estimated ω is obtained, it can be subtracted from the instantaneous phase angle $\theta(t)$ to obtain the initial phase angle.

The formula given in (3-12) provides the instantaneous frequency of S(t) which is constant at 50 Hz, as expected. The instantaneous frequency is shown in Figure 3.3.2.7.

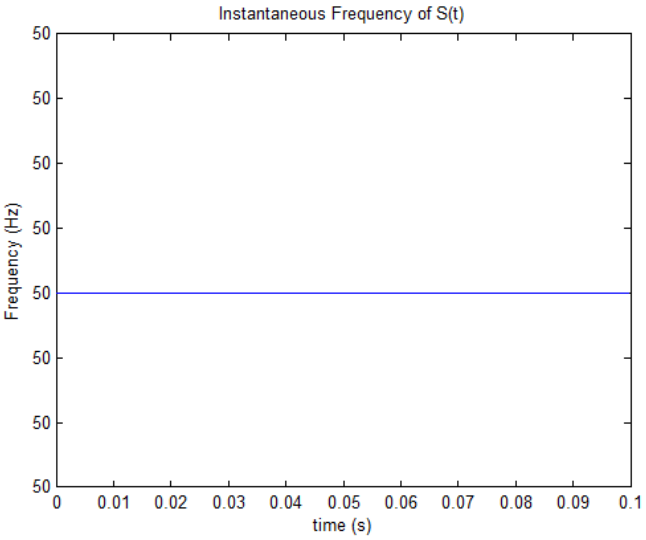

Figure 3.3.2.7 The instantaneous Frequency of S(t).

Now the instantaneous frequency of IMF_2 can be calculated using the relation given in (3-12), and the estimated instantaneous frequency is shown in Figure 3.3.2.8. As previously, the end effect due to the EMD sifting process also appears in the Hilbert Transform result.

To improve the result of instantaneous frequency estimation, a Matlab function instfreq.m available online [40] is used. For an analytic signal x at time instant(s) t, instfreq.m performs the instantaneous frequency estimation of x by using trapezoidal integration rule. The estimated instantaneous frequency using instfreq.m is also shown in Figure 3.3.2.8 which demonstrates an improvement at both ends of the instantaneous frequency waveform.

To find the actual frequency, the impact of the end effect should be avoided by taking the mean of the instantaneous frequency from 10% - 90% of the data which result in the estimated actual frequency 50.04 Hz.

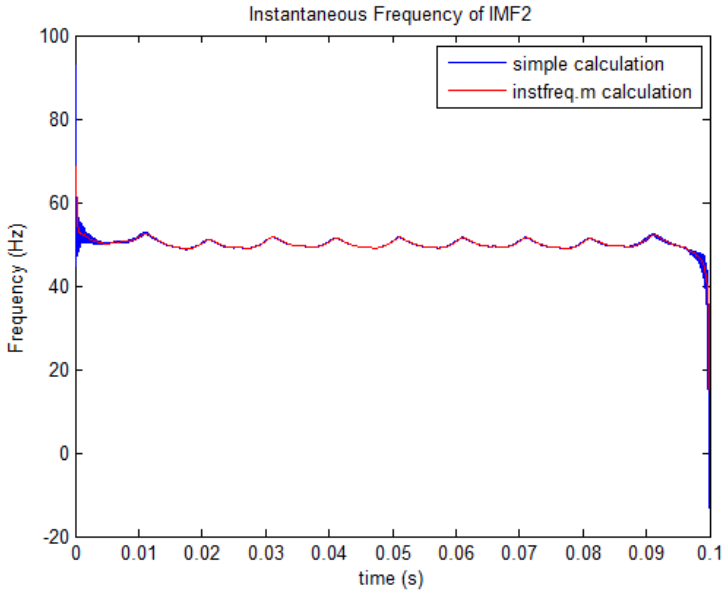

Figure 3.3.2.8: The instantaneous Frequency of IMF_2.

The initial phase angle can now be calculated for IMF_2 by calculating the Instantaneous phase using Equation (3-11) and subtract it by ω as previously and the result is shown in Figure 3.3.2.9. The mean of the result from 10% - 90% of data is also used to determine the phase angle of the signal, which is equal to -10^0.

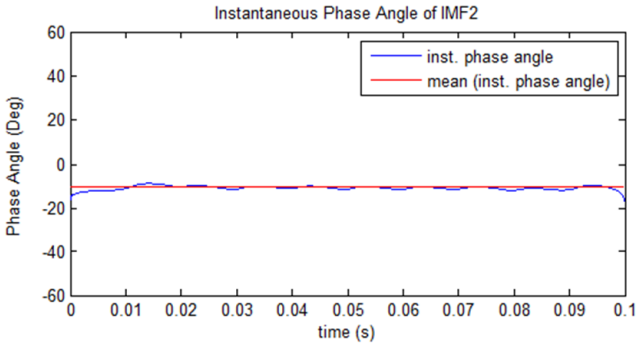

Figure 3.3.2.9: The instantaneous phase angle of IMF_2.

Figures 3.3.2.4, 3.3.2.8 and 3.3.2.9 show that the end effect issue causes inaccuracy in the calculated instantaneous amplitude, frequency and phase since the IMF is not a pure sinusoid with a constant amplitude. To avoid this end effect issue, the mean of the instantaneous values from 10% - 90% of the data is used to calculate the estimated value of the amplitude, frequency and phase. Such technique to avoid the end effect issue is used in the whole thesis to obtain the more accurate value of amplitude, frequency and phase to correct the original result from applying Hilbert Transform to each IMF.

Applying the Hilbert transform directly to a multi-component signal provides values of *a(t)* and *f(t)* which are unusable for describing the signal. For example if the Hilbert Transform is applied directly to the signal given in (3-1) then the result is shown in Figure 3.3.2.10.

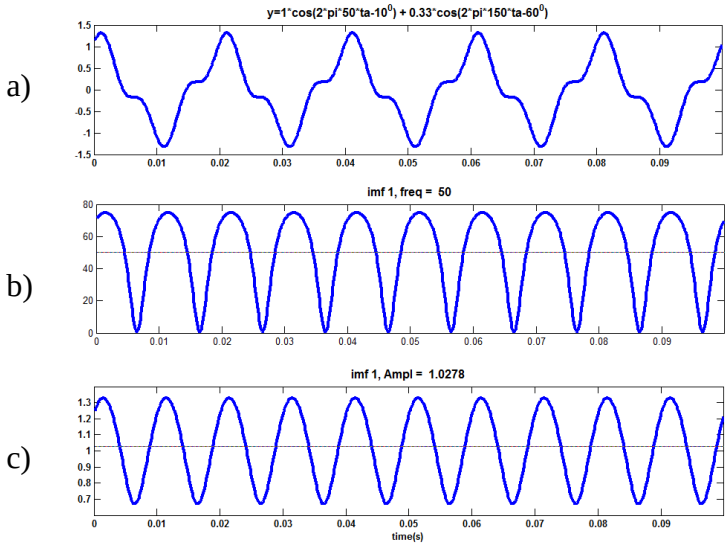

Figure 3.3.2.10. The Hilbert Transform applied on a multicomponent signal. (a) The multi-component signal (b) Instantaneous frequency (c) Instantaneous Amplitude

Figure 3.3.2.10 shows that applying HT on a multi-component signal produces fluctuating instantaneous frequency and instantaneous amplitude which is caused by the mixed frequency (multi-components) contained in the signal.

For this reason, the Empirical Mode Decomposition is needed to first decompose the signal into IMFs each of which contains single component of the signal, which can then be processed by the Hilbert Transform to obtain meaningful instantaneous attributes of the IMFs.

3.4 Applying HHT to Stationary Signals

To demonstrate the effectiveness of HHT to decompose stationary signals, several PQ signals such as harmonics and flicker are analysed.

3.4.1 PQ waveform with harmonics

Consider a signal that contains 3rd and 11th harmonic

$$S(t) = \sin(2\pi\, 50t + 30^0) + 0.33 \sin(2\pi\, 150t + 30^0) + 0.09 \sin(2\pi\, 550t + 30^0) \quad (3\text{-}13)$$

The results from applying the EMD process to the signal given by (3-13) are shown in Figure 3.23. Figure 3.23 shows that the EMD process has decomposed the signal correctly to three IMFs, each of which represents the component of the signal.

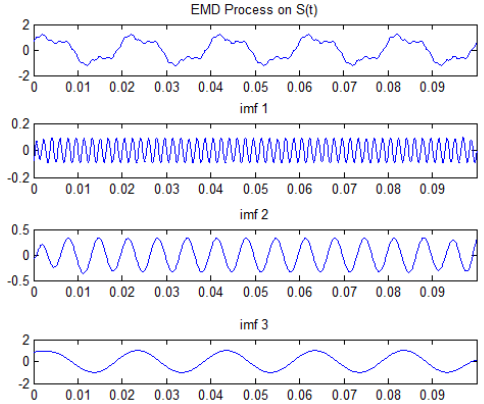

Figure 3.4.1.1 The EMD process of *S(t)*

Applying the Hilbert Transform to each of the IMFs produces the instantaneous amplitude, frequency and phase of each component as shown in Figure 3.4.1.2.

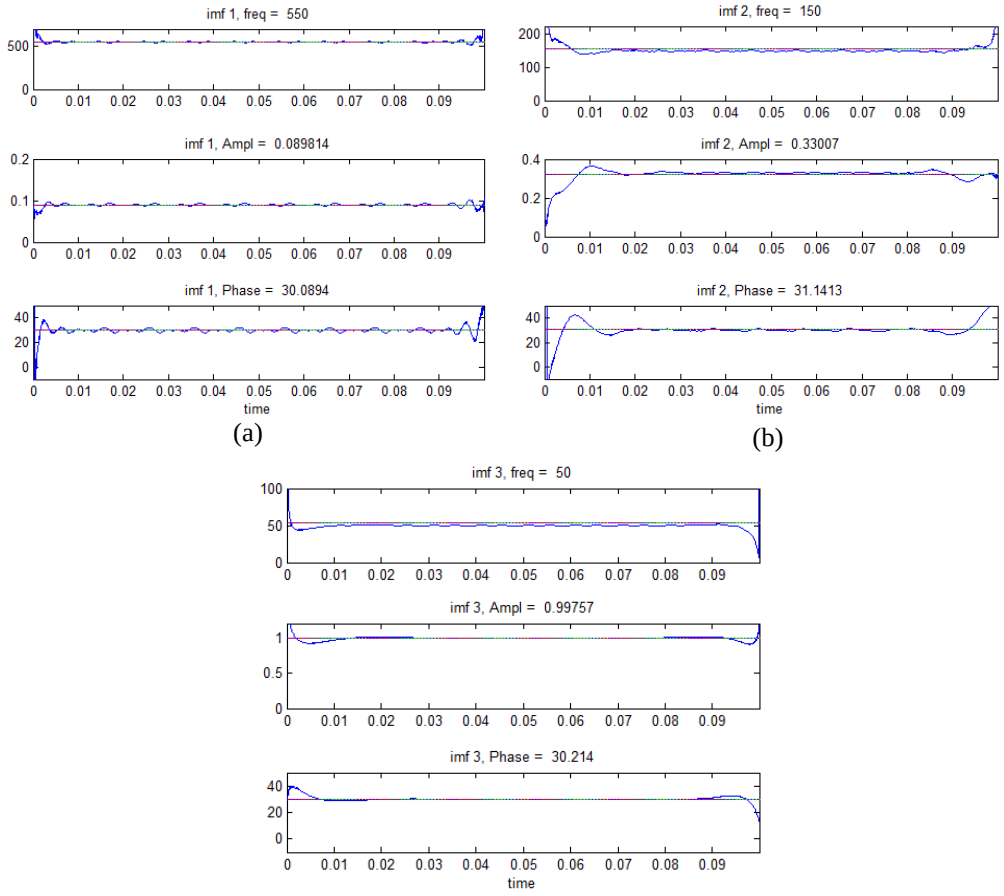

Figure 3.4.1.2 The instantaneous frequency, amplitude and phase of the detected IMFs of S(t). (a) IMF_1, (b) IMF_2, (c) IMF_3

Since the IMFs generated by the EMD process suffer the end effect problem, the mean value of 10% - 90% length of the instantaneous variable is used to obtain the actual amplitude, frequency and initial phase shown in Table 3.1.

Table 3.1

The result of The Hilbert Transform of the IMFs of S(t)

True Freq (Hz)	Freq calc. by HHT (Hz)	True Amp (p.u)	Amp calc. by HHT (Hz)	True Phase (deg)	Phase calc. by HHT (deg)
550	550	0.09	0.09	30	30.1
150	150	0.33	0.33	30	31.14
50	50	1	1	30	30.2

Table 3.1 shows that the results obtained using HHT are quite accurate in determining the amplitude, frequency and phase of the components of the analysed signal.

3.4.2 Stationary PQ waveform containing Flicker

The HHT is applied to a flicker disturbance described by the amplitude modulated signal given in (3-14):

$$S(t) = sin(2\pi f_c t)\left(1 + \frac{A_1}{2} sin(2\pi f_m t)\right) \quad (3\text{-}14)$$

where:

f_c = fundamental (carrier) frequency set at 50 Hz and amplitude of 1 pu.

f_m = modulation (flicker) frequency set at 5 Hz .

A_1 = amplitude of flicker set at 0.2 pu.

Figure 3.4.2.1 shows the signal *S(t)* and the only IMF obtained from the EMD process.

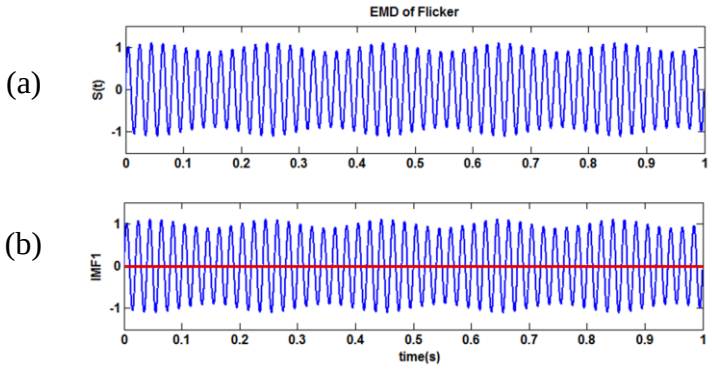

Figure 3.4.2.1. The EMD process of a signal S(t) containing flicker, (a) The signal S(t), (b) IMF_1

Figure 3.4.2.1 shows that the S(t) has already met the conditions to be an IMF and therefore, the only IMF is very similar to S(t).

The Hilbert Transform is then applied to the IMF to obtain the instantaneous amplitude, frequency and phase of fundamental component contained in the signal S(t) as shown in Figure 3.4.2.2(a). It can be observed that the instantaneous amplitude shows the waveform of the flicker component. Therefore, the Hilbert Transform is again applied to the instantaneous amplitude signal to obtain the instantaneous amplitude, frequency and phase of the flicker component. Figure 3.4.2.2(b) shows the Hilbert Transform result of the instantaneous amplitude from Figure 3.4.2.2(a) which indicates the instantaneous amplitude, frequency and phase of the flicker component.

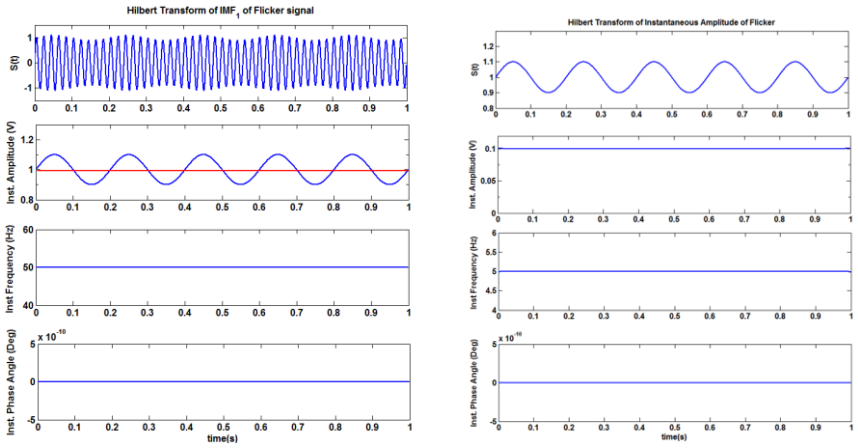

a) b)

Figure 3.4.2.2: The Hilbert Transform to obtain instantaneous frequency, amplitude and phase angle of (a) The signal contains Flicker (b) The flicker signal

To obtain more accurate result of the Hilbert Transform, the mean value of 10% - 90% length of the instantaneous amplitude, frequency and phase of the IMFs is again used. The result from the Hilbert Transform is shown in Table 3.2.

Table 3.2

The Hilbert Transform of IMFs of Flicker signal

fc (carrier component)					
True Freq (Hz)	Freq calc. by HHT (Hz)	True Amp (p.u)	Amp calc. by HHT (Hz)	True Phase (deg)	Phase calc. by HHT (deg)
50	50	1	1	0	0

fm (modulation / flicker component)					
True Freq (Hz)	Freq calc. by HHT (Hz)	True Amp (p.u)	Amp calc. by HHT (Hz)	True Phase (deg)	Phase calc. by HHT (deg)
5	5	0.1	0.1	0	0

Table 3.2 shows that the HHT method has succesfully decomposed the signal contains flicker.

3.5 Applying HHT to Non-Stationary Signals

To demonstrate the effectiveness of HHT to decompose non-stationary signals, several PQ signals such as sag, swell and transient are analysed in this section.

3.5.1 Non-stationary PQ waveform with harmonics and sag

The HHT is applied to a non-stationary PQ signal with harmonics and sag as follows :

$$S_A(t) = \begin{cases} \sin(2\pi 50 t_a) + 0.2\sin(2\pi 250 t_a), & 0 \le t_a < 0.1s \\ 0.8\sin(2\pi 50 t_b) + 0.16\sin(2\pi 250 t_b), & 0.1 \le t_b < 0.2s \\ \sin(2\pi 50 t_c) + 0.2\sin(2\pi 250 t_c), & 0.2 \le t_c < 0.3s \end{cases} \quad (3\text{-}15)$$

The resulting IMFs obtained from the EMD process from the signal given in (3-15) are shown in Figure 3.5.1.1 and the associated instantaneous amplitude, frequency and phase obtained from the Hilbert Transform of the IMFs are shown in Figure 3.5.1.2.

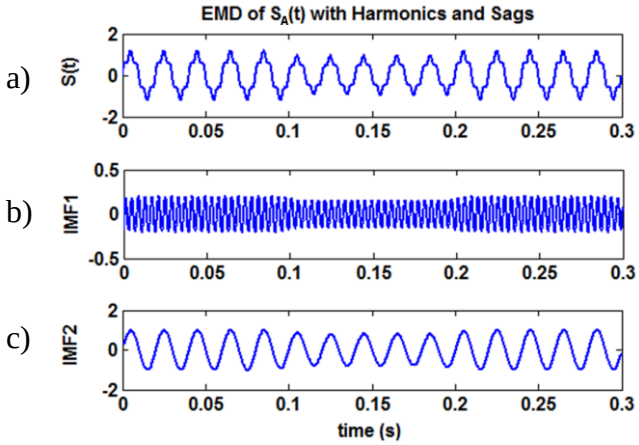

Figure 3.5.1.1 The EMD process on a signal $S_A(t)$ with harmonic and sag. (a) The Signal $S_A(t)$ (b) IMF_1 (c) IMF_2

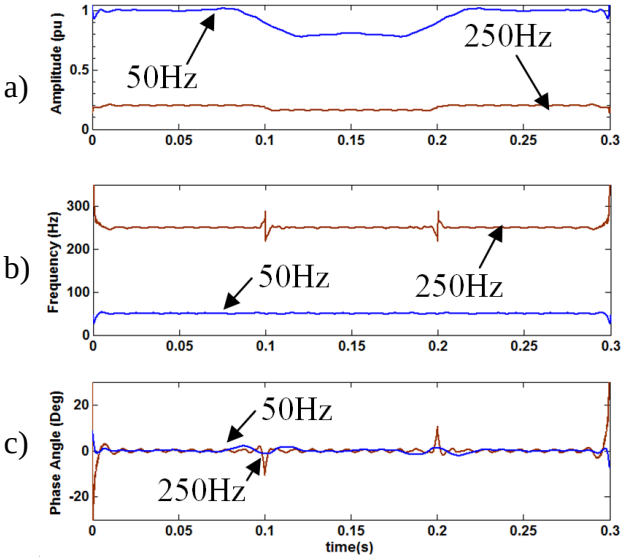

Figure 3.5.1.2. The result from Hilbert Transform of $S_A(t)$: (a) Instantaneous Amplitude, (b) Instantaneous frequency (c) Instantaneous Phase

It is observed in Figure 3.5.1.2, that the HHT method can obtain automatically the instantaneous amplitude, frequency and phase of both signals in the non-stationary signal. However, inaccuracies occur in the calculated instantaneous amplitude, frequency and phase around the area of transitions / discontinuities leading to overshoot and ambiguity.

3.5.2 Windowing Technique [38]

The inaccuracy issue around the area of transitions can be mitigated by using a windowing technique [38] which applies the HHT over a sliding window of the signal *S(t)* to identify the instant of changes (boundaries) of the non-stationary signal. Once the boundaries are identified, the HHT can then be applied to each segment (the area between two boundaries) which contains stationary part of the original signal. For example, a window size of 0.02 sec is chosen and therefore the HHT is applied to *S(t)* from 0.0 to 0.02 sec, 0.02 - 0.04 sec and so on. When there is a change in frequency or amplitude of the first IMF of a particular window, the first point of the window is marked as a boundary of a segment of the signal. For the signal with harmonic and sag, the instant of changes are found at 0.1 sec and 0.2 sec. When the boundaries of all the segments are identified, the HHT is applied to the individual segment to obtain more accurate result.

The result of the windowing technique for signal *S(t)* is shown in Figure 3.5.2.1 and Table 3.3 which shows that an accurate instantaneous amplitudes, frequencies and phases are found with clear points of change during transition and very accurate results are obtained for each component of each segment from the non-stationary signal. For a more accurate method to determine the instant of change, a novel use of Symbolic Aggregate Approximation will be introduced and described in Chapter 5.

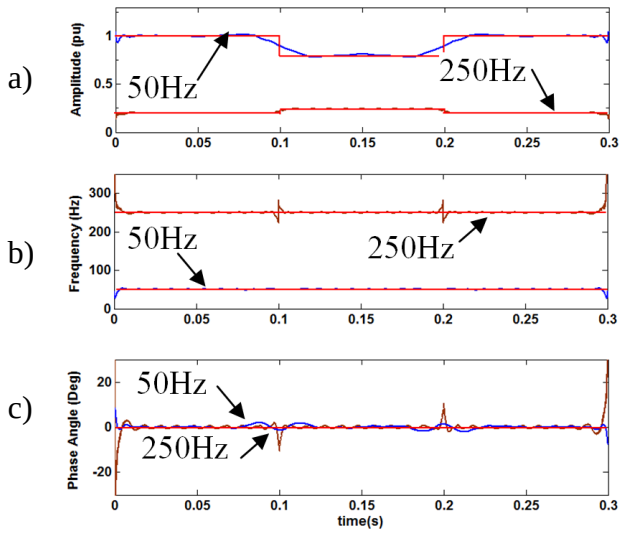

Figure 3.5.2.1. The result from windowing technique on $S_A(t)$: (a) Instantaneous Amplitude, (b) Instantaneous frequency (c) Instantaneous Phase

Table 3.3

The result from windowing technique and HHT of $S_A(t)$

0s ≤ t < 0.1s			0.1 s ≤ t < 0.2 s			0.2 s ≤ t ≤ 0.3 s		
Amp (p.u)	Freq (Hz)	Phase (deg)	Amp (V)	Freq (Hz)	Phase (deg)	Amp (p.u)	Freq (Hz)	Phase (deg)
0.2	250	- 0.02	0.16	250	0	0.2	250	0.02
1.0	50	0.1	0.8	50	0	1.0	50	-0.1

3.5.3 Non-stationary PQ waveform with harmonics and swell

The HHT is applied to a non-stationary signal $S_B(t)$ with harmonics and swell as follows :

$$S_B(t) = \begin{cases} \sin(2\pi 50 t_a) + 0.2\sin(2\pi 250 t_a), & 0 \le t_a < 0.1s \\ 1.2\sin(2\pi 50 t_b) + 0.24\sin(2\pi 250 t_b), & 0.1 \le t_b < 0.2s \\ \sin(2\pi 50 t_c) + 0.2\sin(2\pi 250 t_c), & 0.2 \le t_c < 0.3s \end{cases} \quad (3\text{-}16)$$

The resulting IMFs obtained from the EMD process of the signal given in (3-16) are shown in Figure 3.5.3.1 and the associated instantaneous amplitude, frequency and phase are shown in Figure 3.5.3.2.

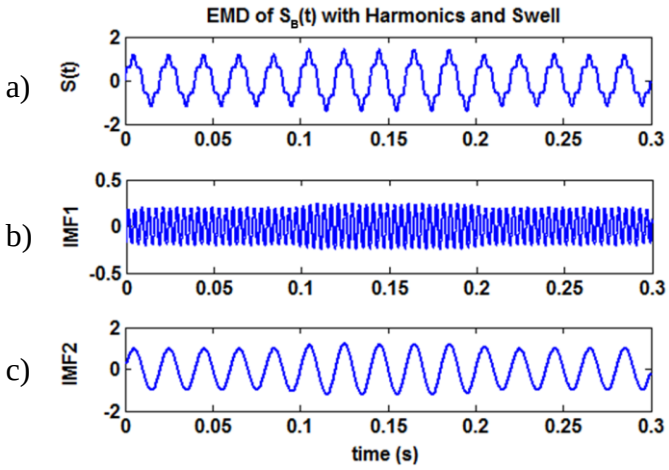

Figure 3.5.3.1 The EMD process of signal $S_B(t)$ with harmonic and swell (a) The Signal $S_B(t)$ (b) IMF_1 (c) IMF_2

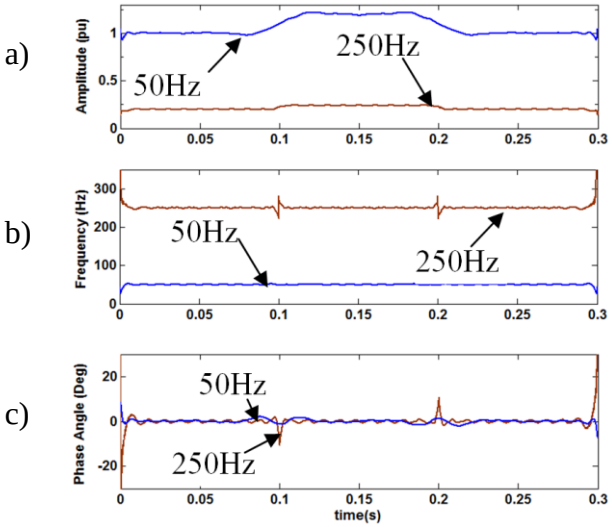

Figure 3.5.3.2 The result from Hilbert Transform of $S_B(t)$: (a) Instantaneous Amplitude, (b) Instantaneous frequency (c) Instantaneous Phase

It is observed in Figure 3.5.3.2, that the HHT method can obtain automatically the instantaneous amplitude, frequency and phase of both components in the non-stationary signal. However, inaccuracies occur on the instantaneous variables due to overshoot and ambiguity around the area of a transition/discontinuity. To overcome this, the windowing technique is also used to reduce these ambiguities. The result of the windowing technique for signal $S_B(t)$ is shown in Figure 3.5.3.3 and Table 3.4. Again Table 3.4 shows that good results have been obtained from the decomposition process, where the amplitudes, frequencies and phases of each segment of the signal have been calculated correctly.

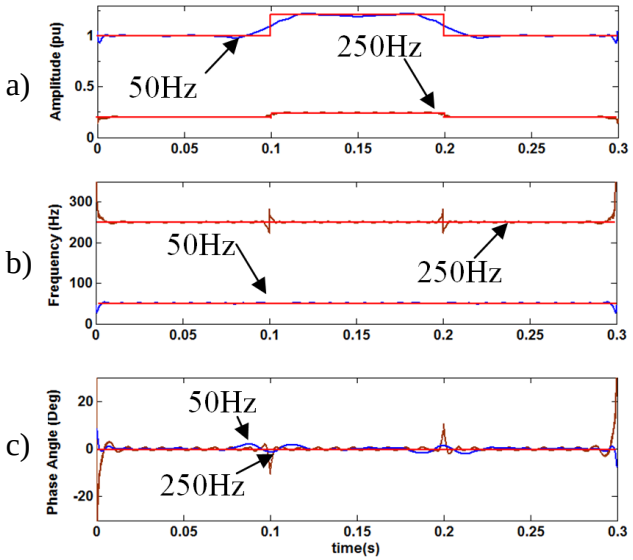

Figure 3.5.3.3: The result from windowing technique of signal $S_B(t)$:

(a) Instantaneous Amplitude, (b) Instantaneous frequency (c) Instantaneous Phase

Table 3.4.

Result from windowing technique and HHT of $S_B(t)$

0s ≤ t < 0.1s			0.1 s ≤ t < 0.2 s			0.2 s ≤ t ≤ 0.3 s		
Amp (p.u)	Freq (Hz)	Phase (deg)	Amp (p.u)	Freq (Hz)	Phase (deg)	Amp (p.u)	Freq (Hz)	Phase (deg)
0.2	250	- 0.02	0.239	250	0	0.2	250	0.02
1.0	50	0.1	1.2	50	0	1.0	50	-0.1

3.5.4 Non-stationary PQ waveform with transient

The HHT is applied to a non-stationary signal with harmonics and transient $S_C(t)$ as follows (3-17):

$$S_C(t) = \begin{cases} \sin(2\pi 50 t_a) + 0.2\sin(2\pi 250 t_a), & 0 \le t_a < 0.1s \\ \sin(2\pi 50 t_b) + 0.2\sin(2\pi 250 t_b) + \sin(2\pi 500 t_b) e^{(-30 t_b - 0.1)}, & 0.1 \le t_b < 0.18s \\ \sin(2\pi 50 t_c) + 0.2\sin(2\pi 250 t_c), & 0.18 \le t_c < 0.3s \end{cases} \quad (3\text{-}17)$$

The transient signal is shown in Figure 3.5.4.1. The resulting IMFs obtained from the EMD process from the signal in (3-17) are given in Figure 3.5.4.2 and the associated instantaneous amplitude, frequency and phase obtained from the Hilbert Transform are given in Figure 3.5.4.3.

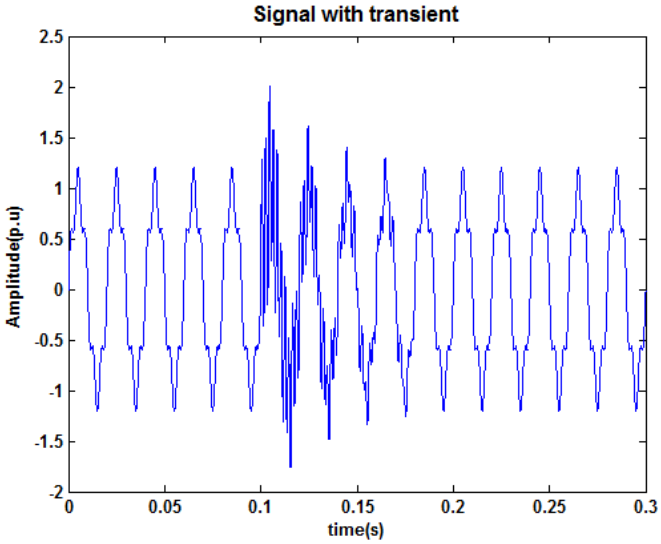

Figure 3.5.4.1 The signal $S_C(t)$ contains transient

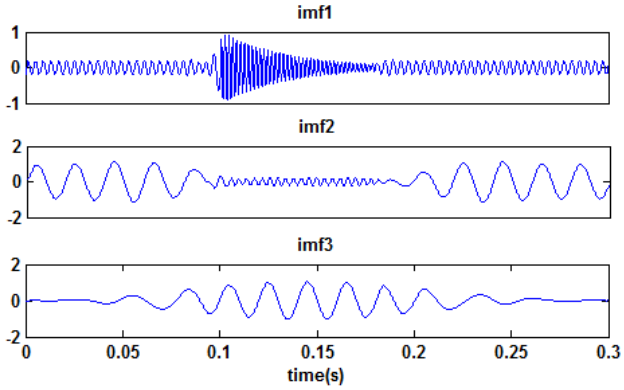

Figure 3.5.4.2 The resulting IMFs of a transient signal $S_C(t)$

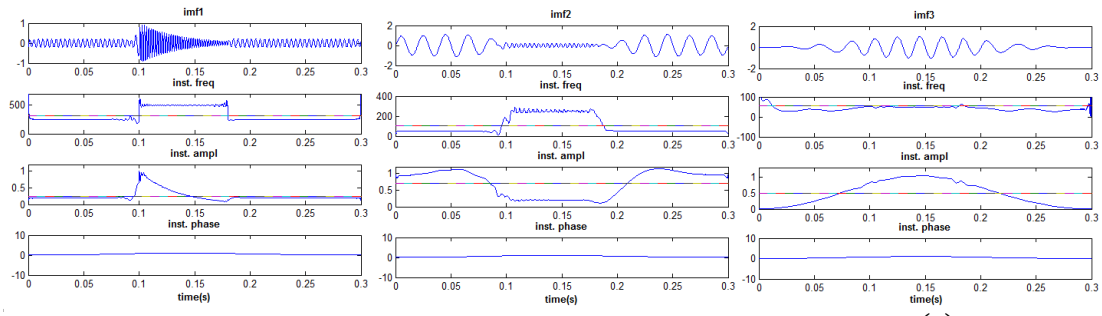

(a) (b) (c)

Figure 3.5.4.3 The Hilbert Transform of IMFs of $S_C(t)$: (a) IMF_1, (b) IMF_2, (c) IMF_3

It is observed in Figure 3.5.4.3, that the HHT method can obtain automatically the instantaneous amplitude, frequency and and phase of signal components in the non-stationary signal $S_C(t)$. However, inaccuracies occur in the instantaneous variables due to overshoot and ambiguity around the area of a transition/discontinuity. To overcome this, the windowing technique is then used to

reduce these ambiguities. The windowing technique is applied to detect if any change in frequency occurs in the first IMF of a particular window, then the first point of the window is marked as a boundary for a segment.

The boundaries are identified correctly at t_1 = 0.1sec and t_2 = 0.18sec. Once the segments are identified, the HHT is then applied to the signal over the identified segments to obtain the instantaneous frequency, amplitude and phase. The result of the windowing technique for signal $S_C(t)$ is shown in Figure 3.5.4.4 and Table 3.5.

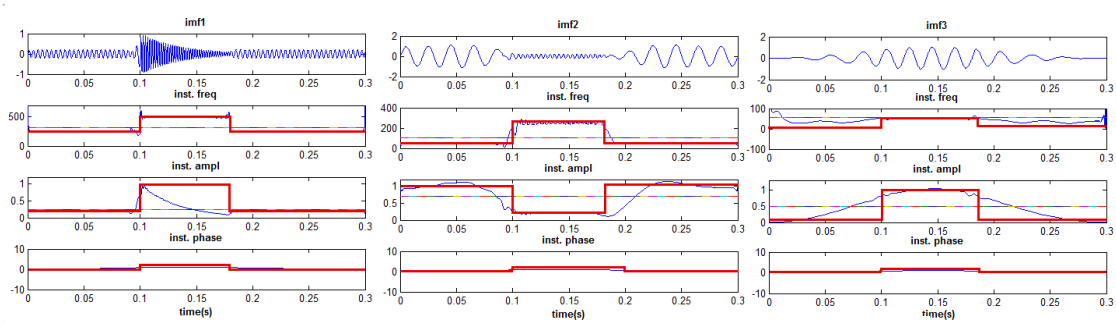

(a) (b) (c)

Figure 3.5.4.4 The result from windowing technique of signal $S_C(t)$: (a) IMF_1, (b) IMF_2, (c) IMF_3

Table 3.5
The result from windowing technique and HHT of a transient signal $S_C(t)$

IMF No	Seg 1, 0s ≤ t < 0.1			Seg 2, 0.1 s ≤ t < 0.18 s			Seg 3, 0.18 s ≤ t ≤ 0.3 s		
	Amp (p.u)	Freq (Hz)	Phase (deg)	Amp (p.u)	Freq (Hz)	Phase (deg)	Amp (p.u)	Freq (Hz)	Phase (deg)
1	0.2	250	0.2	$e^{(-30t-0.1)}$	500	0.4	0.2	250	0.15
2	1.0	50	0.0	0.2	250	3.3	1.0	50	0.01
3	0	0	0.0	1.0	50	2.6	0	0	0

Table 3.5 shows the detected amplitudes, frequencies and phases of the IMFs from the EMD process of signal $S_C(t)$. In the EMD process, the highest frequency component of the signal will be captured by IMF_1 and the next highest frequency component is represented by IMF_2 and so on. Therefore, IMF_1 captures the highest frequency component of each segment, 250 Hz at segment 1, 500 Hz at segment 2 and 250 Hz at segment 3. The waveform of IMF_1 and the associated instantaneous amplitude, frequency and phases are shown in Figure 3.5.4.4(a). IMF_2 captures the lower frequency component of each segment, 50 Hz at segment 1, 250 Hz at segment 2 and 50 Hz at segment 3. The waveform of IMF_2 and the associated instantaneous amplitude, frequency and phases are shown in Figure 3.5.4.4(b). IMF_3 captures the

lowest frequency component of each segment. Since there is no lower than 50 Hz frequency in the signal, no frequency, amplitude and phase are detected in segment 1 and 3. The lowest frequency 50 Hz is detected in segment 2. The waveform of IMF_3 and the associated instantaneous amplitude, frequency and phases are shown in Figure 3.5.4.4(c).

As shown in Figure 3.5.4.4(a), the exponential sinusoidal waveform is captured in second segment of IMF_1 after applying HHT to the IMF. The Hilbert Transform of IMF_1 provides the associated instantaneous frequency, amplitude and phase. The instantaneous amplitude of IMF_1 shows a waveform decays exponentially in segment 2. To identify the waveform, an exponential curve fitting is used to predict an exponential expression as shown in Table 3.5.

Figure 3.5.4.4 and Table 3.5 demonstrate that the EMD method with windowing technique can decompose the non-stationary signal with transient $S_C(t)$ accurately.

3.6 Issues in implementing HHT

There are a number of issues faced when implementing HHT. Cautious steps need to be taken to obtain satisfactory results from the HHT process.

3.6.1 Stopping Criteria

The sifting process used in the EMD algorithm to extract the IMFs from the signal has to be carried out iteratively until the conditions for being an IMF are fulfilled. To guarantee that the local mean is very close to zero (which is the second condition to be an IMF), a stopping criterion using 3 thresholds (θ_1, θ_2 and tol) has been designed [5]. Threshold θ_1 and *tol* are designed to guarantee globally small fluctuations of the IMF while threshold θ_2 is used to take into account locally large excursions of the IMF. The threshold of the stopping criterion needs to be specified appropriately since too small a threshold may cause over decomposition, and too large a threshold may cause poor decomposition i.e some of the signal components remain unidentified.

Based on many simulations, setting the value of stopping criteria smaller than the default can provide a better decomposition result, however, using too small a threshold can lead to over-iteration that can cause over-decomposition.

As an example of the effect of various stopping criteria to the decomposition result, consider a signal *S(t)* as given in (3-18) :

$$S(t) = \sin(2\pi\, 50t + 0^0) + 0.2 \sin(2\pi\, 250t + 0^0) + 0.14 \sin(2\pi\, 350t + 0^0) \quad (3\text{-}18)$$

When the default stopping criteria (θ_1 = 0.05, θ_2 = 0.5 and tol = 0.05) is chosen to decompose the signal by using the HHT, the result is shown in Table 3.6

Table 3.6

Result of HHT decomposition of the signal S(t)

Using θ_1= 0.05, θ_2 = 0.5 and tol = 0.05

True Freq (Hz)	Freq Calc using HHT (Hz)	True Amp (pu)	Amp Calc using HHT (pu)	True Phase (Deg)	Phase Calc using HHT (deg)
350	350	0.14	0.18	0	0.03
250	None	0.2	None	30	None
50	50	1.0	1	0	0.003

Table 3.6 shows that the HHT using the default stopping criteria does not decompose the signal accurately, since the 250 Hz component is not detected.

When a smaller stopping criteria (θ_1= 0.0005, θ_2 = 0.005 and tol = 0.0005) is used, the result of the HHT is shown in Table 3.7.

Table 3.7

Result of HHT decomposition of the signal S(t)

using θ_1= 0.0005, θ_2 = 0.005 and tol = 0.0005

True Freq (Hz)	Freq Calc using HHT (Hz)	True Amp (pu)	Amp Calc using HHT (pu)	True Phase (Deg)	Phase Calc using HHT (deg)
350	350	0.14	0.14	0	0.03
250	250	0.2	0.18	0	0
50	50	1.0	1	0	0

Table 3.7 shows that if a smaller stopping criteria is chosen, a more accurate decomposition result is obtained. The 250 Hz component is now detected and the results of the instantaneous amplitude, frequency and phase are very close to the specified values.

Further check is then performed by using even smaller stopping criteria (θ_1= 5.10^{-11}, θ_2 = 5.10^{-10} and tol = 5.10^{-11}) and the maximum number of iteration is set as 5.10^5. The result of the HHT is shown in Table 3.8.

Table 3.8

Result of HHT decomposition of the signal S(t)

using $\theta_1 = 5.10^{-11}$, $\theta_2 = 5.10^{-10}$, tol = 5.10^{-11} and MAXITERATION = 5.10^5

True Freq (Hz)	Freq Calc using HHT (Hz)	True Amp (pu)	Amp Calc using HHT (pu)	True Phase (Deg)	Phase Calc using HHT (deg)
350	350	0.14	0.14	0	0.03
250	250	0.2	0.182	0	0
50	50	1.0	0.97	0	2.04
None	45	None	0.092	None	77.53
None	35	None	0.06	None	46.25

Table 3.8 shows that when even smaller stopping criteria is chosen, the decomposition results are relatively the same with the result obtained by using greater stopping criteria (Table 3.7). However, some extra signals contain other frequencies (45 and 35 Hz) with significant amplitudes (0.092 and 0.06 pu) emerge in the decomposition result. These extra IMFs are not part of the specified components of the original signal which means that the EMD process does not give accurate result for this case.

The result in Table 3.8 demonstrates that imposing too small a stopping criteria will produce over decomposed result which is not desirable. Therefore, the correct choice of stopping criteria is necessary to obtain accurate results.

The usual practice to select θ_1, θ_2 and tol used in the research is by initially selecting the default stopping criteria for the EMD process. When the result is not accurate, multiply the default stopping criteria by 0.1 to make it smaller. Repeat the process as necessary. Based on many simulations of PQ signals decomposition in the research, the smaller stopping criteria such as 0.01 x default ($\theta_1 = 0.0005$, $\theta_2 = 0.005$ and $tol = 0.0005$) generally produce accurate results to separate the components of PQ signal containing higher frequency components. More discussions on the effect of the stopping criterion to the separation of higher frequency components are presented in Chapter 4.

3.6.2 Close Frequency

The EMD has been found to have difficulty in resolving waveforms containing components with close frequencies with a ratio of less than two [44]. Such signals are often encountered in PQ waveforms, for example 9^{th}, 11^{th} and 13^{th} harmonics.

When the standard EMD is applied to the signal, IMFs with mixed frequencies may be obtained.

As an example, consider a signal *S(t)* as the following :

$$S(t) = \sin(2\pi 50t + 30^0) + 0.091\sin(2\pi 550t + 30^0) + 0.077\sin(2\pi 650t + 30^0) \quad (3\text{-}19)$$

Since the signal contains 11th and 13th harmonic frequencies that are close together, the EMD process will produce IMFs that contains mixed frequency, as shown in Figure 3.6.2.1.

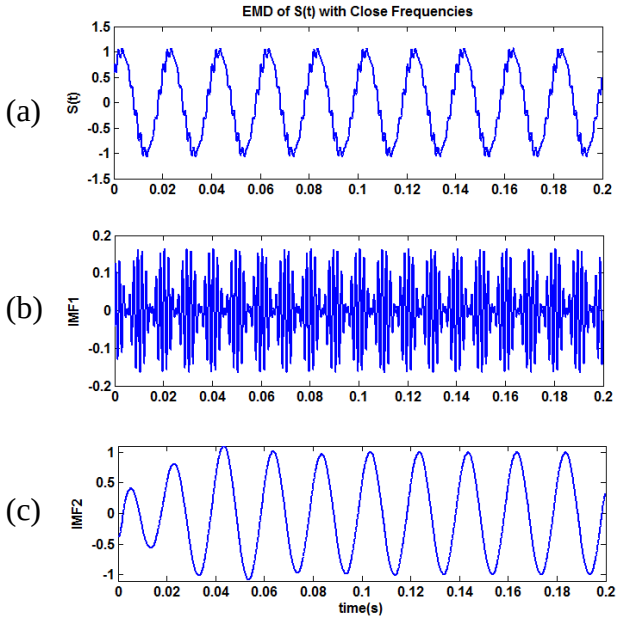

Figure 3.6.2.1. EMD process on a signal that contains close frequency

(a) The signal S(t), (b) IMF_1, (c) IMF_2,

Figure 3.6.2.1(b) shows IMF_1 which looks like a modulated signal composed from more than one frequency. IMF_2 shown in Figure 3.6.2.1(c) looks very similar to a pure sinusoidal which means it is not mixed with any other frequency.

Generally, mixed frequency IMF (or mode mixing) is not desirable, since it would produce incorrect results when the IMFs are processed by the Hilbert Transform as shown in Figure 3.6.2.2 and Table 3.9.

(a) 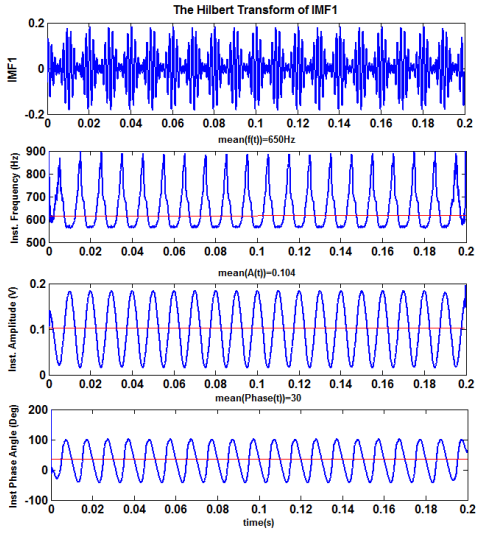

(b) 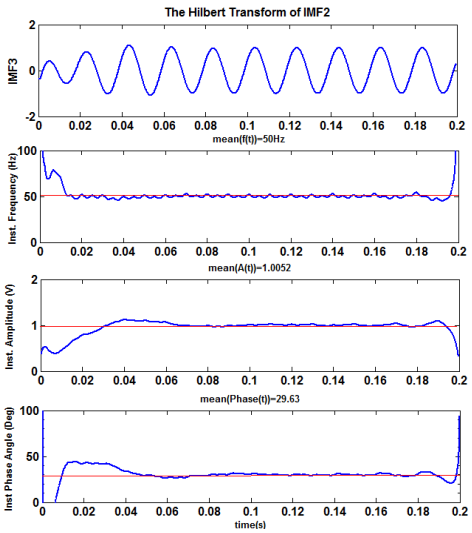

Figure 3.6.2.2 Hilbert Transform of the IMFs from EMD process on a signal that contains close frequency (a) IMF_1, (b) IMF_2,

The IMF_1's waveform in Figure 3.6.2.2(a) shows fluctuating instantaneous frequency, amplitude and phase angle plot which indicates that the IMF contains mixed frequency signal. IMF_2's waveform in Figure 3.6.2.2(b) shows more stable instantaneous frequency, amplitude and phase angle values indicating that the IMF is not mixed. Since one of the IMFs is mixed, applying Hilbert Transform on these IMFs will produce inaccurate results. Table 3.9 shows the result of HHT on signal *S(t).*

Table 3.9

Result of HHT decomposition of the signal *S(t)*

True Freq(Hz)	Freq Calc using HHT (Hz)	True Amp (pu)	Amp Calc using HHT (pu)	True Phase (Deg)	Phase Calc using HHT (Deg)
650	650	0.0770	0.1022	30	31
550	None	0.0910	None	30	None
50	50	1.0000	1.0220	30	30

Table 3.9 shows that the EMD process has succesfully extracted the 650 Hz and 50 Hz components, however, the 550 Hz component is not identified by the EMD algorithm. To overcome the problem with components containing close frequencies, a novel Iterative Hilbert Huang transform (IHHT) will be proposed in Chapter 4.

3.6.3 Noise

The EMD has also been found to have mode mixing issues when it is applied to a signal that contains relatively high level of noise. The noise content of the signal which is usually of high frequency may mix with a high frequency component of the signal in the same IMF [8]. To demonstrate the issue, a simulated noisy signal is created from the formula given by (3-20) :

$$S(t)= cos(2\pi\ 50t) + 0.33cos\ (2\pi\ 150t + 60^0) + 0.2cos(2\pi\ 250t + 50^0) \qquad (3\text{-}20)$$

A Gaussian white noise signal with a *Signal to Noise Ratio* (*SNR*) = 30 is added to *S(t)* to obtain a noisy signal which is then analyzed by the HHT process. The IMFs obtained from the EMD process of the signal are shown in Figure 3.6.3.1. The result of the Hilbert Transform applied to the IMFs are shown in Table 3.10.

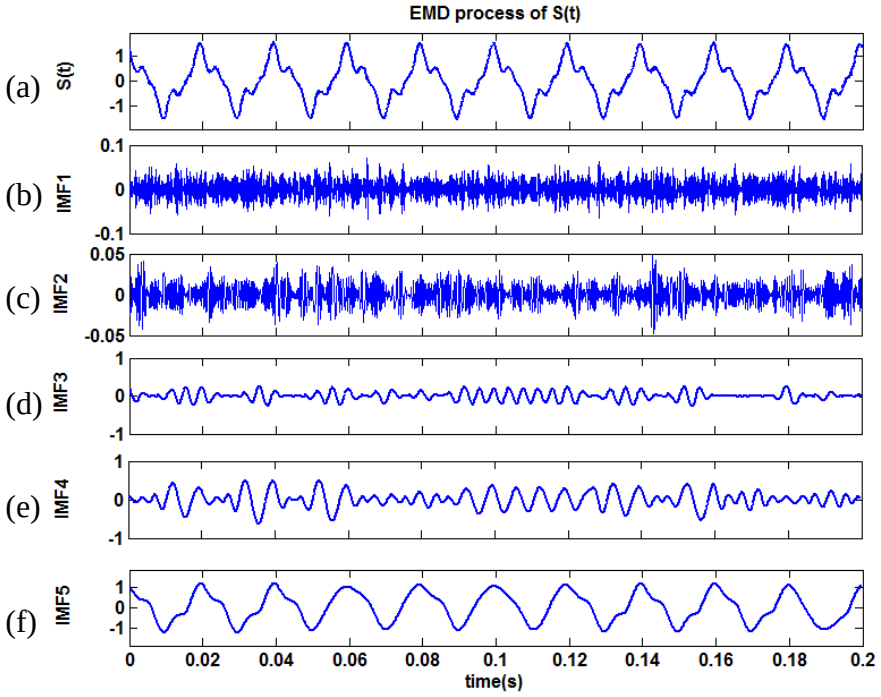

Figure 3.6.3.1 EMD process of a signal that contains noise, (a) The Signal S(t) (b) IMF_1, (c) IMF_2, (d) IMF_3, (e) IMF_4, (e) IMF_5

Figure 3.6.3.1 shows that the EMD process extracts the noise content in IMF_1 and IMF_2. The high frequency noise is mixed with some portions of 250Hz component in IMF_3 which causes the rest of 250 Hz component to mix with the 150 Hz component in IMF_4. This also causes the rest of 150 Hz component is then mixed with 50 Hz component in IMF_5. Table 3.10 shows the results from the Hilbert Transform of the IMFs.

Table 3.10
The Hilbert Transform of the IMFs from EMD process of signal S(t) in (3-20)

IMF	Amp (p.u)	Freq (Hz)	Phase (deg)
1	0.026	3424	-3.42
2	0.015	1786	4.04
3	0.152	335	-3.89
4	0.267	190	-9.39
5	1.019	50	0.18

As shown in Table 3.10, when the Hilbert Transform is applied to process the mixed IMFs, inaccurate results are obtained, such as the calculated mean value of instantaneous frequency 335 Hz and 190 Hz, instead of 250 Hz and 150 Hz.

To overcome the problem with components containing high level of noise, a novel Iterative Ensemble EMD (IEEMD) is proposed in Chapter 6.

3.7 Chapter Summary

This chapter describes the reason of why HHT is used in this research, followed by the explanation of the basic of HHT which consists of EMD and HT. The applications of HHT to stationary and non-stationary PQ signals are also presented showing the effectiveness of HHT to decompose such signals. A simple windowing technique is proposed to overcome the problem with transitions in non-stationary signals. In chapter 5, a more advanced method of solving the transition problems using a Symbolic Aggregated Approximation is described.

Several issues in implementing HHT are also discussed, such as the determination of the stopping criteria, the mode mixing issues caused by signals containing close frequency components and signal containing noise. The problem of mode mixing is the primary difficulty in using HHT for PQ study, since a lot of PQ signals contain close frequency and noise. Solutions to the mode mixing problems will be discussed in Chapter 4 and Chapter 6.

CHAPTER 4 METHODS TO IMPROVE HHT

4.1. Introduction

This chapter initially describes several techniques from the literature to improve the HHT method in resolving the mode mixing problem caused by signals having close frequency components. All these techniques demonstrate the ability to decompose the close frequency components of the signal. However, they have disadvantages, in that some assumptions have to be made prior to the analysis and some requires the use of FFT to obtain the frequency of the components prior to HHT decomposition. A new method using an iterative process is proposed to improve the HHT when dealing with signals containing close frequency components, which does not require the masking signal or FFT to be performed prior to the analysis. The proposed method referred to as the Iterative HHT is then applied on various stationary signals with close frequencies to demonstrate its effectiveness.

4.2. Method to improve HHT using Masking Signal

One of the methods that has been proposed to improve the problem of mode mixing which caused by close frequency components with the ratio of the high frequency to the low (next highest) frequency being less than 2, is to use the masking signal [6], [7].

The basic idea of the method is to add an extra signal to the signal being analysed. Suppose that *x(t)* is a PQ signal containing two close frequencies f_a and f_b (f_a>f_b) which usually cause the mode mixing issue in the EMD process. By adding an appropriately chosen masking signal to *x(t)*, the additional signal will prevent the lower frequency component f_b from being mixed with the higher frequency component f_a in an IMF [6].

4.2.1. EMD using Masking Signal [6]

The following algorithm can be used to perform EMD using masking signal :

1. Apply EMD to the original signal *x(t)* to obtain its IMFs.
2. Estimate the frequency $\hat{f}\ of$ the masking signal, *q(t)*. The frequency $\hat{f}$ can be calculated from instantaneous frequency $f_1(t)$, its mean value $\widetilde{f_1}$ and instantaneous amplitude $a_1(t)$ obtained from the Hilbert Transform of the first IMF. Relation (4-1) provides the estimated masking signal frequency $\hat{f}$,

obtained from the instantaneous value of $f_1(i)$ and the associated $a_1(i)$. The instantaneous value $f_1(i)$ and $a_1(i)$ are used in (4-1) if any data point of $f_1(i)$ *is* greater than $\widetilde{f_1}$:

$$\hat{f} = \frac{\sum_{i=1}^{k} a_1(i) f_1^2(i)}{\sum_{i=1}^{k} a_1(i) f_1(i)} \tag{4-1}$$

3. The masking signal $q(t)$ is then constructed as

$$q(t) = m_1 \bar{a}_1 \sin(2\pi m_2 \hat{f} t) \tag{4-2}$$

Based on his experimental results, Rilling recommends to set the value of m_1 equals to 1.6 to multiply the mean value of the instantaneous amplitude, $\bar{a}_1$[6]. Further, the simulations of PQ signal analysis carried out in the research suggest to use the masking signal with a higher frequency which produce better result to avoid mode mixing. Therefore, to decompose PQ signals, $\hat{f}$ is multiplied by m_2 which is chosen as 1.2.

4. Perform EMD on $x_+(t) = x(t) + q(t)$ to obtain the IMFs $z_+(t)$. Similarly perform EMD on $x_-(t) = x(t) - q(t)$ to obtain the IMFs $z_-(t)$.
5. Define the IMFs as $z(t)=(z_+(t)+ z_-(t))/2$, The averaging step will cancel out the positive and negative instances of the masking signal leaving only the portion of the signal at the highest frequency.

In the original paper [6], the algorithm is used to analyze a signal with two components as given by (4-3):

$$x(t) = \sin(2\pi 1776t) + \sin(2\pi 1200t) \tag{4-3}$$

A masking signal with frequency $\hat{f}$ 2100 Hz is chosen to be inserted to $x(t)$ to avoid the mode mixing issue. The result is shown in Figure 4.2.1.1.

Figure 4.2.1.1 shows how the masking signal helps in the decomposition process of the signal given by (4-3) by preventing the lower frequency (1200 Hz) from being mixed with the higher frequency (1776 Hz) component in IMF_1. Figure 4.2.1.1 (b) shows IMF_1 with mixed frequency components and IMF_2 with smaller than the actual amplitude of 1200 Hz frequency component.

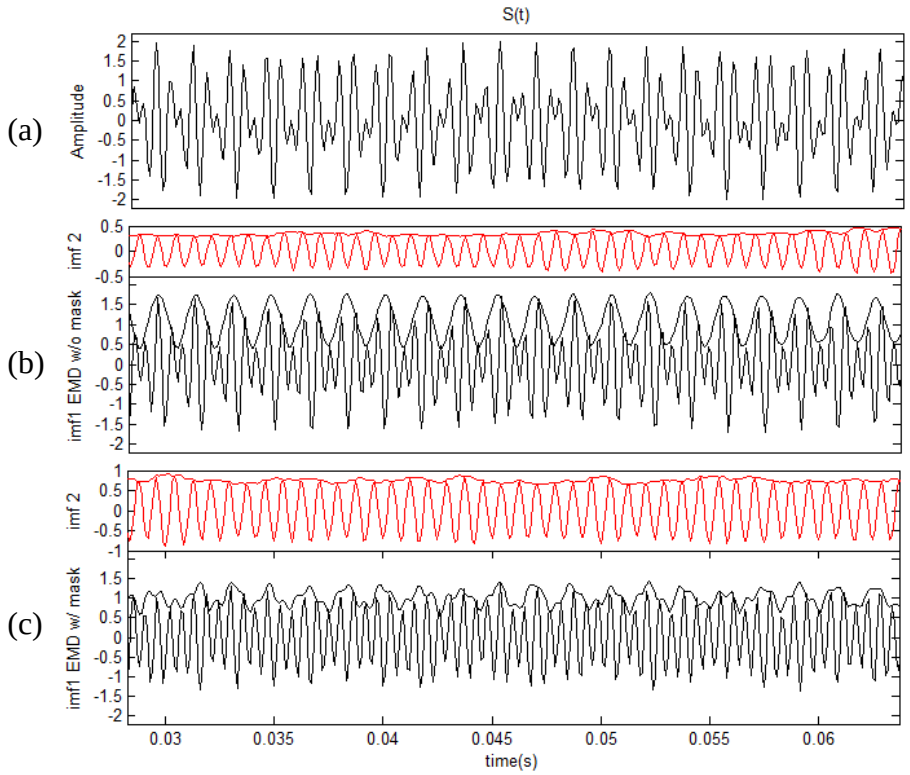

Figure 4.2.1.1 The result of Standard EMD and EMD with masking signal
(a) The original signal *x(t)* (b) The result without masking signal
(c) The result with masking signal

Figure 4.2.1.1 (c) shows the effect of masking signal causing IMF_1 to be less mixed with the lower frequency, IMF_2 is now larger since the 1200 Hz frequency component is more concentrated in IMF_2. The mean amplitude of IMF_2 is however still smaller than the specified value.

A signal with two components can be analyzed by carrying out steps 1 – 5 mentioned above [6]. However, for PQ signals which usually contain more than 2 components, it is necessary to repeat the process to obtain more components by applying the EMD with masking signal to the residue. The additional steps are described as follows :

6. Apply Hilbert Transform to the first IMF to get its instantaneous amplitude, frequency and phase
7. Subtract the IMF from the original signal to obtain the residue.
8. If the residue is below a specified threshold (0.5% of the maximum value of the original signal), stop the process, otherwise take the residue as the signal to be processed *x(t)* and repeat step 1 to 5 to *x(t)*.

4.2.2. Results from EMD with Masking Signal

As mentioned in section 3.6.2, mixed IMF may be generated when a standard EMD is applied to a signal containing close frequency components as given by (4-4).

$$X_1(t) = \sin(2\pi 50t + 30^0) + 0.091\sin(2\pi 550t + 30^0) + 0.077\sin(2\pi 650t + 30^0) \quad (4\text{-}4)$$

Figure 4.2.2.1(a) shows $X_1(t)$ and Figure 4.2.2.1(b)-(c) show the IMFs obtained from the EMD process.

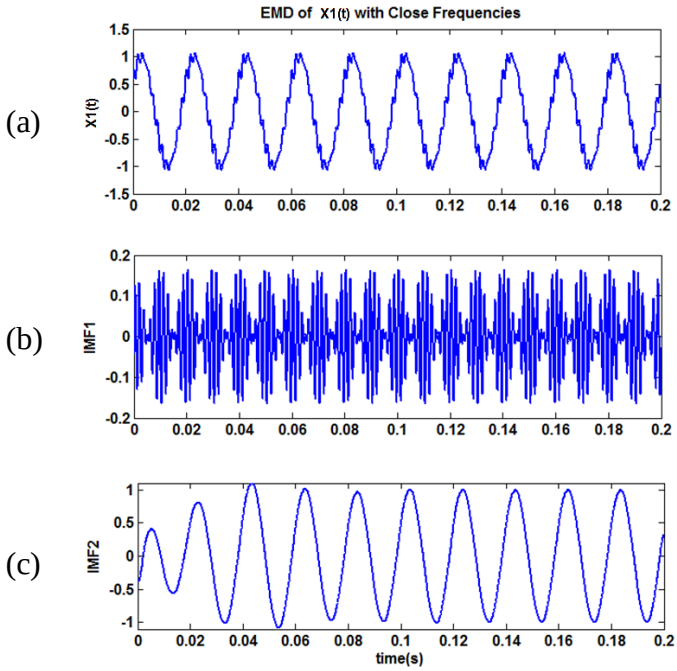

Figure 4.2.2.1 The original $X_1(t)$ and the IMFs obtained from EMD process of $X_1(t)$

Figure 4.2.2.1 shows that only 2 IMFs are obtained from the process which means that one of the components is unidentified and may be mixed in IMF_1 since the IMF shows some fluctuations in the instantaneous amplitude waveform. The result from the Hilbert Transform is shown in Table 4.1

Table 4.1

Result of HHT decomposition of the signal $X_1(t)$

True Freq(Hz)	Freq Calc using HHT (Hz)	True Amp (pu)	Amp Calc using HHT (pu)	True Phase (Deg)	Phase Calc using HHT (deg)
650	650	0.0770	0.1022	30	31
550	None	0.0910	None	30	None
50	50	1.0000	1.0220	30	90

Table 4.1 shows that the EMD process has succesfully extracted the 650 Hz and 50 Hz components. However, the 550 Hz component is not identified by the EMD algorithm.

To overcome the problem, The EMD with masking signal method is then used to decompose $X_1(t)$. To estimate the appropriate masking signal frequency for the separation of components mixed in IMF_1, the Hilbert Transform is used to obtain the mean value of instantaneous amplitude, frequency and phase of IMF_1 as shown in Figure 4.2.2.2(b)-(d)

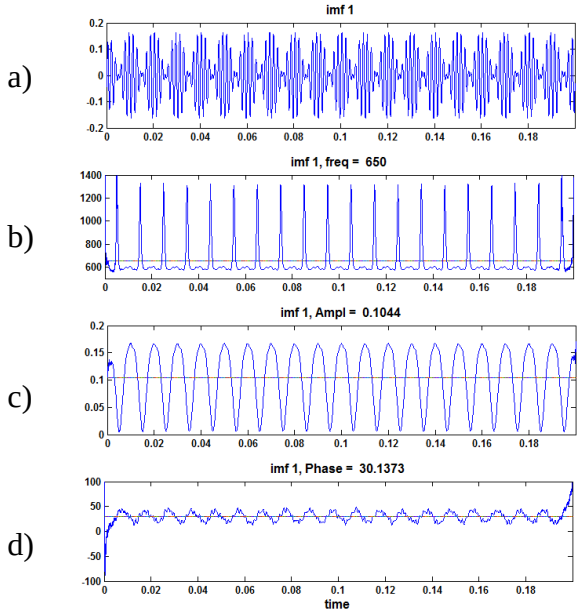

Figure 4.2.2.2. The Hilbert Transform of IMF_1 of $X_1(t)$.

The waveform of IMF_1 in Figure 4.2.2.2 shows more clearly that the IMF is mixed which can be seen from the fluctuations of the instantaneous amplitude and the instantaneous frequency waveform. To resolve the mode mixing issue, a masking signal frequency is then estimated by using the formula given in (4-1) which results in $\hat{f}$ = 879 Hz. The mean value of instantaneous amplitude of IMF_1 is 0.1045 p.u. as shown in Figure 4.2.2.2(c) which is then used by the formula given by (4-2) to construct the masking signal $q(t) = 0.1672 \sin(2\pi\ 1054.8\ t)$.

When the masking signal is applied to the original signal $X_1(t)$ according to step 4 of the algorithm, the first IMF of $x_+(t)$ and the first IMF of $x_-(t)$ denoted by IMF_+ and IMF_- respectively are shown in Figure 4.2.2.3 as follows :

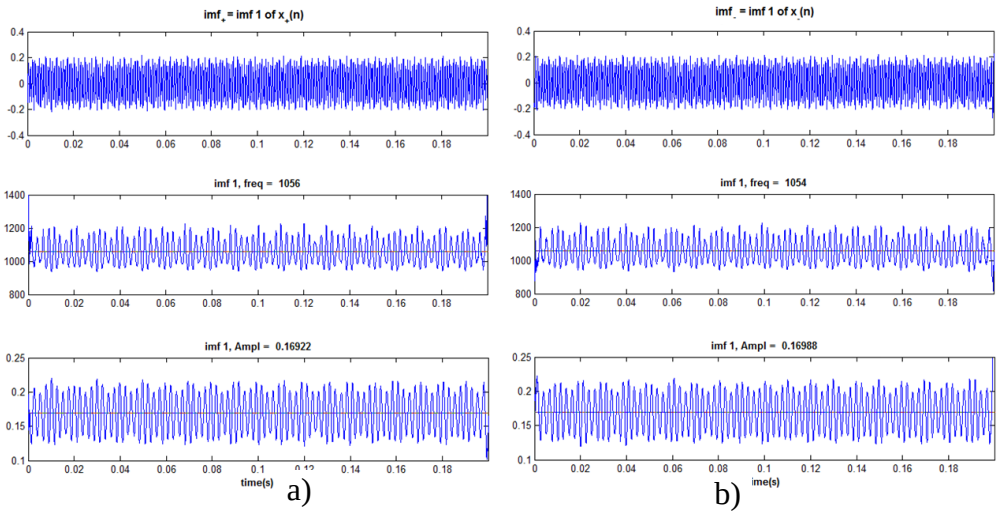

Figure 4.2.2.3: The EMD process using masking signal.
a) IMF_+ b). IMF_-

Figure 4.2.2.3 shows the IMFs obtained from the EMD with masking signal process. The mean value of the instantaneous frequency is greater than the highest frequency component of $X_1(t)$ (650 Hz) which is caused by the masking signal added to the original signal. Averaging the above IMFs following step 5 of the method will produce an IMF as shown in Figure 4.2.2.4.

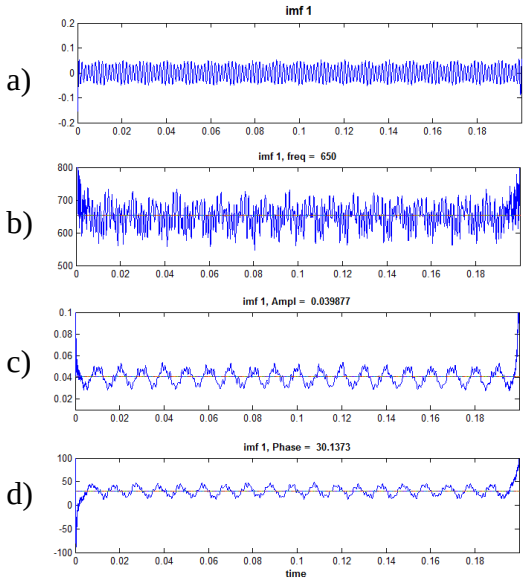

Figure 4.2.2.4: a) The average of IMF_+ and IMF_-, b) the inst. frequency,
c) the inst. amplitude, d) the inst. phase.

Figure 4.2.2.4 shows that the averaged IMF contains less mixed frequency than the IMF without masking signal as shown in Figure 4.2.2.1(b). The IMF represents correctly the frequency of the highest signal component (650 Hz). However, the

amplitude of the IMF 0.0398 p.u is smaller than the actual amplitude for 650 Hz component specified as 0.077 p.u.

The IMF is taken as the first IMF of the process which is then subtracted from the original signal $X_1(t)$ to obtain the residue. The original signal, IMF_1 and the residue are shown in Figure 4.2.2.5

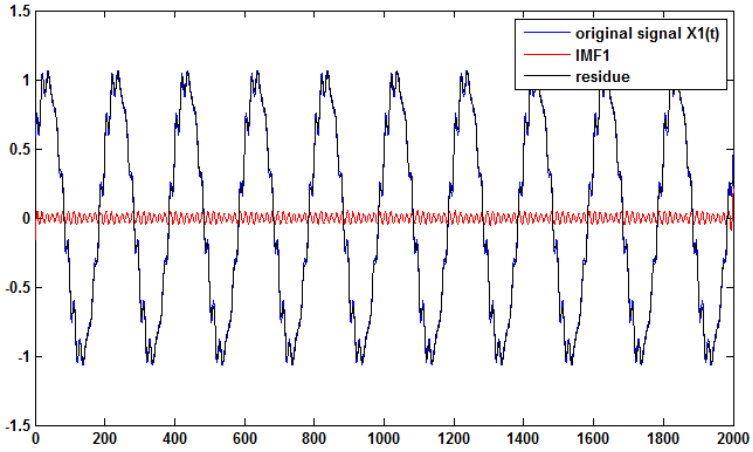

Figure 4.2.2.5 The original signal $X_1(t)$, IMF_1 and the residue after iteration 1

Figure 4.2.2.5 shows that the residue is still above the specified threshold. Therefore, according to step 8 of the algorithm, the residue is considered as the signal $x(t)$ to be processed and the process is then repeated.

The IMFs obtained from the whole decomposition process using the EMD with masking signal are shown in Figure 4.2.2.6.

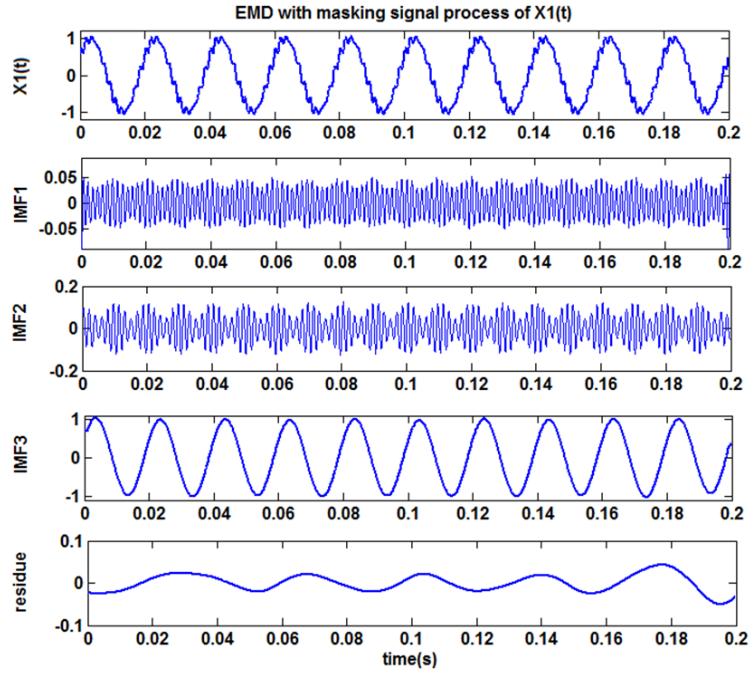

Figure 4.2.2.6 The EMD with masking signal process of $X_1(t)$

Figure 4.2.2.6 shows that the method has succesfully identified all the components of the signal containing close frequency. The waveforms of the IMFs are less mixed with other frequency which demonstrates the advantage of using the masking signal with the EMD process. However, the use of masking signal does not guarantee that the IMF obtained from the process will be free from mixing with other frequency. For example, the waveform of IMF_2 in Figure 4.2.2.6 clearly indicates that it is a modulation of more than one frequency components.

Further, all IMFs in Figure 4.2.2.6 show the existence of end effect problem at both ends of their waveforms. The error at both ends of the IMF may propagate to the interior of the data span that may corrupt the subsequent lower frequency IMFs [45].

The results from the Hilbert Transform of the IMFs are shown in Table 4.2.

Table 4.2
The results of HT of the IMFs from EMD process of $X_1(t)$

	Amp (p.u)	Freq (Hz)	Phase (deg)
IMF_1	0.0399	650	30.14
IMF_2	0.0863	550	29.93
IMF_3	0.9958	50	29.99
IMF_4	0.0208	28	128.80

Table 4.2 shows that all the frequencies and the phase angles of the signal components have been detected correctly. However, the amplitude of each IMF does not show an accurate decomposition result since all the harmonic (550Hz and 650 Hz) amplitudes are smaller than the actual values specified in (4-5), particularly for IMF_1.

4.2.3. EMD with Masking Signal and FFT method [46]

While the algorithm described in section 4.2.1 estimates the frequency of masking signal using an empirical formula, another algorithm is proposed [46] to use FFT to guide the construction of the masking signal. The FFT is applied to identify the frequency and amplitude of the signal components which are then used to construct appropriate masking signal to help the EMD process for the decomposition of the signal containing close frequencies.

The algorithm is described as follows [46]:

1. Apply FFT to the signal being analysed, $x(t)$, to estimate its frequency components , $f_1, f_2, f_3, ... f_n$ where $f_1 < f_2 < f_3 .... < f_n$.
2. Starting from the highest frequency, for every f_k, $k = n, n-1, n-2, ...2$, construct masking signals, $mask_k = M_k \times sin(2\pi(f_k + f_{k-1})t)$. It is suggested to use M_k as 5.5 x amplitude of f_k obtained in FFT spectrum. The value of M_k is empirical.
3. Compute two signals $x(t) + mask_k$ and $x(t) - mask_k$. Apply EMD to both signals to obtain their first IMFs, IMF_+ and IMF_-.
4. IMF_k is defined as $(IMF_+ + IMF_-) / 2$. The averaging step will cancel out the positive and negative instances of the masking signal leaving only the portion of the signal at frequency f_k.
5. Each IMF obtained is assumed as a modulation of 2 sinusoids. To identify the sinusoids, apply the demodulation process to IMF_k to obtain the amplitude, frequency and phase of these sinusoids which may mix in IMF_k.

   A fluctuating IMF indicates that the signal contains a mixture of more than one sinusoid. The waveform is similar to an AM (Amplitude Modulation) signal usually used in radio communication. The AM signal can be produced from an original signal (which is usually of lower frequency) and modulate (multiply) it by another signal. A demodulation process is the reverse of the modulation process which means that it basically works to obtain the components of the modulated signal.
6. Create two sinusoidal representations of IMF_k denoted by $c_k(t)$ using the amplitudes, frequencies and phase angles of the sinusoids obtained from the demodulation process.
7. Compute the residue, $r_k(t) = x(t) - c_k(t)$ then replace $x(t)$ with $r_k(t)$.
8. Perform steps 3 – 7 iteratively using the next masking signals and replacing $x(t)$ with the residue obtained until $n-1$ IMFs containing frequency components $f_2, f_3, ... f_n$ are extracted. The n^{th} residue $r_n(t)$ will contain the remaining component f_1.
9. Compute the residue, $r_k(t) = x(t) - c_k(t)$

10. If the residue, $r_n(t)$, is below a threshold value of error tolerance (0.5% of the maximum value of the original signal), stop the process. Otherwise replace the signal $x(t)$ with $r_n(t)$ and repeat steps 1 – 9 on the new $x(t)$, to obtain the next IMF and a new residue.

4.2.4. Results from EMD with Masking Signal and FFT method

A simple test is also made to see the performance of the method to decompose the same PQ signal containing close frequency specified in section 4.2.2 as follows:

$$X_1(t) = \sin(2\pi 50t + 30^0) + 0.091\sin(2\pi 550t + 30^0) + 0.077\sin(2\pi 650t + 30^0) \quad (4\text{-}5)$$

To decompose $X_1(t)$ by using the technique, the FFT is carried out first to identify the amplitudes and frequencies of the harmonic components of $X_1(t)$. The amplitude M_k and frequency $\hat{f}_k$ of masking signal are then calculated from the highest to the lowest frequency component as shown in Table 4.3.

Table 4.3

The calculated masking signals

$mask_k$		
k	M_k (p.u)	$\hat{f}_k$ (Hz)
3	0.424	1200
2	0.5005	600

Each of the masking signals shown in Table 4.3 is used to help the EMD process to reduce the mixing of the close frequency components in the same IMF.

In the first iteration (k = 3) of the process, the $mask_3$ masking signal is used to obtain IMF_+ and IMF_- shown in Figure 4.2.4.1:

a) b)

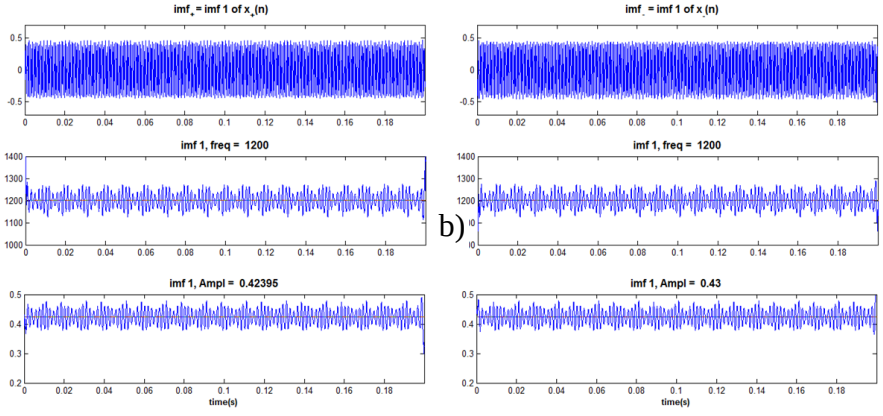

Figure 4.2.4.1. The EMD process using masking signal and FFT at iteration 1 (k = 3)
a) IMF_+ , b) IMF_-

Averaging the above IMFs following step 4 of the method results an IMF as shown in Figure 4.2.4.2 (a). The Hilbert Transform of the averaged IMF is shown in Figure 4.2.4.2 (b)-(d).

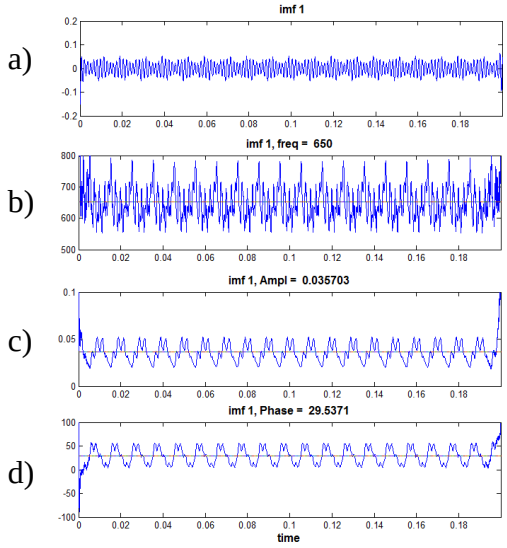

Figure 4.2.4.2.: a) The average of IMF_+ and IMF_- for k=3,
b) the inst. amplitude, c) the inst. frequency, d) the inst. phase.

Figure 4.2.4.2(a) shows that the averaged IMF contains less mixed frequency. The mean value of the instantaneous frequency obtained from HT of the IMF, as shown in Figure 4.2.4.2 (b), represents correctly the frequency of the highest signal component (650 Hz). However, the mean value of the instantaneous amplitude waveform obtained from HT of the IMF shown in Fig. 4.2.4.2 (c) is 0.0357 p.u, which is smaller than the actual amplitude for 650 Hz component specified as 0.077 p.u.

According to step 5 of the algorithm, each IMF obtained from the averaging process is considered as a mixture of a dominant high frequency component, along with a remnant lower frequency component. A demodulation process is therefore required to further identify the components of the IMF.

The demodulation technique used in the algorithm basically assumes that the IMF contains two sinusoids [46], which can be demodulated by using parametric methods such as MUSIC algorithm to estimate the amplitudes, frequencies and phases of these sinusoids. By applying the demodulation process to the IMF shown in Figure 4.2.4.2(a), the components are obtained as given by Table 4.4 :

Table 4.4

The result of demodulation process of IMF from iteration 1, k=3

Amp (p.u)	Freq (Hz)	Phase (deg)
0.0126	550	20
0.0340	650	30

Table 4.4 shows that the demodulation process has identified 550Hz component which is mixed with the dominant 650 Hz component in IMF_1. The 550 Hz component was not detected by the Hilbert Transform as shown in Figure 4.2.4.2. Table 4.4 demonstrates the advantage of the EMD using masking signal and FFT over the original EMD using masking signal only, which does not perform any post processing of the resulting IMF. Further, the detected sinusoids in the mixed IMF can be used to represent the IMF as a two sinusoidal representations $c_3(t)$ which are free from the inaccuracy caused by the end effect issue. These representation can then be subtracted from the original signal, instead of subtracting the original IMF, to obtain more accurate result.

The detected sinusoids $c_3(t)$ from Table 4.4 are then subtracted from the original signal to obtain the residue $r_3(t)$. Since k is still greater than 2, the residue is then considered as the new signal to be processed $x(t)$ and the process is repeated from step 3 to step 7.

The second iteration is performed by using the next masking signal (k=2) to obtain the next IMF_+ and IMF_- which are then averaged and demodulated. The result from iteration 2 is shown in Table 4.5.

Table 4.5

The result of demodulation process of IMF from iteration 2, k=2

Amp (p.u)	Freq (Hz)	Phase (deg)
0.0774	550	30
0.042	650	30

The result in Table 4.5 is used to create the sinusoidal representation $c_2(t)$ which is then subtracted from the signal $x(t)$ to obtain the next residue $r_2(t)$.

According to step 8 of the algorithm, when two IMFs contain frequency components of 550 Hz and 650 Hz have been subtracted from the signal consists of 3 components as given by (4-5), the final residue $r_2(t)$ will contain the remaining

fundamental component 50 Hz. The Hilbert Transform can then be used straight away to obtain the instantaneous amplitude, frequency and phase of $r_2(t)$ as shown in Table 4.6.

Table 4.6

The residue after iteration 2

Amp (p.u)	Freq (Hz)	Phase (deg)
1	50	30

The detected amplitude, frequency and phase in Table 4.6 is then subtracted from the signal to obtain the new residue. The signal reconstructed from detected components, $X_1(t)$ and the residue of the process is shown in Figure 4.2.4.3

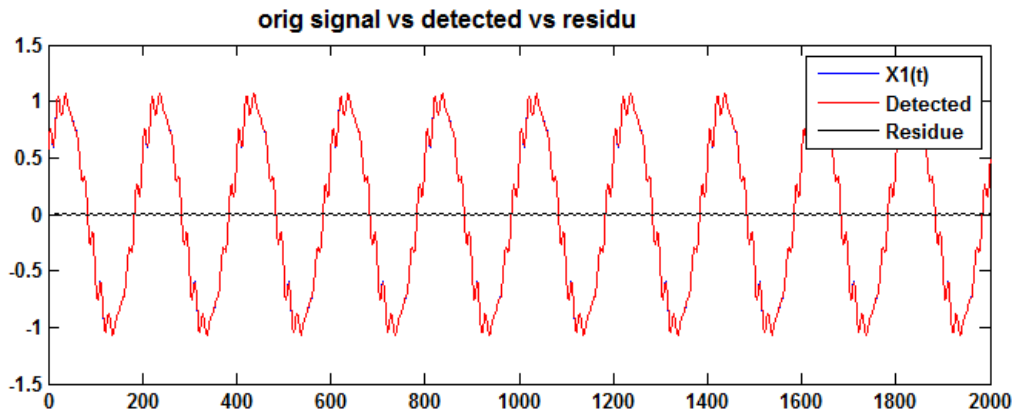

Figure 4.2.4.3 The original signal $X_1(t)$, reconstructed signal, and the residue

Figure 4.2.4.3 shows that the reconstructed signal is quite close to the original signal. However, the residue is still greater than the specified threshold (0.5% of the maximum value of the original signal), and therefore more iterations are required to obtain more accurate result.

The process is then repeated by applying FFT to the residue in the next iterations. The whole result of the algorithm is shown in Table 4.7.

Table 4.7

The result of EMD with Masking Signal and FFT method

Amp (p.u)	Freq (Hz)	Phase (deg)
0.0126	550	20
0.0340	650	30
0.0774	550	30
0.0420	650	30
1.0000	50	30
0.0001	550	90
0.0003	650	30
0.0023	550	94.86
0.0004	650	30
0.0000	550	280
0.0002	650	30

Table 4.7 shows that more components of the correct frequencies are detected in the next iterations. Similar frequencies from Table 4.7 can be combined to obtain the final result of the process shown in Table 4.8.

Table 4.8

The Final result of EMD with Masking Signal and FFT method

Amp (p.u)	Freq (Hz)	Phase (deg)
0.0769	650	30
0.0909	550	30.00
1.0000	50	30.00

Table 4.8 demonstrates that the algorithm has accurately decomposed the PQ signal containing close frequency.

In order to test the performance of the algorithm to decompose close frequency signal, a signal containing even higher frequency $X_2(t)$ given by (4-6) is used.

$$X_2(t) = \sin(2\pi 50t + 30^0) + 0.0182\sin(2\pi 2750t + 30^0) + 0.0175\sin(2\pi 2850t + 30^0) \quad (4\text{-}6)$$

The result of the decomposition process is shown in Table 4.9.

Table 4.9

The result of EMD with masking signal and FFT of $X_2(t)$

Amp (p.u)	Freq (Hz)	Phase (deg)
0.0089	2750	30
0.0106	2850	30
0.0092	2750	30
0.0068	2850	30
1	50	30

Similar frequencies can be combined to obtain the final result as shown in Table 4.

Table 4.10

The Final result of EMD with masking signal and FFT on $X_2(t)$

Amp (p.u)	Freq (Hz)	Phase (deg)
0.0175	2850	30
0.0181	2750	30
1	50	30

Table 4.10 demonstrates that the algorithm has successfully decomposed signal $X_2(t)$ which containing higher and closer frequency by using masking signal and FFT. The decomposition result shows the accuracy of the EMD with masking signal and FFT method over the EMD with masking signal only.

However, the EMD process using masking signal and FFT algorithm may not be efficient, since the use of FFT is required to guide the masking signal estimation. If one already has the amplitude, frequency and phase solution for each component from FFT, why further work is needed by using HHT?

Further, the use of masking signal does not guarantee that the IMF obtained will not be mixed with other frequency component [46] and therefore the demodulation process using parametric method is required to identify the component of the (still mixed) IMF by assuming that the IMF consists of 2 sinusoids. If one knows exactly the total number of components in the original signal, a decomposition process using parametric method (such as MUSIC algorithm) can be applied directly to decompose the signal. The difficulty lies in the fact that the total number of harmonic components is usually unknown.

4.3. The proposed Iterative HHT

As described in section 3.6.2, the HHT has been found to have difficulty in resolving waveforms containing components with close frequencies with a ratio of less than two. Although efforts have been made to resolve the problem by using the EMD with masking signal [6] and EMD with masking signal and FFT [46], there are still some issues with the methods.

In the EMD with masking signal method [6], the IMFs obtained from the process suffer from the end effect problem which causes inaccuracies at both ends of the IMFs. When the error is processed further by the EMD algorithm, it may propagate to the inner part of the data span which can corrupt the next lower frequency IMFs.

In EMD with masking signal and FFT method, the FFT needs to be carried out to correctly calculate the masking signal frequency. However it appears that there is a duplication of work in doing this because the FFT can already perform the decomposition process.

In order to perform more efficient computation of EMD, a modified EMD technique is proposed in this research. The proposed method uses an iterative process of HHT to estimate the signal components and therefore is referred to as the iterative HHT [47].

Since the application of EMD to the signal containing close frequency usually produce mixed IMF, appropriate steps in the proposed method need to be carried out to utilize the mixed IMF in the decomposition process. The stopping criteria may need to be adjusted to obtain a correct mean value of the instantaneous frequency. Experiments carried out in the research has found that the following stopping criteria (or smaller) should be used (θ_1 = 0.005, θ_2 =0.05 and tol= 0.005).

Each mixed IMF obtained from the EMD process of a signal containing close frequency components can be assumed as a combination of a dominant high frequency component, along with a remnant lower frequency component [46]. While the IMF is still mixed, The Hilbert Transform of the IMF generally produce the instantaneous frequency of the IMF with the mean value equals to the frequency of the dominant component.

Therefore, in this approach, a sinusoidal representation of the dominant component is then created by using the mean value of the instantaneous frequency,

amplitude and phase of the first IMF. Although the value of instantaneous amplitude and phase angle of the IMF may not be accurate, they can be calculated iteratively to improve the accuracy of the result.

The sinusoidal representation of the first IMF is then subtracted from the original signal and the process is then repeated. Any error obtained during the calculation in any of these IMFs can be recovered in the succeeding iterative steps [47].

Since the highest frequency component has been taken out from the original signal in the first iteration, the lower frequency component can be found more easily in the next iteration by applying EMD process to the residue.

In this way, the issue of mixed IMFs obtained from the EMD process of a signal containing close frequency components with ratio of the signal frequency much less than 2 is resolved. The proposed method does not require any treatment (such as by introducing masking signal) to make the IMF less mixed or to estimate the components in the mixed IMF by using any extra technique such as demodulation process.

The proposed iterative HHT differs from the standard HHT process in two important respects [38].

First, in the standard HHT all of the obtained IMFs are taken as the final decomposition result. Therefore, no more calculation is needed. The HT is then performed on these IMFs. In the proposed iterative method, at each iteration only the first IMF is taken from each EMD process, then the HT is applied to that IMF to obtain the sinusoidal representation of the IMF. The sinusoidal representation is then subtracted from the signal. Therefore, further calculation is needed to repeat the process on the remainder.

Second, the standard HHT uses the original IMF waveform obtained from the sifting process to be subtracted from the signal before doing the next sifting in the EMD algorithm, despite the fact that the IMF may be mixed. In the proposed iterative method, at each iteration, the IMFs are represented by pure sinusoids whose amplitude, frequency and phase are obtained from the mean values of the instantaneous amplitude, frequency and phase given by the HT. The errors in the calculated amplitude and phase angle of the sinusoidal representation of the signal components can be corrected as the iterative process progresses.

The steps for the iterative HHT of a signal x(t) are described as follows:

1. Find the first IMF using the standard EMD process of x(t).
2. Use the HT to approximate the instantaneous frequency, amplitude and phase of the first IMF. These approximation are then used to create the sinusoidal representation of the IMF given by:

$$P(t) = \tilde{A}_1 \sin(2\pi \tilde{f}_1 \, t + \tilde{\varphi}_1) \tag{4-7}$$

   Where:

   $P(t)$= sinusoidal representation of the first IMF

   $\tilde{A}_1$ = approximated amplitude of the first IMF

   $\tilde{f}_1$ = approximated frequency of the first IMF

   $\tilde{\varphi}_1$ = approximated phase angle of the first IMF

   Since the IMF usually contain inaccuracies at both ends as shown in section 3.4.1 and Figure 3.4.1.1, the approximated amplitude, frequency and phase are taken by averaging the 10% - 90% length of the instantaneous amplitude, frequency and phase data points obtained from the HT of the IMF.
3. Subtract the sinusoidal representation of the first IMF from the original signal to obtain the residue, *r(t)*

$$r(t) = x(t) - P(t) \tag{4-8}$$

4. Steps 1-3 are repeated on *r(t)* until the amplitude of the first IMF reaches a low threshold value. The smaller the threshold, the longer the program will keep going to decompose and subtract detected components from the original signal. From experience, a threshold of 0.5% of the maximum value of the simulated signal has been found to be sufficient to obtain an accurate result. However, for a measured signal, the threshold needs to be increased to 3% to take the noise in the signal into account [47].
5. In the iterative HHT method, it is possible that similar frequencies are obtained during the iterative process of decomposition. For each frequency f_k, obtained in the Iterative HHT process, the sinusoidal representation associated with that frequency can be added together as given in (4-9) and then the Hilbert Transform is applied to obtain the

amplitude, frequency and phase of that frequency component. These sinusoids are then sorted by frequency.

$$R_k = \tilde{A}_1 \sin(2\pi \tilde{f}_k \, t + \tilde{\varphi}_1) + \tilde{A}_2 \sin(2\pi \tilde{f}_k \, t + \tilde{\varphi}_2) + \ldots\ldots$$

$$\ldots\ldots + \tilde{A}_n \sin(2\pi \tilde{f}_k \, t + \tilde{\varphi}_n) \qquad (4\text{-}9)$$

4.4. Results from the Iterative HHT

To evaluate the performance of the proposed method, the Iterative HHT is then tested to decompose the stationary signal $X_1(t)$ given in (4-5). The result of the first iteration is shown in Figure 4.4.1

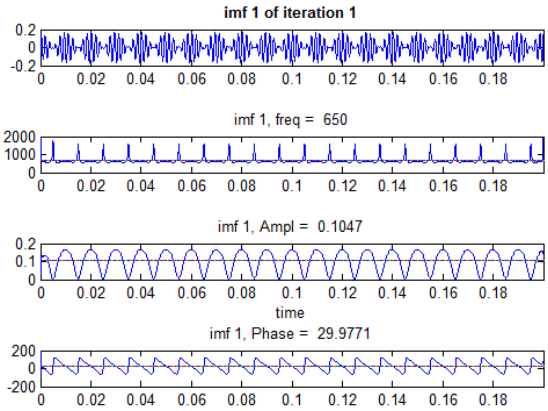

Figure 4.4.1 The first IMF from iteration 1 of the IHHT process on $X_1(t)$

Figure 4.4.1 shows the first IMF from iteration 1 of the IHHT process on $X_1(t)$, which contains mixed frequencies due to the close frequency components which were not separable by the EMD process of the signal. The mean value of the instantaneous amplitude 0.1047 p.u is also higher than the specified value 0.0769 p.u which indicates that the IMF contains other signal components.

However, the mean value of instantaneous frequency of the dominant component of IMF_1 is correctly identified as 650 Hz, which is the most important thing at this stage since the next iteration will be able to correct the error in amplitude and phase angle value. The Hilbert Transform of the first IMF at the first iteration is shown in Table 4.11.

Table 4.11

The HT of IMF_1 at iteration 1

Amp (p.u)	Freq (Hz)	Phase (deg)
0.1047	650	29.97

A sinusoidal representation is then constructed based on the mean value of the instantaneous amplitude, frequency and phase shown in Table 4.11. The sinusoid is then subtracted from the original signal to obtain the first residue $r_1(t)$ which will then be considered as the new signal to be processed in the second iteration. The result of the second iteration is shown in Figure 4.4.2.

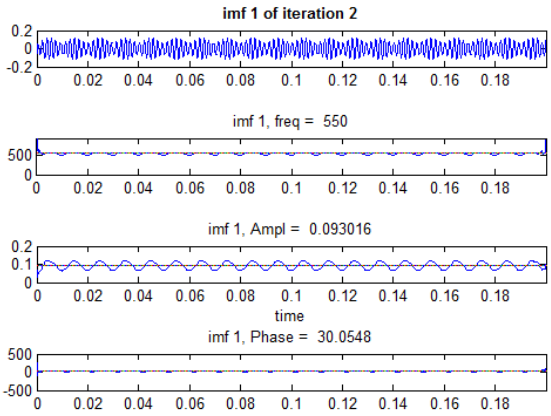

Figure 4.4.2 The first IMF from iteration 2 of the IHHT process on $X_1(t)$

Figure 4.4.2 shows the first IMF from iteration 2 which looks a bit mixed. The mean value of the instantaneous amplitude 0.093 p.u is also higher than the specified value 0.091 p.u. The mean value of the instantaneous frequency is correctly identified as 550 Hz. The Hilbert Transform of the first IMF at iteration 2 is shown in Table 4.12.

Table 4.12

The Hilbert Transform of IMF_1 at iteration 2

Amp (p.u)	Freq (Hz)	Phase (deg)
0.093	550	30.05

A sinusoidal representation is then constructed based on the mean value of the instantaneous amplitude, frequency and phase shown in Table 4.12. The sinusoid constructed from Table 4.12 is then subtracted from the signal being analysed to obtain the second residue $r_2(t)$ which will then be considered as the new signal to be processed in the 3rd iteration, the process is iteratively repeated until the threshold is reached. The whole result of the IHHT process on signal $X_1(t)$ is shown in Table 4.13.

Table 4.13

The result of IHHT process on $X_1(t)$

iteration	Amp (p.u)	Freq (Hz)	Phase (deg)
1	0.105	650	29.98
2	0.093	550	30.05
3	0.028	650	209.81
4	1.000	50	30.00

Table 4.13 shows that some of the sinusoids obtained have the same frequency value. The sinusoids of the same frequency are then combined to obtain the final result as shown in Table 4.14.

Table 4.14

Final result of IHHT process on $X_1(t)$

True Freq (Hz)	Freq Calc using IHHT (Hz)	True Amp (pu)	Amp Calc using IHHT (pu)	True Phase (deg)	Phase Calc using IHHT (deg)
650	650	0.077	0.077	30	30.04
550	550	0.091	0.093	30	30.05
50	50	1.000	1.000	30	30.00

Table 4.14 shows the final results of the Iterative HHT for the stationary signal $X_1(t)$ which demonstrates that this process can decompose the signal correctly.

The Iterative HHT is also tested to decompose the stationary signal containing higher frequencies $X_2(t)$ given in equation (4-6). The result of the first iteration is shown in Figure 4.4.3.

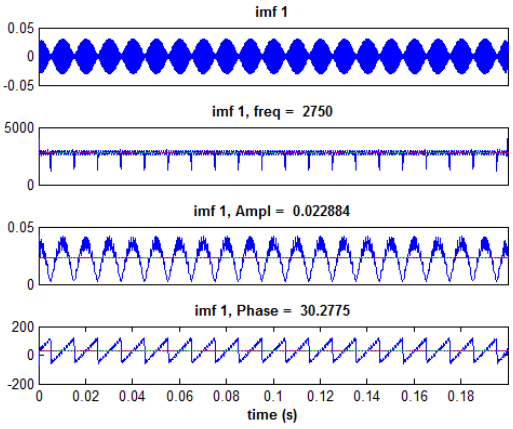

Figure 4.4.3 The first IMF from 1st iteration of the IHHT process on $X_2(t)$.

Figure 4.4.3 shows the first IMF from iteration 1 of the IHHT process on $X_2(t)$, the mean value of instantaneous frequency is correctly identified as 2850 Hz, the mean value of the instantaneous amplitude and phase angle are identified as 0.018 p.u and 30^0 respectively. The Hilbert Transform of the IMF is shown in Table 4.15.

Table 4.15

The HT of IMF_1 at iteration 1

Amp (p.u)	Freq (Hz)	Phase (deg)
0.023	2750	30.3

A pure sinusoid is then constructed based on the mean value of the instantaneous amplitude, frequency and phase shown in Table 4.15. The sinusoid is then subtracted from the original signal to obtain the first residue $r_1(t)$ which will then be considered as the new signal to be processed in the second iteration. The result of the second iteration is shown in Figure 4.4.4.

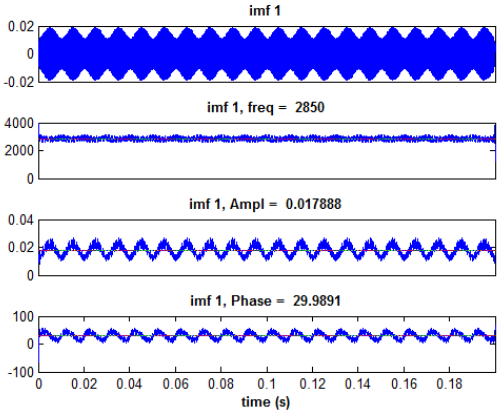

Figure 4.4.4 The first IMF from 2nd iteration of the IHHT process on $X_2(t)$.

Figure 4.4.4 shows the first IMF from iteration 2 of the IHHT process on $X_2(t)$, the mean value of instantaneous frequency is correctly identified 2750 Hz. The mean value of the instantaneous amplitude and phase angle are identified as 0.0185 p.u. and 30^0 respectively. The Hilbert Transform of the IMF is shown in Table 4.16.

Table 4.16

The HT of IMF_1 at iteration 2

Amp (p.u)	Freq (Hz)	Phase (deg)
0.0179	2850	29.99

A pure sinusoid is then constructed based on the mean value of the instantaneous amplitude, frequency and phase shown in Table 4.16. The sinusoid is

then subtracted from the signal being analysed to obtain the second residue $r_2(t)$ which will then be considered as the new signal to be processed in the 3rd iteration, the process is iteratively repeated until the threshold is reached. The whole result of the IHHT process on signal $X_2(t)$ is shown in Table 4.17.

Table 4.17

The result of IHHT process on $X_2(t)$

iteration	Amp (p.u)	Freq (Hz)	Phase (deg)
1	0.023	2750	30.28
2	0.018	2850	29.99
3	0.005	2750	211.35
4	1	50	30.00

Table 4.17 shows that some of the sinusoids obtained have the same frequency value. The sinusoids of the same frequency are then combined to obtain the final result as shown in Table 4.18.

Table 4.18

Final result of IHHT process on $X_2(t)$

True Freq (Hz)	Freq Calc using IHHT (Hz)	True Amp (pu)	Amp Calc using IHHT (pu)	True Phase (deg)	Phase Calc using IHHT (deg)
2850	2850	0.0175	0.0179	30	29.99
2750	2750	0.0182	0.0182	30	30.01
50	50	1.000	1.000	30	30.00

Table 4.18 shows the final results of the Iterative HHT for the signal $X_2(t)$ which demonstrates that the proposed method of successively subtracting sinusoidal representation of the first IMF instead of the original IMFs (which is used in the standard HHT) has led to greater accuracy when dealing with harmonic signals.

To examine the performance of the proposed method, the standard HHT and the proposed iterative HHT are then tested to decompose various combinations of harmonic signal from 1 to 4 harmonic components. To do the test, a harmonic signal with n components is constructed [38] as given by (4-10) :

$$S(t) = A\sin(2\pi ft + \varphi_1) + \frac{A}{k(\beta)}\sin(2\pi k(\beta) ft + \varphi_2) + \ldots$$
$$\frac{A}{k(\beta + n - 1)}\sin(2\pi k(\beta + n - 1) ft + \varphi_{n+1}) \quad (4\text{-}10)$$

Where :

A = the amplitude of the fundamental signal

f = 50 Hz

$k(m)$ = 3,5,7,9..., for m=1,2,3,4,....

φ = phase in radians

β = constant offset

For example, a signal containing 50, 350,450,550 Hz will have n=3 since there are three harmonics (7^{th}, 9^{th} and 11^{th}), β =3 since $k(3) = 7$, followed by $k(4) = 9$ and $k(\beta + n-1) = k(5) = 11$. So the signal will be of the form given by (4-11):

$$S(t) = A\sin(2\pi ft + \varphi_1) + \frac{A}{7}\sin(2\pi k7\, ft + \varphi_2) + ... \\ \frac{A}{9}\sin(2\pi 9\, ft + \varphi_3) + \frac{A}{11}\sin(2\pi 11\, ft + \varphi_4) \quad (4\text{-}11)$$

In the research, all of the harmonic signals analysed contain the fundamental component with frequency f at 50 Hz and one to four other harmonic components. The test signals are sampled at 30 kHz over the range 50 Hz to 4950 Hz.

To see the effect of the stopping criteria, different stopping criteria (0.1 x default value and 0.01 x default value) are used. The results are shown in Table 4.19 and Table 4.20.

Table 4.19

Separation of Harmonic Signals using standard HHT

Number of harmonic components (n)	Frequencies separated corectly	
	Stopping criteria : 0.1x default	Stopping criteria : 0.01x default
1	50, 150 Hz to 50, 4950 Hz	50, 150 Hz to 50, 4950 Hz
2	50, 150, 250 to 50, 450, 550 Hz	50, 150, 250 to 50, 850, 950 Hz
3	50, 150, 250, 350 Hz only	50, 150, 250, 350 Hz to 50, 350, 450, 550 Hz
4	50, 150, 250, 350, 450 Hz only	50, 150, 250, 350, 450 Hz to 50, 250, 350, 450, 550 Hz

Table 4.20

Separation of Harmonic Signals using Iterative HHT

Number of harmonic components (n)	Frequencies separated corectly	
	Stopping criteria : 0.1xdefault	Stopping criteria : 0.01xdefault
1	50, 150 Hz to 50, 4950 Hz	50, 150 Hz to 50, 4950 Hz
2	50, 150, 250 Hz to 50, 4850, 4950 Hz	50, 150, 250 Hz to 50, 4850, 4950 Hz
3	50, 150, 250, 350 Hz to 50, 350, 450, 550 Hz , then intermittent success	50, 150, 250, 350 Hz to 50, 750, 850, 950 Hz , then intermittent success
4	50, 150, 250, 350, 450 Hz to 50, 250, 350, 450, 550 Hz then intermittent success	50, 150, 250, 350, 450 Hz to 50, 450, 550, 650, 750 Hz then intermittent success

As shown in Table 4.19 and Table 4.20, for n=1, both HHT and IHHT are able to separate the frequencies upto 50 and 4950 Hz. There is no difference of the performance of both methods, since the signal does not contain close frequency components. For signals containing 2 harmonic components (n=2), the Iterative HHT has successfully separated the components up to 4850, 4950 Hz, while the standard HHT can separate upto 850, 950 Hz only.

When the number of harmonic components increases, the separation of the harmonic components is more difficult. However, the Iterative HHT has successfully separated signals up to the frequency 50, 450, 550, 650, 750 Hz by using the stopping criteria 0.01 x default. Beyond this point, the separation is not always successful.

Tables 4-19 and 4-20 also demonstrate the effect of stopping criteria to the accuracy of the decomposition process. For the stopping criteria used in the Tables, the smaller the stopping criteria, the more accurate the results are.

4.5. **Chapter summary**

This chapter has described several techniques to resolve the mode mixing problem in HHT method. First, the EMD method with masking signal [6] is discussed. In the algorithm, the masking signal was used to reduce the mixing level of 2 or more frequencies in the first IMF. The masking signal is constructed from the

instantaneous frequency and amplitude data, $f_1(t)$ and $a_1(t)$ obtained from the Hilbert Transform of the first IMF. The masking signal is added and subtracted from the original signal, and the average of the resulting IMFs is then assumed to be the correct IMF. The method was found to be effective for the signal investigated by the author. However, the analysis of PQ signal using the method demonstrates that all IMFs obtained from the process suffer end effect problem. The issue may cause the propagation of error to the interior of the data span of the particular IMF and may corrupt the subsequent lower frequency IMFs [45]. In addition, the identified amplitudes of the components are usually lower than the actual specified amplitudes.

Another method of using EMD with masking signal is by carrying out FFT of the signal first, from which the frequency and amplitude of the masking signal can be estimated to reduce the frequency mixing in each IMF [46]. The masking signal is added and subtracted from the original signal, and the average of the two resulting IMFs is assumed to be the the correct IMF. A demodulation process is then applied to estimate the components of each IMF obtained. This method works quite well for most PQ signal investigated, even one with the high frequency component. Its main disadvantage is that the FFT has to be calculated first.

Because of the above issues with both methods, a novel Iterative HHT method is proposed which can carry out the decomposition process without the need of masking signals or calculating the FFT spectrum of the original signal. In this method, only the first IMF is used to obtain the instantaneous amplitude, frequency and phase using the Hilbert Transform. Based on the values of these waveforms, a sinusoidal representation of the IMF is formed and subtracted from the original signal. The process is repeated in an iterative fashion, until the amplitude of the sinusoidal representation is below a certain defined value. The algorithm has been tested with various PQ harmonic waveforms and it has been found to be effective in decomposing them even when the signal contains high frequency components.

The purpose of the method discussed in chapter 4 is to improve the performance of HHT to separate close frequency signal. The separation of such signal should be examined by using signals containing multiple frequencies which are close each other. Therefore, harmonics signals with such frequencies are considered as the most suitable signal for this purpose [6], [7].

The proposed method will also be tested to process the non-stationary signal by first identifying the boundaries of the segments (each of which contains stationary signal) of the original signal. In the next chapter a new method based on the Symbolic Aggregate Approximation will be introduced to determine the boundaries when the signal is non-stationary.

CHAPTER 5 THE SAX BASED BOUNDARY DETECTOR METHOD AND ITERATIVE HHT TO DECOMPOSE NON-STATIONARY SIGNAL

5.1. Introduction to SAX

Most PQ signals are non-stationary in nature whose frequency, amplitude, and phase vary over time. In principle, these could also be assumed as a series of signal segments, which individually would be stationary [47]. As each signal segment is potentially composed of a mixture of different elements, the transition from one segment to the next would be occasioned at an instance where the former mixture is modified to represent that of the latter segment, such as a change in frequencies elements and or phases, which in-turn result in manifested different patterns.

Although the standard HHT can automatically obtain the instantaneous amplitude, frequency, and phase of the components in the non-stationary signal, uncertainties will occur around the area of a transition. To resolve the problem, a new method referred to as Symbolic Aggregate Approximation (SAX) analysis is proposed to identify the instant of changes in the original signal [48]. SAX is a translation method which works by converting the original time series signal into an equitable symbolic sequence. The symbolic representation is then processed to characterize the original signal into various repeating patterns that can be used to identify particular instants, such as those that relate to sudden change. Once the instants of sudden changes have been identified, the composite non-stationary signal could then be divided into a sequence of stationary signals segments. Subsequently, the HHT and the Iterative HHT can then be applied to decompose each of these (stationary signal) segments.

5.2. SAX Algorithm

The algorithm was first introduced in 2002 by Patel, Keogh and colleagues [49], who proposed a symbolic representation which is referred to as SAX (Symbolic Aggregate ApproXimation) of a time series which can be used for data mining purposes such as pattern recognition, anomaly detection and data size reduction .

The first step to obtain a SAX representation of a long time series Q of length n with the elements $q_1, q_2, \ldots . q_n$ is to convert the elements of Q to a dimensionality

reduced representation D of length w with the elements $d_1, d_2, \ldots . d_w$, typically, $w << n$. The dimensionality reduced representation is referred to as Piecewise Aggregate Approximation (PAA) which is obtained by dividing the n-dimensional time series data into w equal sized "frames". The mean value of the normalized data within a frame is calculated to obtain the approximated value d_i of the associated data by implementing the expression given by [48]:

$$d_i = \frac{w}{n} \sum_{j=\frac{n}{w}(i-1)+1}^{\frac{n}{w}i} q_j \tag{5-1}$$

Where :

w = window size

n = length of the signal

The PAA representation is obtained from a series of these approximated values. The subsequent step is to obtain a discrete representation by converting the lower dimensional time series D into a number of symbols with equiprobability. The number of symbols is denoted here by "a". Since a normalized subsequence typically reveals a highly Gaussian distribution characteristic [50], it is required to divide the areas under Gaussian curve equally by determining appropriate "breakpoints".

To map the PAA representation into a sequence of symbols containing an alphabet of "a" symbols, (a-1) breakpoints are needed to segment the region under the Gaussian curve to "a" equally sized areas. These breakpoints $B = \beta_1, \ldots, \beta_{a-1}$ are chosen such that the area under the Gaussian curve from β_i to $\beta_{i+1} = 1/a$. For example, the required breakpoints that divides the Gaussian curve from 3 to 5 of equiprobable regions is shown in Table 5.1 [48].

Table 5.1:

A lookup table that contains the breakpoints that divides a Gaussian distribution in an arbitrary number (from 3 to 5) of equiprobable regions (source: Keogh et.al, "HOT SAX: Efficiently Finding the Most Unusual Time Series Subsequence," 2005 [48]).

β_i \ a	3	4	5
β_1	-0.43	-0.67	-0.84
β_2	0.43	0	-0.25
β_3		0.67	0.25
β_4			0.84

Figure 5.1.1 illustrates a time series which is to be discretized into a PAA approximation using window size w = 32.

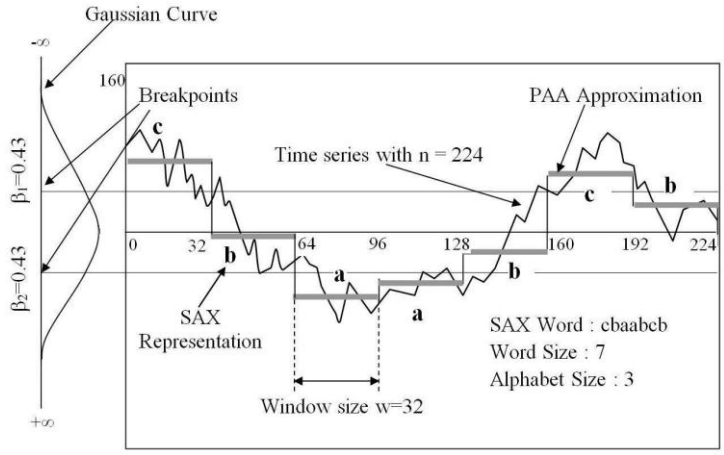

Figure 5.1.1. The process to discretize the time series or signal (thin black line) to obtain a PAA approximation (heavy gray line) and then to convert the PAA coefficients into symbols (bold letters) by using the predetermined breakpoints. In the example above, with n = 224, w = 32 and a = 3, the signal is mapped to a word-size of 7 SAX representation "cbaabcb" (adapted from [48]).

The discrete representation is then symbolized using an alphabet of three symbols (a=3). Two or (a-1) breakpoints are then chosen by looking at Table 5.1, which are β_1 = -0.43 and β_2 = 0.43. (β_0 and β_a are defined as -∞ and ∞, respectively). A sequence of symbols from the PAA representation is referred to as the SAX word, the total number of symbols used in SAX word is the word size, and the range or number of discrete symbols possible in this vocabulary is called the alphabet size.

5.2.1. Applications of SAX

The method of transforming time series data into the SAX representation has been applied to various data mining tasks such as data indexing, anomaly detection, signal classification and clustering [51]. A couple of the applications of SAX representation are explained in more details in the following sub sections.

5.2.1.1. Fault Detection

The SAX method has been applied for rotor bar fault detection of an induction motor [52]. The faulty signatures are determined from the IMF obtained from the EMD process of the start-up current of the induction motor. Based on the experience [53], the second IMF can be used to determine the faulty condition in the rotor bar, as shown in Figure 5.2.1.1.1.

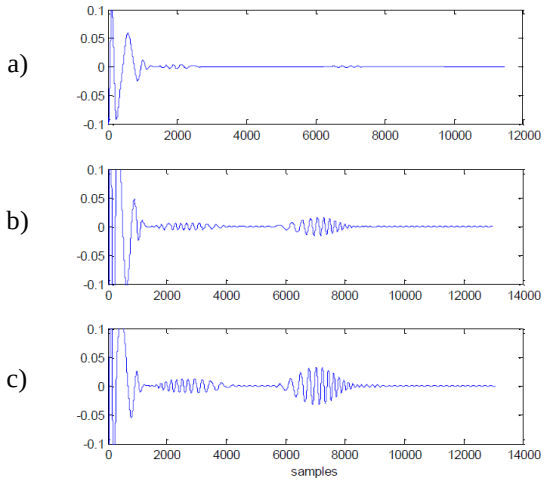

Figure 5.2.1.1.1. : The second IMF of the start-up current for a) healthy machine, b) a machine with one broken bar and c) a machine with two broken bars (source: P. Karvelis et.al, "An intelligent icons approach for rotor bar fault detection," *2013* [53])

Figure 5.2.1.1.1 shows that three categories of the rotor bar healthy conditions (a healthy machine, a machine with one broken bar and a machine with two broken bars) are used as the target classes of the identification process. Each target class has a unique pattern of IMF_2 obtained from the decomposition process of start-up current.

To test the proposed method, the start-up currents from a healthy machine and from a machine with one and two broken rotor bars were recorded. Three different current transducers are used in the recording process to obtain three recordings for each faulty condition. The machine start up were performed 10 times for each faulty condition to obtain 30 recordings for healthy condition, 30 recordings for faulty condition with one broken bar and 30 recordings for faulty condition with two broken bars. The recordings are named based on the faulty conditions, sample #1 to sample #30 are the recordings of healthy machines, sample #31 to sample #60 are the data of machines with one broken bar, sample #61 to sample #90 are the data of machines with two broken bars. Each of the second IMF of the data is normalized and transformed to SAX representations as shown in Figure 5.2.1.1.2

The symbolic representation of the data is used to measure the Euclidean distance of a particular sample to the other samples. A distance matrix of 30 normal machines and 60 faulty machines is then obtained and shown in Figure 5.2.1.1.3

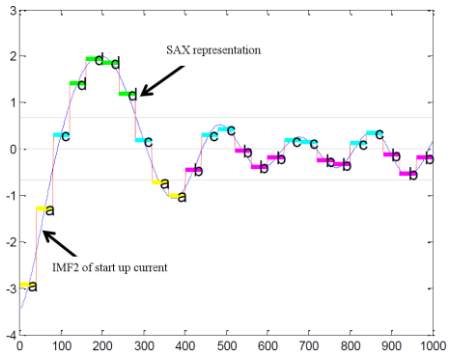

Figure 5.2.1.1.2 IMF_2 of the start up current and the SAX representation (source: P. Karvelis et.al, "An intelligent icons approach for rotor bar fault detection," *2013* [53])

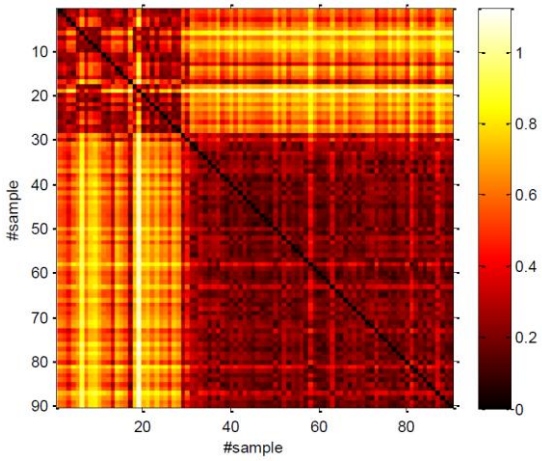

Figure 5.2.1.1.3 The distance matrix of normal and faulty signal (source: P. Karvelis et.al, "An intelligent icons approach for rotor bar fault detection," *2013* [53])

The distance matrix shows small distances (marked by dark colour) between the samples in the same faulty condition and larger distances (marked by light colour) between the samples of different faulty condition. Since the distances of samples #1 to #30 are close to each other, a dark region is manifested at the top right of the matrix. Similarly, the distances of samples #31 to #90 are close to each other which causes a dark region in the bottom left of the matrix. In this way, the distance matrix indicates 2 classes of faulty condition ie. healthy and faulty machine.

An NN classifier is then trained by using the distance data of 89 samples to be able to discriminate the faulty and normal conditions, the last 1 sample is used to test the accuracy of the classifier to estimate the correct class for the test data [52].

5.2.1.2. Data size reduction

Another use of the SAX representation is reported in data size reduction process to classify electrical load consumption patterns. The load consumption patterns which is referred to as Representative Load Pattern (RLP) of each consumer can be represented by using the data points in the time domain or using a reduced number of features. The study proposes the use of Symbolic Aggregate Approximation (SAX) method to form the reduced set of features.

The use of the SAX representation to classify electrical load consumption patterns is clearly simpler than the implementation of principal component analysis (PCA) or Sammon map on a local board [54]. The SAX representation is more intuitive for the operators than the PCA or Sammon map outputs.

5.2.1.3. Anomaly Detection

The SAX symbolic representation can also be used to find anomalies (discords) in ECG signal [48]. By converting the signal to SAX representation, the time series discords can be found as subsequences of a longer time series that are maximally different to all the rest of the time series subsequences. Keogh and colleagues have found in their work that the identified discords coincide with heart disorder. Figure 5.2.1.3.1 shows an ECG signal with 3 anomalies (discords).

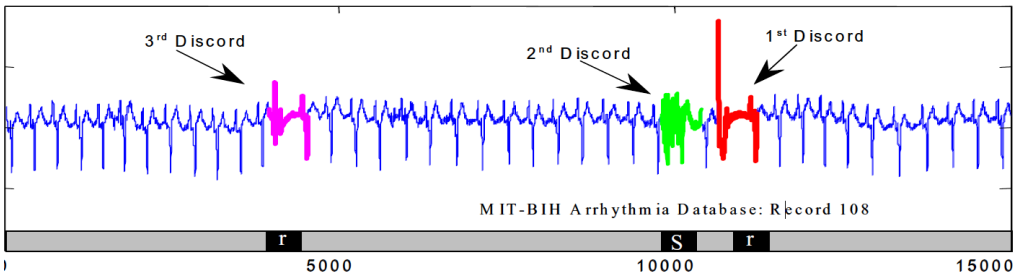

Figure 5.2.1.3.1. An ECG signal with 3 detected anomalies (discords)which exactly coincides with the heart anomaly (source: Keogh et.al, "HOT SAX: Efficiently Finding the Most Unusual Time Series Subsequence," 2005.)

Anomalous pattern detection by using the SAX representation is also used in the assessment of clustered rooftop solar PV impacts in smart grid [55]. Figure 5.2.1.3.2 shows the detection of unusual voltage profile due to distortion by cloud passing. The signal is converted to a SAX representation which is then characterized by using a pattern detector to identify the most unusual patterns.

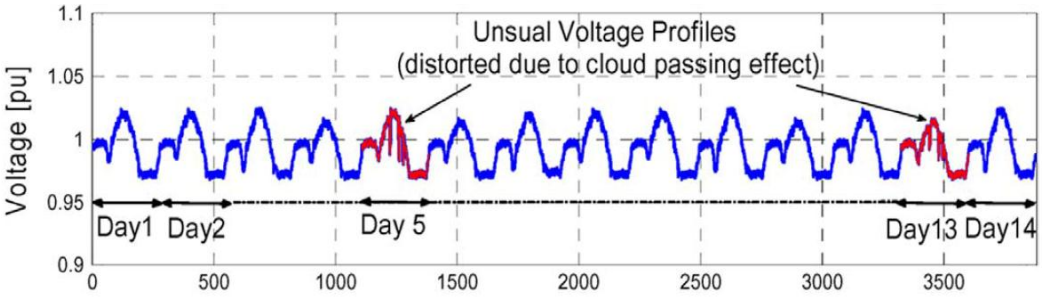

Figure 5.2.1.3.2. Detection of unusual voltage profile (source: Alam et.al, "A SAX-based advanced computational tool for assessment of clustered rooftop solar PV impacts on LV and MV networks in smart grid,", 2013.)

5.2.2. Determination of window size and alphabet size of the SAX representation

In order to transform the non-stationary signal into an accurate SAX representation, the window size "*w*" and alphabet size "*a*" have to be determined properly. If a very large value of "*w*" is chosen, some important details may not be represented clearly in the SAX representation. Basically, the reduced dimensionality in the SAX representation should be able to represent the data properly without loosing any essential feature of the data [56].

For example, a signal S(t) given in (5-2) is transformed to two SAX representations using alphabet size a = 50. The first representation uses w = 20, while the second one uses w = 40. The signal changes at sample point no 1040 as shown in Figure 5.2.2.1.

$$S(t)=\begin{cases}\sin(2\pi 50t_a)+0.091\sin(2\pi 550t_a)+0.077\sin(2\pi 650t_a), & 0\le t_a<0.104s\\ 1.2\sin(2\pi 50t_b)+0.109\sin(2\pi 550t_a)+0.092\sin(2\pi 650t_a), & 0.104\le t_b<0.3s\end{cases} \quad (5\text{-}2)$$

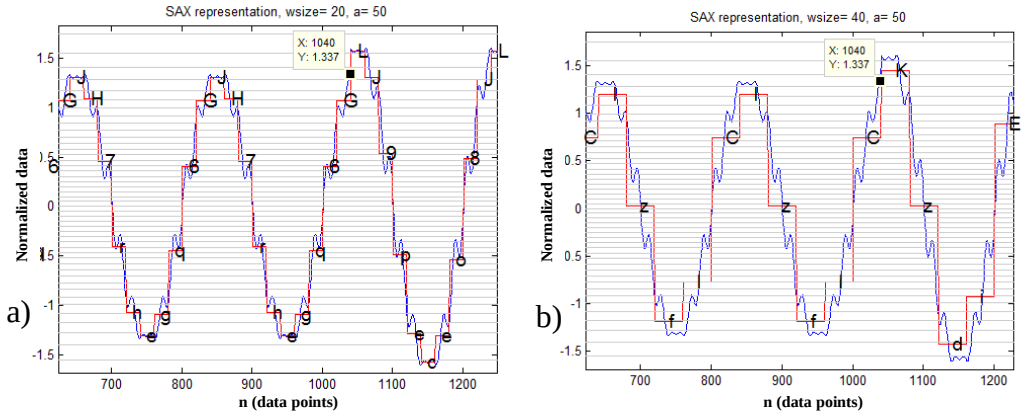

Figure 5.2.2.1: SAX representation of signal *S(t)* with alphabet size a = 50. (a). Using window size w = 20 (b). Using window size w = 40.

Figure 5.2.2.1 (a) shows that the SAX representation with window size 20 can represent the signal before and after the change at point no 1040 as completely

different words. However, when the window size is increased to 40 as shown in Figure 5.2.2.1 (b), the SAX representation transforms two or more sub sequences which are significantly different to a same symbol (in this example, "z" is used to represent such sub sequences). When a boundary detector algorithm is applied to such SAX representation, inaccuracies may occur.

On the contrary, if a very small value of "w" is chosen, The SAX representation may translate insignificant variations (such as the variations due to noise content in the signal) to different symbols which may cause inaccuracy in the boundary detection process.

For example, a noisy periodic signal is generated by using the same formula of the signal *S(t)* given in (5-2) but now it is added with white gaussian noise with Signal – To - Noise Ratio (SNR) = 30. The noisy signal is then transformed to a SAX representation using window size *w* = 5 as shown in Figure 5.2.2.2.

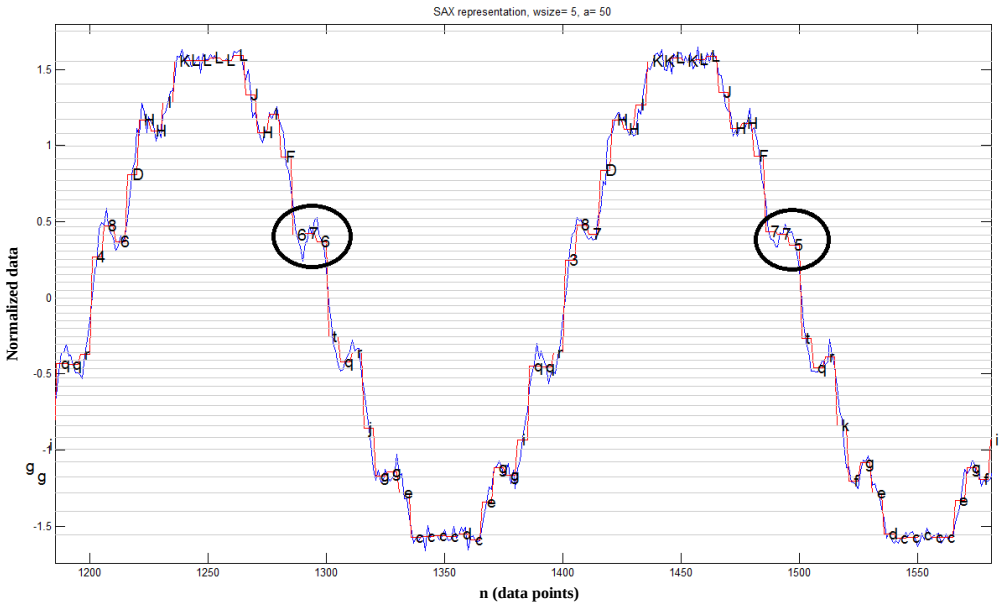

Figure 5.2.2.2 SAX representation of a noisy signal using *w*= 5

Figure 5.2.2.2 shows two consecutive cycles in a noisy periodic signal. It is expected that these two cycles are translated to the same symbolic representation. However, the choice of the window size "*w*" = 5 affects the translation process to obtain inconsistent symbolic representation "676" in former cycle and "775" in the latter cycle. The inconsistency occurs since the symbolic code is obtained by averaging the inconsistent noisy data within a short window. A sufficiently longer window size is needed to let the mean value of the noise content to be very small which can be neglected to obtain an accurate symbolic representation.

To get rid of the inconsistent translation, a larger window size w = 10 is used to transform the noisy signal to another SAX representation, as shown in Figure 5.2.2.3.

It is then necessary to note here, that the dimensionality reduced representation should be able to ignore any insignificant variations of the original data and to obtain patterns, which represents all the essential feature of the original signal. By choosing a proper window size "*w*", the noise content or insignificant variations can be ignored in the averaging process of the noisy data, while at the same time retain the essential feature of the data.

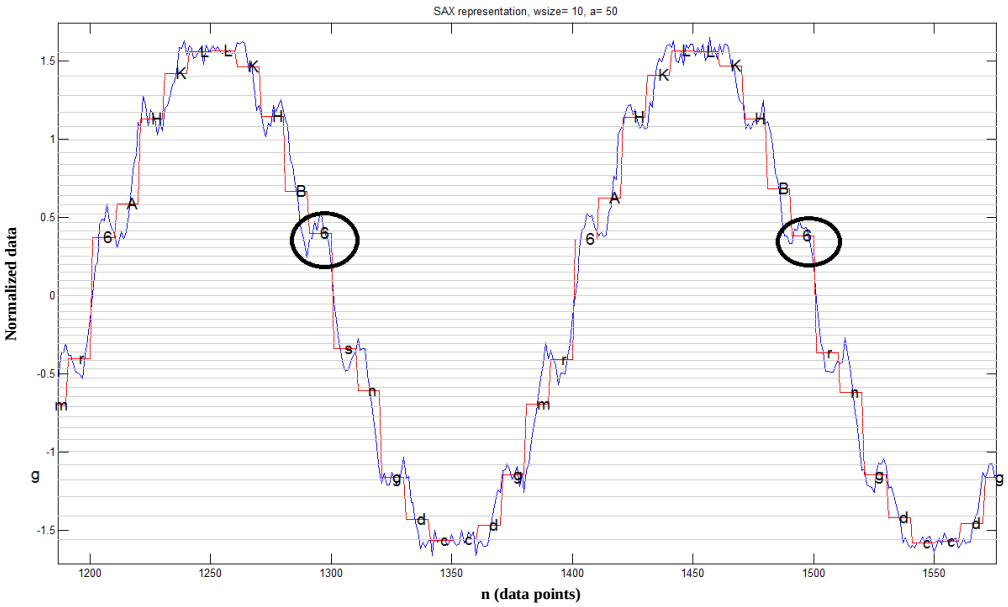

Figure 5.2.2.3 SAX representation of a noisy signal using *w*= 10

Figure 5.2.2.3 shows that by changing the window size *w* to 10, the periodic sub-sequence is now translated to the same symbol as expected.

In the research, when the alphabet size used to represent the signal is larger, usually the boundary detection process is more accurate. However, when the alphabet size is too large, insignificant variations may be translated as different symbols in the SAX representation, which is undesireable. The experiments carried out in the research has found that the alphabet size of 50 is quite effective for accurate boundary detection of PQ signal.

5.3. The SAX Based Boundary Detector Algorithm

Once the SAX representation of a non-stationary signal is obtained, the next process is to identify any pattern change which may indicate a change in frequencies,

amplitudes or phases of the signal components. The technique to detect the changes in the signal is referred to as the boundary detector algorithm, which can be described as follows :

1. Convert the symbols of SAX representation to a numeric alias (for example "a" = 1, "b" = 2 and so on) to facilitate the comparison process.
2. Find out the cycle length *cyc* of the periodic signal.
3. Set the base point of searching *bsearch* equals to *cyc+1*
4. Set the starting point of the search *i* equals to *bsearch*
5. Compare the value of window *i* to window *i-cyc* (the window of previous cycle). A window contains only a number / symbol of SAX representation.
6. If the difference of the numerical value of window *i* to window *i-cyc* ≥ 1 AND

   the difference of the numerical value of window *i + 1* to window *i-cyc+1* $\geq$ 1, mark the window as the change window, then compare the cumulative sum of the Euclidean distance to a predefined threshold.
7. If the cumulative sum of the Euclidean distances of the previous and current sub-sequences of a cycle exceeds a predefined threshold, mark the first point of change as the boundary *bnd*, set the base point of next search *bsearch* equals to *bnd + cyc +1* then reset the cumulative sum to zero.
8. If the the cumulative distance does not satisfy step 6, repeat step 5 to 7 on the next window *(i+1)*.
9. Stop the process if the sliding window *i* reaches the end of the signal.

5.4. Applying IHHT and SAX-based Boundary Detector to non-stationary signals

To test the ability of the SAX-based boundary detector, as well as the Iterative and standard HHT algorithms to decompose a nonstationary harmonic signal contains close frequency, a couple of examples are described in the following sections.

5.4.1. Non-stationary PQ waveform with harmonics variations

A non-stationary signal contains variations of harmonic components is given by (5-3) and shown in Figure 5.4.1.1.

$$S_k(t) = \begin{cases} \sin(2\pi 50 t_a) + 0.33\sin(2\pi 150 t_a), & 0 \le t_a < 0.1s \\ \sin(2\pi 50 t_b) + 0.091\sin(2\pi 550 t_b) + 0.077\sin(2\pi 650 t_b), & 0.1 \le t_b < 0.2s \\ \sin(2\pi 50 t_c) + 0.2\sin(2\pi 250 t_c) + 0.143\sin(2\pi 350 t_c), & 0.2 \le t_c < 0.3s \end{cases} \quad (5\text{-}3)$$

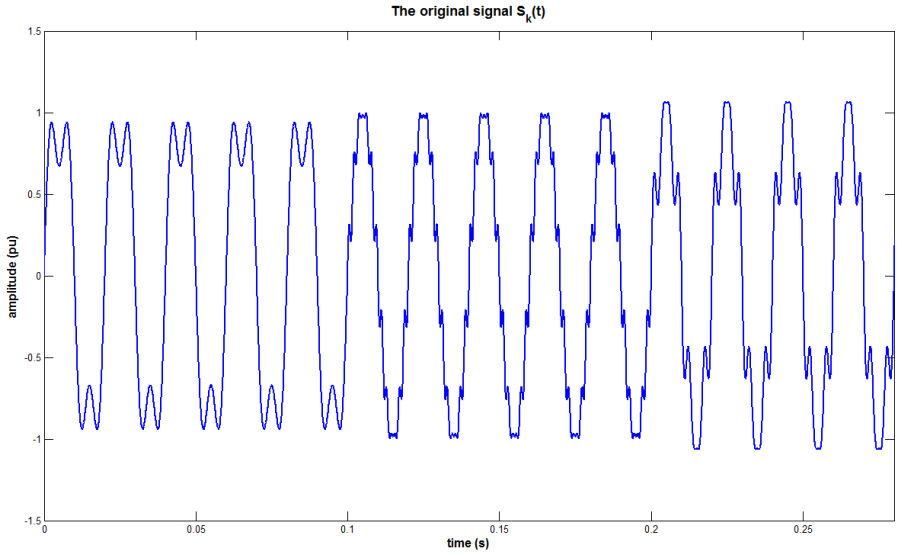

Figure 5.4.1.1. A Non-stationary signal with harmonics variations $S_k(t)$

The instants of the transitions are specified at t_1 = 0.1 s and t_2 = 0.2 s. The data are normalized by first evaluating the mean (μ) and the standard deviation (σ) of the data series. Each data point is subtracted by μ and the result is divided by σ. The normalized signal is then converted to the SAX representation. This is subsequently used to detect and resolve where these instants of sudden change occur within the SAX sequence which, in turn, represents the boundaries of each stationary segment. Once these have been determined, the stationary signal in each segment is consequently decomposed using the standard HHT and the Iterative HHT approach.

A window size of 20 (w = 20) is utilized for this signal, that is every 20 sample points in the original signal will be converted into a window of SAX representation. The whole time series (here 3000 points) is thus transformed into a SAX sequence of 150 characters (symbols). An alphabet size of 50 symbols (a = 49 breakpoints) is used. The SAX representation of $S_k(t)$ is shown in Figure 5.4.1.2.

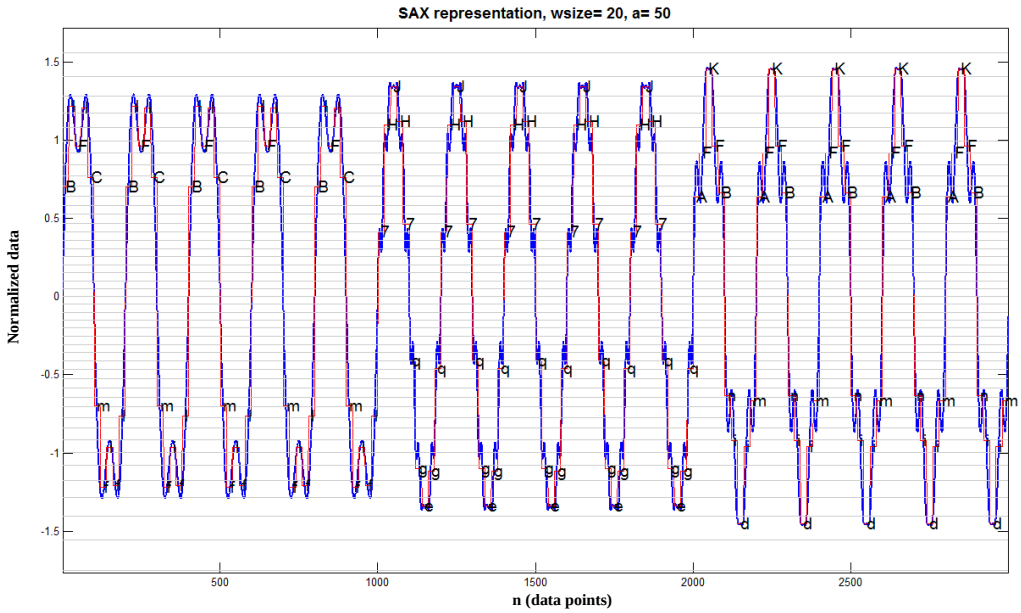

Figure 5.4.1.2: the SAX representation of non-stationary signal $S_k(t)$ with harmonic variations

As successive cycles of the raw signal are translated into the approximated stream of symbols, any change of the patterns within this temporal sequence become immediately apparent. The longest common sub sequence (LCCS) of these would naturally correspond to the cycle.

Since $S_k(t)$ is a periodic signal , the SAX word representation for each period will be repeated after each cycle if there is no change of the signal component. The word representing a typical cycle of the signal can then be determined accordingly. For example, in Figure 5.4.1.2, each cycle is represented as a SAX string of 10 symbols. Having converted the signal into a SAX representation, repeating subsequences of these symbol patterns (or motifs) will obviously correspond to any reoccurring stationary cycles of the signal (regular or distorted). Subsequently, significant pattern changes, will be manifested as changes of these symbol subsequences.

The advantage of using SAX symbols (rather than instantaneous values), to collectively form a quantized approximation of the signals numeric range is that any pattern change is readily detected through the (self) non-matching comparison via a sliding window, when a cumulative sum of the Euclidean distance of two corresponding subsequences (at the previous and current cycle respectively) exceeds a predefined threshold. This is predicated on the Lower Bounding property of SAX,

where any such instances in the waveform will correspond to the boundary of transition for each segment of a non-stationary signal [48].

Subsequently, a boundary detection algorithm is utilized in order to detect and further establish the boundary times for any differing segments using a cycle-by-cycle comparison of the SAX numeric values within the word. The boundary can be identified when a cumulative sum of the Euclidean distance of two corresponding subsequences (at the previous and current cycle respectively) exceeds a predefined threshold. At the beginning of the cycle the sum is reset to zero. A threshold of 2.2 have been chosen in this research work. The first boundary is detected at the sample point n_1=51 since it is the first point of change which produce the cumulative sum of the Euclidean distances of the previous and current sub-sequences exceeded the threshold as shown in Table 5.2. The next boundary is found at n_2=101. These points in SAX representation coincide with: t_1 = 0.1 sec and t_2 = 0.2 sec which are the actual boundaries specified above. The period of each cycle is 0.02 sec in the original signal.

Table 5.2

The SAX word for two consecutive cycles of Signal $S_k(t)$

$S_1(n_1)$			$S_2(n_2)$			Euclidean
n_1	symbol l_1	value	n_2	symbol l_2	value	Dist Sum
49	‘f’	6	39	‘f’	6	0
50	‘l’	12	40	‘l’	12	0
51	‘7’	34	41	‘B’	38	4
52	‘H	44	42	‘I’	45	4.12
...	...	...	...	...	...	...
99	‘g’	7	89	‘g’	7	0
100	‘q’	17	90	‘q’	17	0
101	‘A’	37	91	‘7’	34	3
102	‘f’	42	92	‘H’	44	3.6
.....	.....	.....	.....	.....	.....	.....

Table 5.2 shows how the SAX representation can be processed by a boundary detector to identify the boundaries of signal $S_k(t)$. The identified boundaries are then used to segment the signal into 3 segments, each of which contains stationary signal which can be processed by the standard HHT and the proposed IHHT. Table 5.3

shows the results of the signal decomposition using the standard HHT and Table 5.4 shows the results using the proposed Iterative HHT methods.

Table 5.3

Result of HHT decomposition of Signal $S_k(t)$

0s ≤t<0.10s			0.10 s ≤t<0.20 s			0.20 s ≤t<0.30s		
A	f	φ	A	f	φ	A	f	φ
0.33	150	0.2	0.0997	650	0.0	0.148	350	0
1.0	50	0	0.0189	450	180	1.01	50	3.7
			1	50	3.98			

Table 5.4

Result of IHHT decomposition of Signal $S_k(t)$

0s ≤t<0.10s			0.10 s ≤t<0.20 s			0.20 s ≤t<0.30s		
A	f	φ	A	f	φ	A	f	φ
0.33	150	0.2	0.077	650	0.0	0.148	350	0.0
1.0	50	0	0.092	550	0.0	0.2	250	0.1
			1.0	50	0.0	1.000	50	2.3

Comparing the result given in Table 5.3 and Table 5.4 to the specified values given in (5-3) shows that the IHHT is more accurate in decomposing these segments of non-stationary signal obtained through the SAX – based boundary detector.

5.4.2. Non-stationary PQ waveform with harmonics and sag

A nonstationary signal contains harmonic and sag $S_L(t)$ with transition time close to signal $S_A(t)$ in equation (3-15) is used. The instants of the transitions are specified at t_1 = 0.102 sec. and t_2 = 0.202 sec, which are different to the specified boundary points of $S(t)$. The reason of choosing these points is to show the ability of SAX – based boundary detector to identify correctly the boundary points which are located between the cycles. Such boundary points cannot be identified accurately by the windowing technique described in Chapter 3. The components are also modified from $S(t)$ to contain close frequency like the signal in equation (3-19). The purpose of the modification is to show the ability of IHHT to decompose close frequency signal which was not identified accurately by using the standard HHT. The signal $S_L(t)$ is given by equation (5-4) and shown in Figure 5.4.2.1.

$$S_L(t) = \begin{cases} \sin(2\pi 50 t_a) + 0.091\sin(2\pi 550 t_a) + 0.077\sin(2\pi 650 t_a), & 0 \le t_a < 0.102s \\ 0.8\sin(2\pi 50 t_b) + 0.073\sin(2\pi 550 t_b) + 0.062\sin(2\pi 650 t_b), & 0.102 \le t_b < 0.202s \\ \sin(2\pi 50 t_c) + 0.091\sin(2\pi 550 t_c) + 0.077\sin(2\pi 650 t_c), & 0.202 \le t_c < 0.3s \end{cases}$$

(5-4)

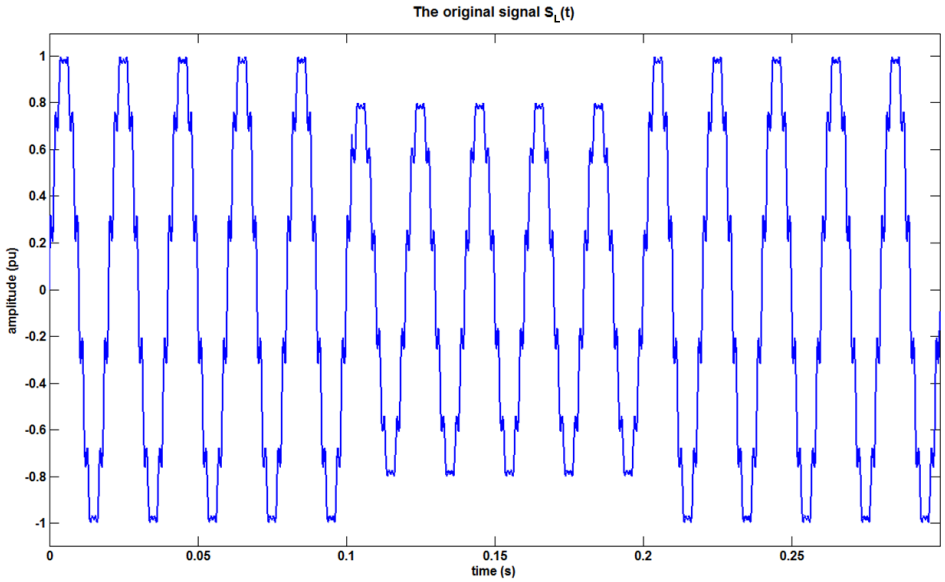

Figure 5.4.2.1. Non-stationary signal with harmonics and sag $S_L(t)$

A window size of 10 (w = 10) is utilized for this signal, that is every 10 sample points in the original signal will be converted into a window of SAX representation. The whole time series (here 3000 points) is thus transformed into a SAX sequence of 300 characters (symbols). An alphabet size of 20 symbols (a = 19 breakpoints) is used. The SAX representation of $S_L(t)$ is shown in Figure 5.4.2.2.

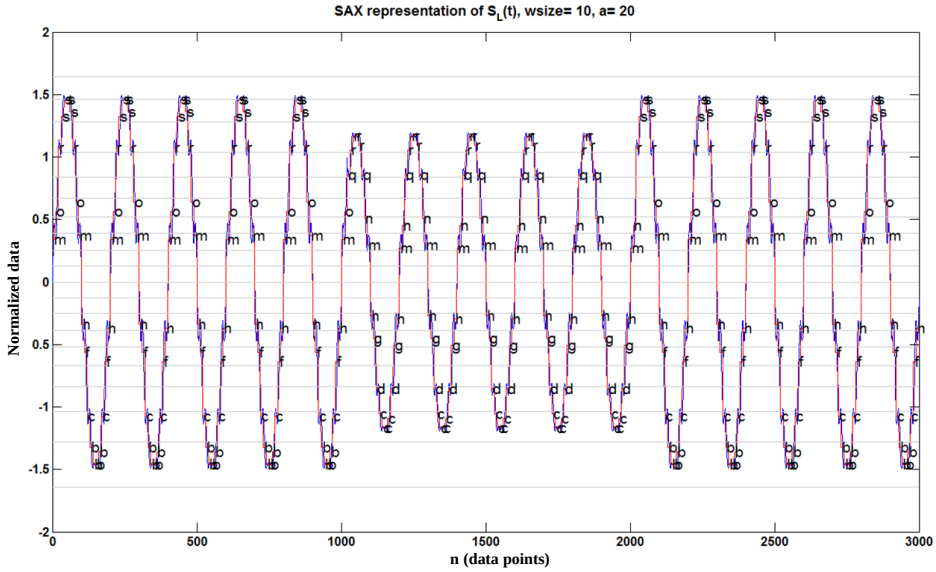

Figure 5.4.2.2 SAX representation of $S_L(t)$

Since $S_L(t)$ is a periodic signal , the SAX word representation for each period will be repeated after each cycle as long as there is no change of the signal component.

A threshold of 2.2 have been chosen in this research work. The boundary is detected at the sample point n_1 = 103 since it is the first point of change which produce the cumulative sum of the Euclidean distances of the sub-sequences at the previous and current cycles exceeded the threshold as shown in Table 5.5. Using the above criterion, the boundaries are detected at n_1 = 103 and n_2 = 203. These points in SAX representation coincide with: t_1 = 0.102 sec and t_2 = 0.202 sec which are the actual boundaries specified above.

Table 5.5

The SAX word for two consecutive cycles of the Signal $S_L(t)$

$S_1(n_1)$			$S_2(n_2)$			Euclidean
n_1	symbol l_1	value	n_2	symbol l_2	value	Dist Sum
99	‘f’	6	79	‘f’	6	0
100	‘h’	8	80	‘h’	8	0
101	‘m’	13	81	‘m’	13	0
102	‘o’	15	82	‘o’	15	0
103	‘q’	17	83	‘r’	18	1
104	‘r’	18	84	‘s’	19	1.41
105	‘r’	18	85	‘s’	19	1.73
106	‘r’	18	86	‘s’	19	2
107	‘r’	18	87	‘s’	19	2.23
.....	.....	.....	.....	.....	.....	.....
199	'g'	7	179	'g'	7	0
200	'h'	8	180	'h'	8	0
201	'm'	13	181	'm'	13	0
202	'n'	14	182	'n'	14	0
203	'r'	18	183	'q'	17	1
204	's'	19	184	'r'	18	1.41
205	's'	19	185	'r'	18	1.73
206	's'	19	186	'r'	18	2
207	's'	19	187	'r'	18	2.23

Table 5.5 shows how the SAX representation can be processed by a boundary detector to identify the boundaries of the non-stationary signal $S_L(t)$.

The identified boundaries are then used to segment the signal into 3 segments, each of which contains stationary signal which can be processed by the standard HHT and the proposed IHHT. Table 5.6 shows the results of the signal decomposition using the standard HHT and Table 5.7 shows the results using the proposed Iterative HHT methods.

Table 5.6

Result of HHT decomposition of signal $S_L(t)$

0s ≤t<0.102s			0.102 s ≤t<0.202 s			0.202 s ≤t<0.30s		
A	f	φ	A	f	φ	A	f	φ
0.105	650	4.1	0.084	650	4.1	0.105	650	4.1
0.009	350	8.3	0.007	350	8.3	0.009	350	8.3
1.000	50	0.0	0.800	50	0.0	1.000	50	0.0

Table 5.7

Result of IHHT decomposition of signal $S_L(t)$

0s ≤t<0.102s			0.102 s ≤t<0.202 s			0.202 s ≤t<0.30s		
A	f	φ	A	f	φ	A	f	φ
0.077	650	0.0	0.061	650	0.0	0.077	650	0.0
0.091	550	0.0	0.073	550	0.0	0.091	550	0.0
1.000	50	0.0	0.800	50	0.0	1.000	50	0.0

Comparing the result given in Table 5.6 and Table 5.7 to the specified values given in (5-4) shows that IHHT is more accurate in decomposing these segments of non-stationary signal obtained through SAX – based boundary detector.

5.4.3. Non-stationary PQ waveform with harmonics and swell

The Iterative HHT is also applied to a non-stationary PQ signal $S_M(t)$ with harmonics and swell as given by equation (5-5) and shown in Figure 5.4.3.1.

$$S_M(t) = \begin{cases} \sin(2\pi 50 t_a) + 0.091\sin(2\pi 550 t_a) + 0.077\sin(2\pi 650 t_a), & 0 \le t_a < 0.106s \\ 1.2\sin(2\pi 50 t_b) + 0.109\sin(2\pi 550 t_b) + 0.092\sin(2\pi 650 t_b), & 0.106 \le t_b < 0.208s \\ \sin(2\pi 50 t_c) + 0.091\sin(2\pi 550 t_c) + 0.077\sin(2\pi 650 t_c), & 0.208 \le t_c < 0.3s \end{cases} \quad (5\text{-}5)$$

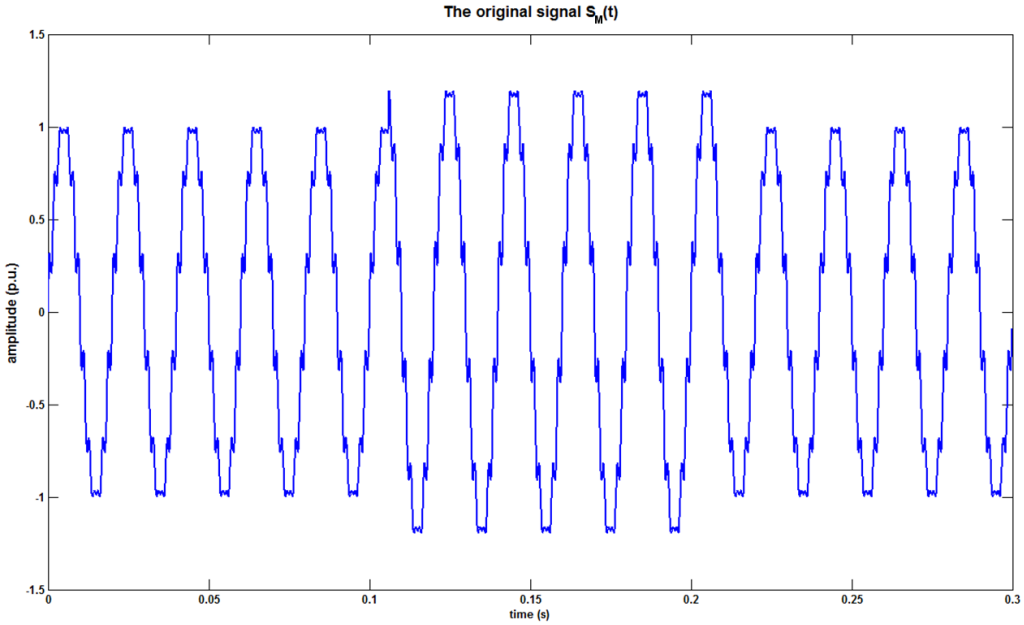

Figure 5.4.3.1 The original signal $S_M(t)$

The SAX representation of signal $S_M(t)$ is then obtained by using a window size of 10 (w = 10) and alphabet size of 50 symbols (a = 49 breakpoints). The SAX representation of $S_M(t)$ is shown in Figure 5.4.3.2.

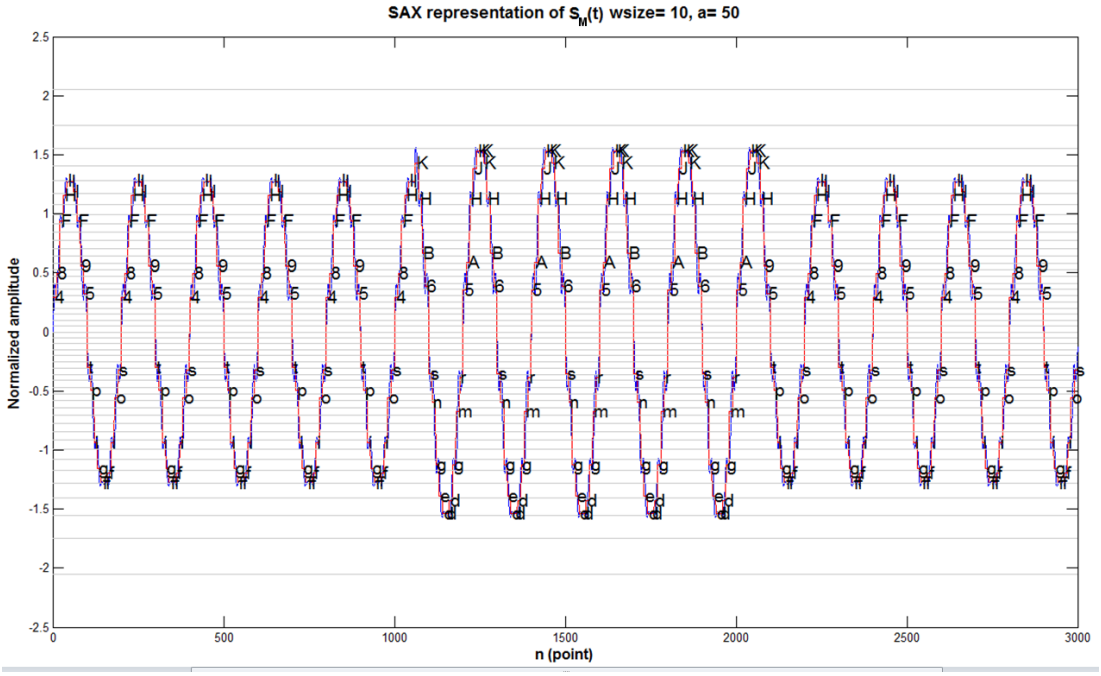

Figure 5.4.3.2: The SAX representation of signal $S_M(t)$

The boundary detector is then applied to detect a cumulative distance which exceeds a threshold of 2.2. The boundary is detected at the sample point n_1 = 107 which is the first point of change that produces the cumulative sum of the Euclidean

distances of the sub-sequences at the previous and current cycles exceeds the threshold as indicated in Table 5.8. Using the above criterion, the boundaries are detected at n_1 = 107 and n_2 = 209. These points in SAX representation coincide with: t_1 = 0.106 sec and t_2 = 0.208 sec which are the actual boundaries specified above.

Table 5.8

The SAX word for two consecutive cycles of Signal $S_M(t)$

$S_1(n_1)$			$S_2(n_2)$			Euclidean
n_1	symbol l_1	value	n_2	symbol l_2	value	Dist Sum
105	'I'	45	85	'I'	45	0
106	'I'	45	86	'I'	45	0
107	'K'	47	87	'I'	45	2
108	'H'	44	88	'F'	42	2.82
109	'B'	38	89	'9'	36	3.46
.....	.....	.....	.....	.....	.....	.....
208	'H'	44	188	'H'	44	0
209	'9'	36	189	'B'	38	2
210	'5'	32	190	'6'	33	2.23
211	't'	20	191	's'	19	2.45
212	'p'	16	192	'n'	14	3.16

Table 5.8 shows how the SAX representation can be processed by a boundary detector to identify the boundaries of the non-stationary signal $S_M(t)$.

The identified boundaries are then used to segment the signal into 3 segments, each of which contains stationary signal which can be processed by the standard HHT and the proposed IHHT. Table 5.9 shows the results of the signal decomposition using the standard HHT and Table 5.10 shows the results using the proposed Iterative HHT method.

Table 5.9

Result of HHT decomposition of signal $S_M(t)$

0s ≤t<0.102s			0.102 s ≤t<0.202 s			0.202 s ≤t<0.30s		
A	f	φ	A	f	φ	A	f	φ
0.105	650	4.1	0.126	650	4.1	0.105	650	4.1
0.009	350	8.3	0.011	350	8.3	0.009	350	8.3
1.000	50	0.0	1.200	50	0.0	1.000	50	0.0

Table 5.10

Result of IHHT decomposition of signal $S_M(t)$

0s ≤t<0.102s			0.102 s ≤t<0.202 s			0.202 s ≤t<0.30s		
A	f	φ	A	f	φ	A	f	φ
0.077	650	0.0	0.092	650	0.0	0.077	650	0.0
0.091	550	0.0	0.109	550	0.0	0.091	550	0.0
1.000	50	0.0	1.200	50	0.0	1.000	50	0.0

Comparing the result given in Table 5.9 and Table 5.10 to the specified values given in (5.5) shows that IHHT is more accurate in decomposing these segments of nonstationary swell signal obtained through SAX – based boundary detector.

5.4.4. Non-stationary PQ waveform with transient

The Iterative HHT is also applied to a non-stationary PQ signal $S_N(t)$ with harmonics and transient as given by equation (5-6). The signal is shown in Figure 5.4.4.1:

$$S_N(t) = \begin{cases} \sin(2\pi 50t_a) + 0.091\sin(2\pi 550t_a) + 0.077\sin(2\pi 650t_a), & 0 \le t_a < 0.104s \\ \sin(2\pi 50t_b) + 0.091\sin(2\pi 550t_b) + 0.077\sin(2\pi 650t_b) & \\ \qquad + \sin(2\pi 2000t_b)e^{-60(t_b-0.104)}, & 0.104 \le t_b < 0.164s \\ \sin(2\pi 50t_c) + 0.091\sin(2\pi 550t_c) + 0.077\sin(2\pi 650t_c), & 0.164 \le t_c < 0.3s \end{cases} \tag{5-6}$$

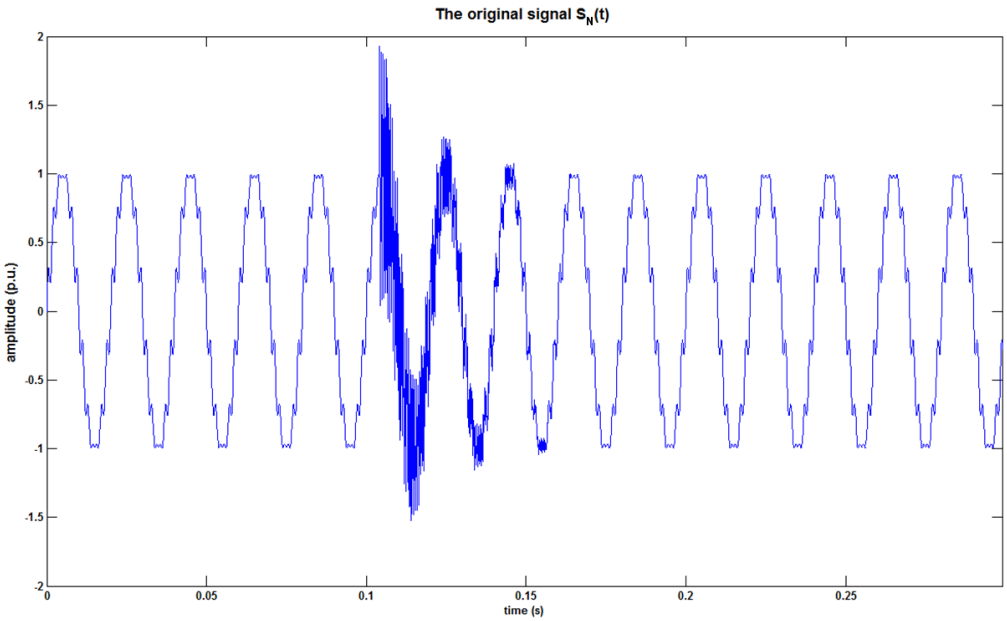

Figure 5.4.4.1 The original signal $S_N(t)$

Identifying the boundaries of such a signal using cycle by cycle search may not obtain an accurate result, since the boundaries of the signal pattern is not easily observed, unlike the sag or swell signal discussed above. An alternative approach is required to accurately identify the boundary of the signal. According to equation (5-6), the frequency of the transient signal is significantly higher than the frequencies of other components of the signal. Therefore, the instantaneous frequency data obtained from the Hilbert Transform of IMF_1 is used to identify the boundaries of the signal. As shown in Figure 5.4.4.2, the instantaneous frequency plot of IMF_1 shows more obvious boundaries of the signal contains transient $S_N(t)$.

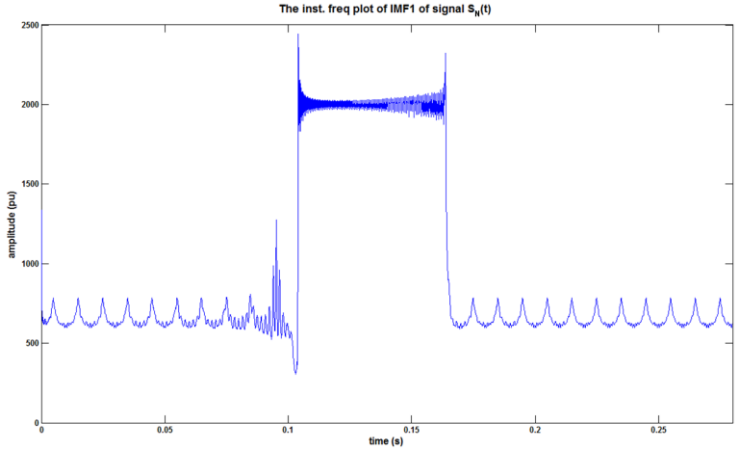

Figure 5.4.4.2: The instantaneous frequency plot of IMF_1 of $S_N(t)$

A window size of 40 (w = 40) is utilized for this signal, that is every 40 sample points in the original signal will be converted into a window of SAX representation. An alphabet size of 10 are used to obtain the SAX representation of the instantaneous frequency of $S_N(t)$ as shown in Figure 5.4.4.3.

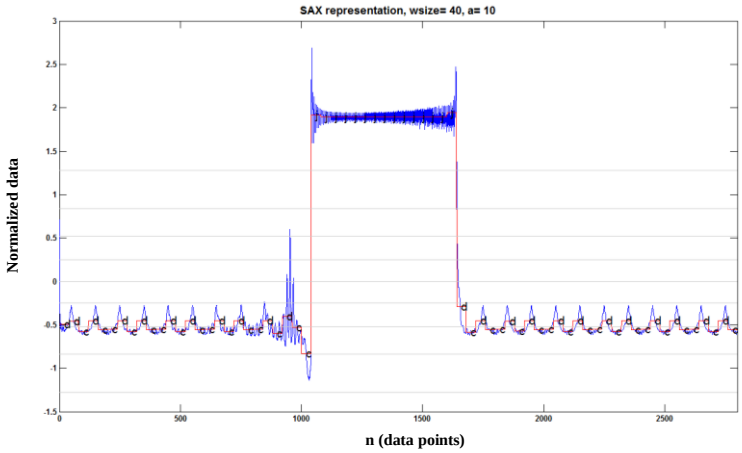

Figure 5.4.4.3: The SAX representation of the instantaneous frequency data of IMF_1 from EMD process of $S_N(t)$

Figure 5.4.4.3 shows that the SAX representation have made the boundary detection of $S_N(t)$ more visible by identifying the level of each window of the instantaneous frequency plot of the signal. The instant when the transient content of the signal occurs is indicated by the higher instantaneous frequency value while the rest of the instantaneous frequency data with lower frequency value indicates the frequency components without transient content. The difference of the signal patterns is then utilized by the boundary detector to identify the boundary of the signal.

A boundary detection algorithm is then applied in order to detect and further establish the boundary times for any differing segments using two consecutive segments comparison of the SAX numeric values within the word. A window is slid on each segment to check the Euclidean distance of the current segment and previous segment.

A threshold of 2.2 has been chosen in this research work. When the distance of the two consecutive segments exceeds the threshold, the boundary is then determined at the end of the first segment being analysed. Using this criterion, the boundaries are detected at n_1 = 26 and n_2 = 41. These points in SAX representation coincide with: t_1 = 0.104 sec and t_2 = 0.164 sec which are the actual boundaries specified above. Table 5.11 shows the boundary detection process.

Table 5.11

The SAX word for two consecutive segments of Signal $S_N(t)$

Segment (i)			Segment(i+1)			Two segments Distance
n_i	symbol l_i	value	n_{i+1}	symbol l_{i+1}	value	
23	‘c’	3	24	‘d’	4	1
24	‘d’	4	25	‘c’	3	1
25	‘c’	3	26	‘c’	3	0
26	‘c’	3	27	‘j’	10	7
27	‘j’	10	28	‘j’	10	0
28	‘j’	10	29	‘j’	10	0
29	‘j’	10	30	‘j’	10	0
.....	.....	.....	.....	.....	.....	.....
39	‘j’	10	40	‘j’	10	0
40	‘j’	10	41	‘j’	10	0
41	‘j’	10	42	‘d’	4	6
42	‘d’	4	43	‘c’	3	1
43	‘c’	3	44	‘d’	4	1

Table 5.11 shows how the SAX representation can be processed by a boundary detector to identify the boundaries of the non-stationary signal $S_N(t)$.

Having identified the boundaries of the signal, the decomposition methods are then applied to each segment of the signal. Table 5.12 shows the results of the signal decomposition using the standard HHT and Table 5.13 shows the results using the proposed Iterative HHT methods.

Table 5.12

Result of HHT decomposition of signal $S_N(t)$

0s ≤t<0.104s			0.104 s ≤t<0.164 s			0.164 s ≤t<0.30s		
A	f	φ	A	f	φ	A	f	φ
-	-	-	decays	2000	0.9	-	-	-
0.105	650	4.1	0.0991	650	3.0	0.105	650	4.1
0.009	350	8.3	0.0190	450	166.1	0.009	350	8.3
1.000	50	0.0	1.0007	50	0.4	1.000	50	0.0

Table 5.13

Result of IHHT decomposition of signal $S_N(t)$

0s ≤t<0.104s			0.104 s ≤t<0.164 s			0.164 s ≤t<0.30s		
A	f	φ	A	f	φ	A	f	φ
-	-	-	decays	2000	0.9	-	-	-
0.077	650	0.0	0.061	650	-0.1	0.077	650	0.0
0.091	550	0.0	0.073	550	0.2	0.091	550	0.0
1.000	50	0.0	0.800	50	1.4	1.000	50	0.0

Comparing the result given in Table 5.12 and Table 5.13 to the specified values given in (5.6) shows that IHHT is more accurate in decomposing these segments of nonstationary signal containing transient obtained through SAX – based boundary detector.

5.5. Chapter summary

This chapter has described the SAX algorithm to transform non-stationary PQ signals into symbolic sequences which is then processed by a boundary detector to detect the instants of sudden changes or boundaries in the signal. The non-stationary signals could then be divided into a sequence of stationary signal segments.

Subsequently, the HHT and iterative HHT can be applied to decompose each of these (stationary signal) segments.

A couple of non-stationary signals have been used to test the accuracy of SAX based boundary detector as well as the Iterative HHT to identify the signal components. The results of the simulations demonstrated that the SAX based boundary detector algorithm is very effective in determing the instants of sudden changes in PQ signals, which can help the proposed iterative HHT to analyse complex non-stationary PQ signals.

CHAPTER 6 ENSEMBLE EMPIRICAL MODE DECOMPOSITION (EEMD)

6.1. Introduction

One of the major drawbacks of the original EMD used in the Iterative HHT is the frequent appearance of mode mixing. The mode mixing is associated with an IMF obtained from an EMD process with either having a uniformly mixed IMF, or an intermittently mixed IMF as shown in Figure 6.1.1(a) and Figure 6.1.1(b) respectively. Mode mixing is often due to the signal having close frequency components [44], [6], [46], [47] or a consequence of signal intermittency [9].

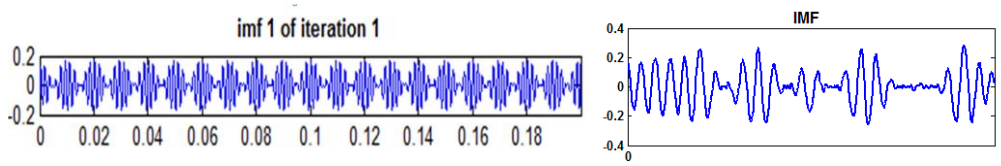

a) b)

Figure 6.1.1 Two types of mixed IMFs, a) Uniformly mixed IMF, b) Intermittently mixed IMF

The uniformly mixed IMF issue may be resolved by using masking signal, demodulation process or Iterative HHT [6],[46],[47] discussed in Chapter 4. However, the use of demodulation process or Iterative HHT may not help to resolve the problem of intermittently mixed IMF.

The research has also found that a relatively higher noise level contained in the signal may cause the IMF to be mixed intermittently in such extent that the mean value of the instantaneous frequency obtained from the Hilbert Transform is also inaccurate. In this situation, the Iterative HHT may not help to obtain accurate decomposition result since the Iterative HHT relies on the accurate mean frequency calculation to analyze the signal correctly.

To resolve the problem, the Ensemble Empirical Mode Decomposition (EEMD) has been proposed by Wu [9], where an ensemble of white noise-added signals is created from the original data. The EMD is applied to each of these signals to produce an ensemble of IMFs which are then averaged to obtain the final IMF which is considered as the true result.

The method has successfully resolved the mode mixing issues for several signals investigated by the authors [9], such as the analysis of climate data showing the interaction between atmosphere and ocean and the analysis of a high resolution

digitalized sound record. Both of these introduce mode mixing and cannot be analysed using the standard EMD method, therefore, the EEMD is used to help in resolving some of these issues [9]. The EEMD method has also been used in various applications such as Atherosclerosis identification [57], bearing fault diagnosis in a machine [58], and signal denoising [59].

However, experiments carried out in the research to decompose noisy PQ signals by using the EEMD method demonstrate that the detected amplitudes obtained from the Hilbert Transform of the IMFs are usually less than the actual value, which means that part of the signal components still remain in the residue. To resolve the problem, a novel algorithm which is referred to as the Iterative EEMD (IEEMD) is proposed in this research to improve the accuracy of the standard EEMD.

To analyse non-stationary signals that contain high level of noise, the SAX based boundary detector proposed in Chapter 5 can be used to determine the time instances of signal changes in a noisy non stationary signal. The proposed IEEMD is then applied to estimate the components of the stationary signal in each identified segment.

6.2. Standard EEMD Algorithm [9]

A simple illustration on the use of the EEMD method is shown using the signal given in (6-1)

$$S(t) = \cos(2\pi\, 50t) + 0.33\cos(2\pi\, 150t + 60^0) + \ldots$$
$$0.20\cos(2\pi\, 250t + 50^0) \qquad (6\text{-}1)$$

Initially, the signal is decomposed using the standard EMD, the result is shown in Figure 6.2.1. Figure 6.2.1 shows that the simulated signal can be decomposed well with the standard EMD method.

To test the performance of the standard EMD to decompose a noisy signal, a white Gaussian noise with a Signal-to-Noise-Ratio (SNR) 30dB is added to $S(t)$. The noisy signal is referred to as $S_1(t)$ and shown in Figure 6.2.2.

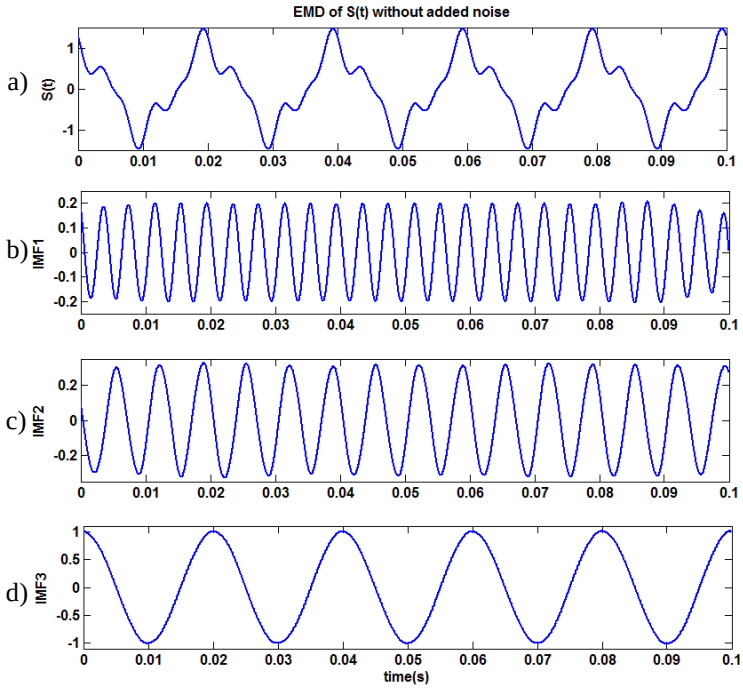

Figure 6.2.1 The EMD process of *S(t)*

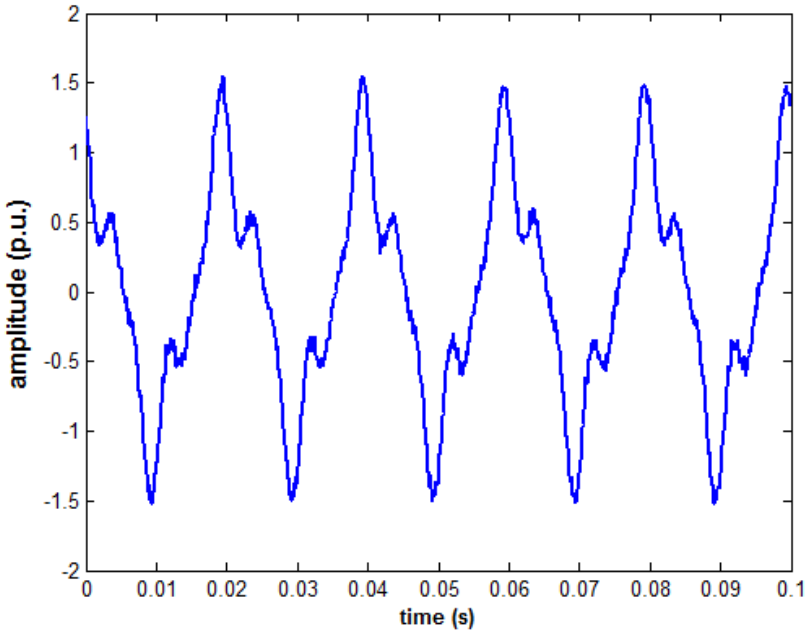

Figure 6.2.2 The noisy signal $S_1(t)$

When the standard EMD is applied to $S_1(t)$, the IMFs obtained demonstrate a typical decomposition result of the noisy signal, as shown in Figure 6.2.3.

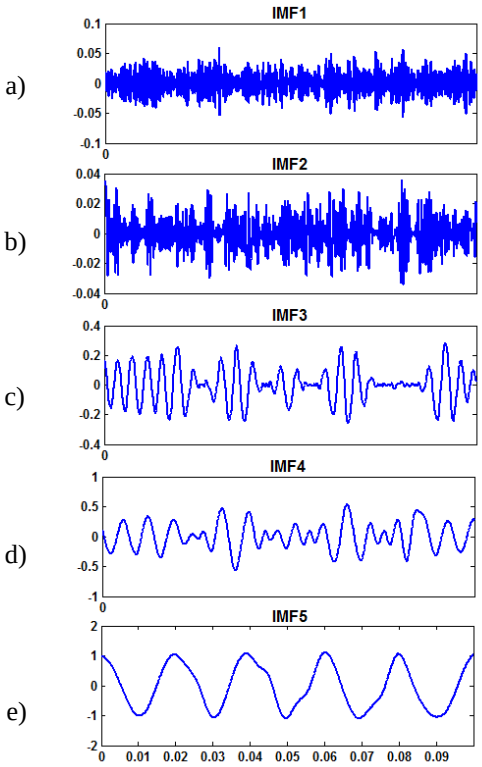

Figure 6.2.3: The results of standard EMD on a noisy signal $S_1(t)$ (a) IMF_1 (b) IMF_2 (c) IMF_3 (d) IMF_4 (e) IMF_5

Figure 6.2.3(a)-(b) show that the EMD process extracts the noise component of the signal due to the addition of the white Gaussian noise in IMF_1 and IMF_2. Figure 6.2.3(c)-(d) show the IMF_3 and IMF_4 waveforms which are intermittently mixed with other frequencies, IMF_3 shows a 250 Hz component intermittently mixed with noise and IMF_4 shows a 150 Hz component intermittently mixed with the 250Hz component. The 50 Hz component is captured in IMF_5. The waveform of IMF_5 indicates that IMF_5 may also be intermittently mixed with a small portion of higher frequency components. The mean of the instantaneous amplitude, frequency and phase obtained from the Hilbert Transform of IMF_1- IMF_5 are shown in Table 6.1.

Table 6.1

The HT of the IMFs obtained by EMD of $S_1(t)$

IMF	Amp (p.u)	Freq (Hz)	Phase (deg)
1	0.026	3280	10.729
2	0.015	1748	-4.539
3	0.127	452	-6.942
4	0.289	211	10.204
5	1.031	50	0.657

Table 6.1 shows that the only frequency correctly identified using the EMD and Hilbert Transform (HT) is the frequency of IMF_5, while the frequencies of the rest of the IMFs are incorrectly calculated by HT. Therefore, the standard HHT cannot decompose the noisy signal accurately. As the mean value of instantaneous frequency of the highest frequency signal from IMF_3 is incorrect, the iterative HHT will also fail to analyze the signal.

To resolve this type of mode mixing issue, the EEMD method is used in the research. The method assumes that a measured (real) data is a mixture of the true (clean) signal and noise. A single measurement of such data may not give consistent and accurate result [9]. Practically, an accurate measurement result is obtained by averaging the results from sufficient trials, each of which contains different noise. The same concept can be used by introducing an artificial random noise $w_i(t)$ to the original data, $x(t)$ to mimick the separate observations made in a physical experiment. The i^{th} "artificial" observation can be expressed as given by (6-2)

$$x_i(t) = x(t) + w_i(t) \tag{6-2}$$

Next observation is made by using different noise until an ensemble of noise added signals is obtained. Finally, the mean of the ensemble is calculated to obtain the final true result which is generally more accurate.

A white noise is defined as the following criterion [60] :

1. A noise signal $x[n]$ is white if it has zero mean

$$E\,(x[n]) = 0 \text{ for all } n, \tag{6-3}$$

with $E\,(x[n])$ being the expected value of the random variable $x[n]$.

2. Further, white noise is defined to have unit variance

$$E\,(x[n]x[n]) = 1, \text{ for all } n, \tag{6-4}$$

3. Lastly, a noise signal $x[n]$ is white if it is independent from sample to sample, i.e. not correlated in time

$$E\,(x[n]x[n-k]) = 0, \text{ for } k \neq 0 \text{ and for all } n \tag{6-5}$$

The above characteristic of white noise is general and applies to many probability distributions. A white Gaussian noise is composed of a set of independent random variables from Gaussian distribution. To generate such noise, a Matlab command **randn** can be used. For example, the following code draws uncorrelated pseudorandom numbers from a normal (Gaussian) distribution with mean (mu) = 0 and variance (sigma) = 1, the signal length is specified as 10 samples:

mu=0;sigma=1;

noise= sigma *randn(1,10)+mu

The research uses the following code to add an original signal *x* with a white Gaussian noise of the same length as *x* and a standard deviation nstd:

x_added=x+nstd*randn(size(x));

The EMD is applied to each of $x_i(t)$ signal in (6-2) to generate an ensemble of IMFs, which are then averaged to obtain the final result. Wu [9] argues that adding white noise may help to extract the true signals in the data, a method that is termed EEMD, which is based on Noise Assisted Data Analysis (NADA) method.

The essential concept of EEMD is based on the following study [9]:

1. White noise is required to allow the ensemble to generate all possible solutions.
2. A collection of white noise neutralizes each other out in the averaging process of the ensemble members; therefore, the final result will contain only the original data.
3. The final result of the EEMD is obtained by applying the EMD to the ensemble of noise added signals and then averaging the ensemble results.

The above concepts have been utilized in the EEMD algorithm in order to resolve the mode mixing issue for signals containing intermittency. The standard EEMD algorithm is described as follows [9]:

1. Add a randomly generated white noise ensemble to the targeted signal to form an ensemble of noise added signal waveforms. Each ensemble member will be introduced by a different white noise.
2. Decompose each of the white noise added signal from the ensemble into IMFs.
3. Perform steps 1-2 repeatedly for the remaining signals in the ensemble. Each EMD process produces a set of IMFs.

   To understand how the ensemble of IMFs can obtain the final true result, the EEMD method is applied to the noisy signal $S_1(t)$ given in Figure 6.2.2. For example, an ensemble of 10 white-noise-added signals are generated. The EMD processes will then be applied 10 times to generate 10 sets of IMFs. The third IMFs of this set are investigated further as shown in Figure 6.2.4.

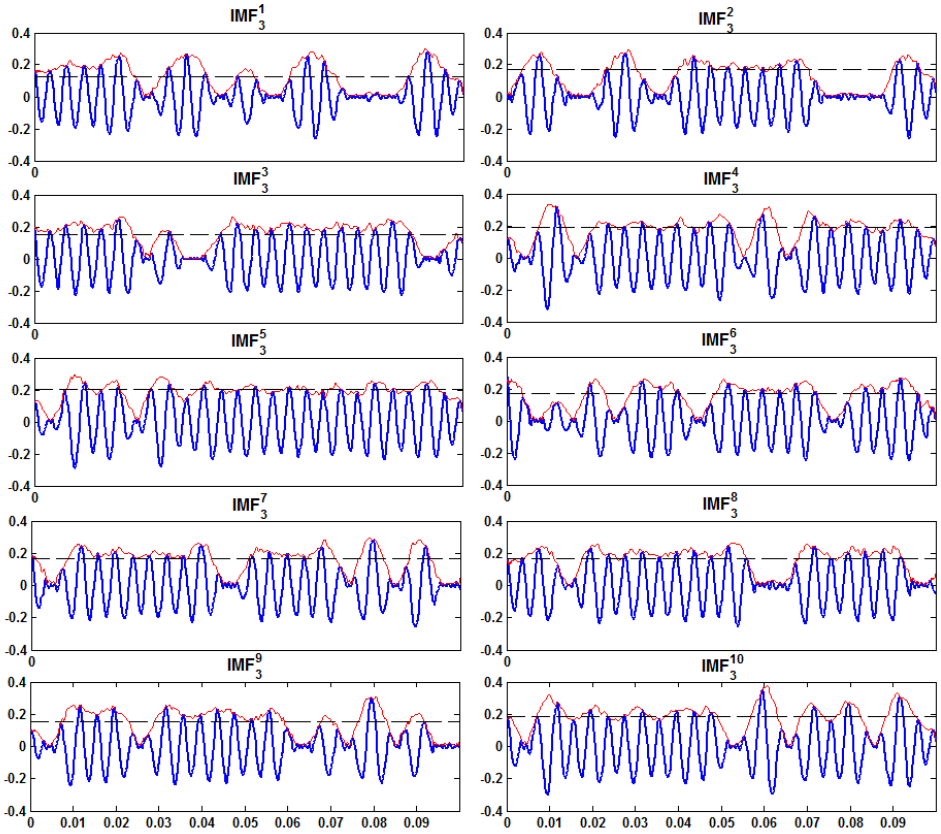

Figure 6.2.4: IMFs$_3$ obtained from 10 times EMD process of $S_1(t)$, x and y in IMF_y^x denote the IMF set (1 to 10), and the IMF number (here 3) from each set respectively. Red line in each IMF plot indicates the instantaneous amplitude, while the dashed black line indicates the mean of instantaneous amplitude obtained from HT.

The means of ten instantaneous amplitudes of IMF$_3$ are given in Table 6.2, which shows the calculated mean value of the amplitude of each IMF. It is shown that most of the calculated amplitudes is lower than the specified amplitude. Further, it is to be noted that all of the IMFs are intermittently mixed with other frequency.

Table 6.2

The calculated mean value of the amplitude of each IMF

IMF_3^x	Mean of inst. Amplitude (p.u)	IMF_3^x	Mean of inst. Amplitude (p.u)
1	0.13	6	0.17
2	0.17	7	0.17
3	0.15	8	0.17
4	0.19	9	0.15
5	0.20	10	0.19

4. Average the (ensemble) of corresponding IMFs to obtain the final result.

The mean of the third IMF is shown in Figure 6.2.5(a) and its corresponding instantaneous amplitude, frequency and phase waveforms obtained from the Hilbert Transform are shown in Figure 6.2.5 (b)-(d)

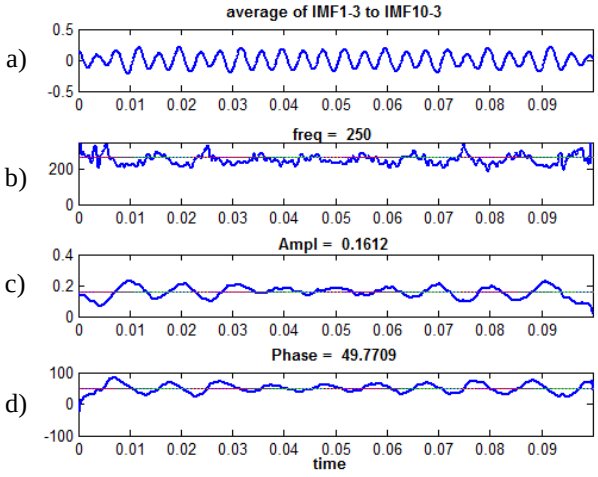

Figure 6.2.5: The Hilbert Transform of the averaged $IMFs_3$ shown in Figure 6.2.4 (a)The averaged $IMFs_3$ (b) The instantaneous frequency (c) The instantaneous amplitude (d) The instantaneous phase angle.

Figure 6.2.5(a) demonstrates how the averaging process of IMF_3^1 to IMF_3^{10} shown in Figure 6.2.4 has successfully reduced the noise mixing intermittently in the IMF_3 component as shown in Figure 6.2.3 and the mean of the instantaneous frequency of the IMF_3 becomes close to the expected value (250Hz), the highest frequency of the signal. The intermittent noise mixing in the $IMFs_3$ has been cancelled out by the averaging process of 10 trials. The noise has been captured in the first and second IMFs. The only part that survives the averaging process of $IMFs_3$ is the waveform of the actual 250Hz component. Figure 6.2.5(b) shows that the instantaneous frequency is much smoother and its mean is close to 250Hz.

However, since the mean of the instantaneous amplitude of IMF_3^1 to IMF_3^{10} are smaller than the specified amplitude of the 250 Hz component, the averaging process of $IMFs_3$ will also produce a mean of the instantaneous amplitude which is smaller than the specified value of the 250 Hz component.

The final results of EEMD process applied to $S_1(t)$ by using the standard deviation of the added noise of 0.2 and using 500 ensembles are shown in Table 6.3.

Table 6.3

The result of EEMD process on $S_1(t)$

IMF	Amp (p.u)	Freq (Hz)	Phase (deg)
1	0.019	3023	-7.19
2	0.011	1618	12.15
3	0.161	250	49.80
4	0.252	150	64.23
5	0.985	50	1.39

Table 6.3 shows the result from HT of the IMFs. IMF_1 and IMF_2 contain the noise component of the signal, while IMF_3 to IMF_5 contain the harmonic and fundamental components of the signal. Table 6.3 demonstrates that the EEMD process has managed to solve the mixed frequency issues associated with EMD (shown in Figure 6.2.3). All the frequency components and the phase angle of the signal have been identified accurately. However, the detected amplitudes are less than the specified value as given by (6-1) resulting in a difference (error).

Since the mean value of the instantaneous frequency is correctly calculated by the EEMD, it is proposed to overcome the inaccuracy of the detected amplitude by using an iterative technique which is referred to as the Iterative EEMD (IEEMD).

6.3. The Proposed Iterative EEMD (IEEMD)

Similar to the Iterative HHT process, in the Iterative EEMD, the calculation process is repeated iteratively in order to decompose additional information that still remains within the residue.

In order to obtain an accurate result of the decomposition process of noisy signal, it is necessary to identify and separate the IMFs associated with noise from the IMFs associated with actual components which should not be mixed with other frequency. The IMFs obtained from the EEMD process which are not related to the noise and not mixed with other frequency are referred to as significant IMFs which will be subtracted from the signal.

Based on many simulations in the research, the identification of the IMFs associated with noise can be performed by checking the mean value of the

instantaneous frequency of the IMF. For example, the noisy signal in (6-1) is specified with highest frequency 250Hz. The IMF frequency which represents the correct component of the signal must not be greater than 250 Hz. Therefore, the IMF frequency greater than 250 Hz does not represent any signal component and it should only come from the noise. Further, our experiments show that the mean value of the IMF frequency related to the noise component is always greater than 1000 Hz.

The IMFs associated with actual components must not be mixed and can be identified by checking the standard deviation of the instantaneous phase angle. A smooth (less fluctuating, low standard deviation) instantaneous phase angle plot is the result from smooth instantaneous frequency and smooth instantaneous amplitude of the IMF which indicates that the IMF is not mixed. In contrary, a high standard deviation of instantaneous phase angle is an indication of mixed IMF which should be considered as insignificant result of the process. Based on the experimental results, the IMFs associated with actual components usually have standard deviations of the instantaneous phase angle below 30.

In addition, the experimental results show that a small amplitude IMF may produce erroneous phase angle calculation. Further, small amplitude also means that it is not large enough to be considered as significant result of the process, therefore it should be ignored. Based on the experiments, the criterion of choosing significant IMF with max amplitude $\geq$ 2 % peak amplitude of S(t) works effectively to obtain accurate results.

To identify the correct IMFs which represent the actual signal components, a significance check is performed in the process, as shown in step 4 of the Iterative EEMD algorithm.

The steps to apply the Iterative EEMD on a signal *S(t)* are as follows:

1. Carry out the steps in EEMD
2. Calculate the amplitude and frequency of IMF_1 to IMF_n by using HT and choose all the significant IMFs. The significant IMFs must satisfy the following conditions :

   * Fundamental freq $\leq$ IMF freq $\leq$ noise freq (1000Hz) AND
   * Max amplitude of (IMF) $\geq$ 2% peak amplitude of S(t)

   AND

   * The standard deviation of the instantaneous phase angle is below 30.

3. Assume the significant k^{th} IMF $P_k(t)$can be approximated by a sinusoidal representation:

$$P_k(t) = \tilde{A}_k sin(2\pi \tilde{f}_k\, t + \tilde{\varphi}_k) \quad (6\text{-}6)$$

Where:

$P_k(t)$= sinusoidal representation of the IMF

$\tilde{A}_k$ = approximated amplitude of k^{th} IMF

$\tilde{f}_k$ = approximated frequency of k^{th} IMF

$\tilde{\varphi}_k$ = approximated phase angle of k^{th} IMF

4. Subtract the approximation for the dominant components of the significant IMFs from the original signal to obtain the residue, $r_k(t)$

$$r_k(t) = S(t) - P_k(t) \quad (6\text{-}7)$$

Steps 1-4 are repeated on $r_k(t)$ until the amplitude of the significant IMFs reaches a low threshold value, which is defined here as 3% of the maximum amplitude of $S(t)$ OR until no more significant IMF obtained by the decomposition process.

5. As in the iterative HHT [47], it is possible that similar frequencies are obtained during the iterative process of decomposition. For each frequency $\tilde{f}_k$, obtained in the iterative EEMD process, the sinusoidal representations associated with that frequency can be added together as given in (6-8) and then the Hilbert Transform is applied to obtain the amplitude, frequency and phase of that frequency component. These sinusoids are then sorted by frequency.

$$R_k = \tilde{A}_1 \sin(2\pi \tilde{f}_k\, t + \tilde{\varphi}_1) + \tilde{A}_2 \sin(2\pi \tilde{f}_k\, t + \tilde{\varphi}_2) + \ldots\ldots$$
$$\ldots\ldots + \tilde{A}_n \sin(2\pi \tilde{f}_k\, t + \tilde{\varphi}_n) \quad (6\text{-}8)$$

6.4. Results from the Iterative EEMD

As an example of applying EEMD iteratively to the simulated signal, consider the result of the standard EEMD process shown in Table 6.3 as the result of first iteration. The significant IMFs should then be chosen according to step 2. Since IMF_1 and IMF_2 have mean frequencies more than 1000Hz, according to step 2 they are not considered as significant. Further, IMF_3, IMF_4 and IMF_5 have mean frequencies that lie between fundamental frequency and 1000Hz. The mean amplitudes are also greater than 2% of the peak amplitude of S(t) and the IMFs are

not mixed with other frequencies. Therefore, IMF_3, IMF_4 and IMF_5 are chosen as the significant IMFs which are then represented as sinusoidal waveforms with mean amplitudes, mean frequencies and mean phases obtained from HT, according to step 3.

The proposed method of successively subtracting sinusoid representations of the significant IMFs instead of the actual IMFs (which is the approach in the standard EEMD) has led to greater accuracy when dealing with the simulated noisy signal, as shown in Table 6.4

Table 6.4

The detected components of noisy signal $S_1(t)$ using IEEMD

Step No	Amp (p.u)	Freq (Hz)	Phase (deg)	MSE (%)
1	0.167	250	49.81	0.44
	0.247	150	62.63	
	0.947	50	0.67	

Step No	Amp (p.u)	Freq (Hz)	Phase (deg)	MSE (%)
2	0.021	250	49.87	0.13
	0.069	150	51.95	
	0.029	50	-9.37	

Step No	Amp (p.u)	Freq (Hz)	Phase (deg)	MSE (%)
3	0.019	50	-14.27	0.11

Table 6.4 shows that some of the sinusoids obtained have the same frequency value. The sinusoids of the same frequency are then combined to obtain the final result as shown in Table 6.5.

Table 6.5

The Final Result of IEEMD process on noisy signal $S_1(t)$

Amp	Freq	phase
0.187	250	49.8
0.315	150	60.3
0.994	50	0.1

Table 6.5 shows the final result of IEEMD process which is more accurate than the result from the standard EEMD process as shown in Table 6.3.

To test the performance of the proposed method, the Iterative EEMD as well as the standard EEMD are used to decompose a couple of simulated noisy signals with various harmonic frequency components. A total 500 ensemble member (*nE*) with the standard deviation of the added noise (*a*) 0.3 is used for the EEMD and IEEMD process. The accuracy of the decomposition processes are evaluated by checking the difference of the reconstructed signal (which is obtained by combining all the detected components) and the original signal by using a Mean Square Error criterion (MSE). Mean Square Error (MSE) of a calculation measures the mean or average of the squares of the "errors", which is the difference between the calculated value and the actual value [61]. The smaller the MSE value, the more accurate the decomposition results are. The result of the accuracy test of the decomposition processes is shown in Table 6.6.

Table 6.6

The MSE of the decomposition results using IEEMD and EEMD

	MSE (%)	
signal (Hz)	EEMD	IEEMD
50-250-450	0.672	0.123
50-350-650	0.268	0.133
50-450-850	0.502	0.162

Table 6.6 shows that for the simulated PQ harmonic signals used in the test, the MSEs of the reconstructed signal (which is obtained by combining all the detected components) and the original signal using the IEEMD process are significantly smaller than the associated MSEs of the EEMD process. The results demonstrate that the accuracy of the proposed IEEMD method is higher than the standard EEMD technique.

6.5. **Chapter Summary**

This chapter has described the Ensemble Empirical Mode Decomposition (EEMD) to resolve the mode mixing issues with the EMD. The EEMD has been tested with noisy signals which usually produce mixed IMF when processed by using EMD. The EEMD has been found to be effective in resolving the mode mixing issues of the noisy signals. However, the identified amplitudes of the detected components are found to be inaccurate. To resolve this problem, an iterative techique which is referred to as the Iterative EEMD is proposed. The evaluation of the

proposed Iterative EEMD method to decompose various PQ signals has demonstrated its accuracy over the standard EEMD.

CHAPTER 7 RESULTS

7.1. Introduction

This chapter will provide the decomposition results of measured signals by using HHT, Iterative HHT, EEMD and the Iterative EEMD. The measured signals are obtained from measurement at an industrial site using Dranetz PQ analyzer and also from PQube cloud storage of PQ events.

First, the standard HHT will be used to decompose the measured signals. Because of the noise content of the measured signals, mixed frequency IMFs will be obtained, which may cause the decomposition process to miss one or more frequency components. The Iterative HHT can decompose the measured signal more accurately than the standard HHT, if the noise content is not too high. However, for more noisy measured signals, the Iterative HHT will also miss one or more frequency components due to mode mixing issue. To overcome this, the EEMD is used to improve the decomposition process by resolving the problems of mixed IMFs. The result of EEMD process of measured signals are found to be more accurate than the Iterative HHT since the mixed IMFs issue are reduced significantly. However, as discussed in the previous chapter, the amplitudes of the identified components by EEMD process are usually smaller than the actual amplitudes. To produce more accurate amplitudes of the decomposed components, the iterative EEMD is then applied. Results from the decomposition process show that the noisy signals from the Dranview measurement and Pqube data can be decomposed correctly using this approach.

To decompose non-stationary signals, SAX method can be utilized to obtain the instant of changes of the signal which are then used to segment the original signal to a sequence of stationary signals. The iterative HHT or the iterative EEMD can then be used to analyse each segment separately.

7.2. Measured Signals

7.2.1. Dranview Signal

The Dranview signal is obtained from a measurement of the 66kV phase ‘a’ current at a point of common coupling to a plastic manufacturing facility in Australia, using a Dranetz PQ monitoring instrument, Power Xplorer PX5. The company produces small plastic pellets which are then used by other manufacturers

to make larger products such as plastic storage tanks. The major loads within the facility include compressors, DC drives and one large AC VSD. The plant is supplied by 2 66kV/11 kV transformers. The rating of transformer 1 is 20/27 MVA (ONAN/ONAF) and the rating of transformer 2 is 20/30 MVA (ONAN/ONAF). This would give an overall firm rating (i.e. assuming n-1 operation) of 27 MVA.

Dranetz is owned by Gossen Metrawatt (GMC-I), a world class company in measurement and test instrumentation. The Dranetz Power Xplorer PX5 PQ monitor is a portable, hand-held PQ analyzer which comes with a color liquid crystal display using touch screen technology. The device is equipped with most advanced features in a power monitoring instrument, such as the capability to identify transients, voltage harmonics, unbalanced and non-sinusoidal systems through 8-channels input for voltage and current with high speed data capture and sampling. The signal captured by using the Dranetz Power Xplorer PX5 can be processed further by using Dranview software installed in a PC.

Figure 7.2.1.1 shows a Dranetz Power Xplorer PX5 used in the measurement of the plastic manufacturing facility. Figure 7.2.1.2 shows the connection diagram of a PQ analyzer to measure 3 phase currents.

Figure 7.2.1.1 Dranetz Power Xplorer PX5 PQ Analyzer
(source: Davis Instruments [62])

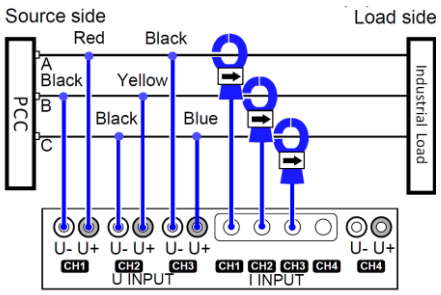

Figure 7.2.1.2 Connection Diagram of a PQ Analyzer
for Current Measurement

The phase ‘a’ current signals captured with sampling frequency 256 / 0.02 Hz at various time from 7th to 9th of August 2012 are shown in Figures 7.2.1.3 (a-d), which can be seen that sometimes the signal has very little noise content as shown by the zoomed box in Figure 7.2.1.3(a) and (d). However, at other times the signals are quite noisy as shown by the zoomed boxes in Figures 7.2.1.3 (b)-(c). Table 7.1 details the time when the signal data are recorded.

The noise content in the signal can be due to the starting of large motors at some time during the day which can generate short term noise as well as possible electromagnetic interference from starting power electronics equipment nearby.

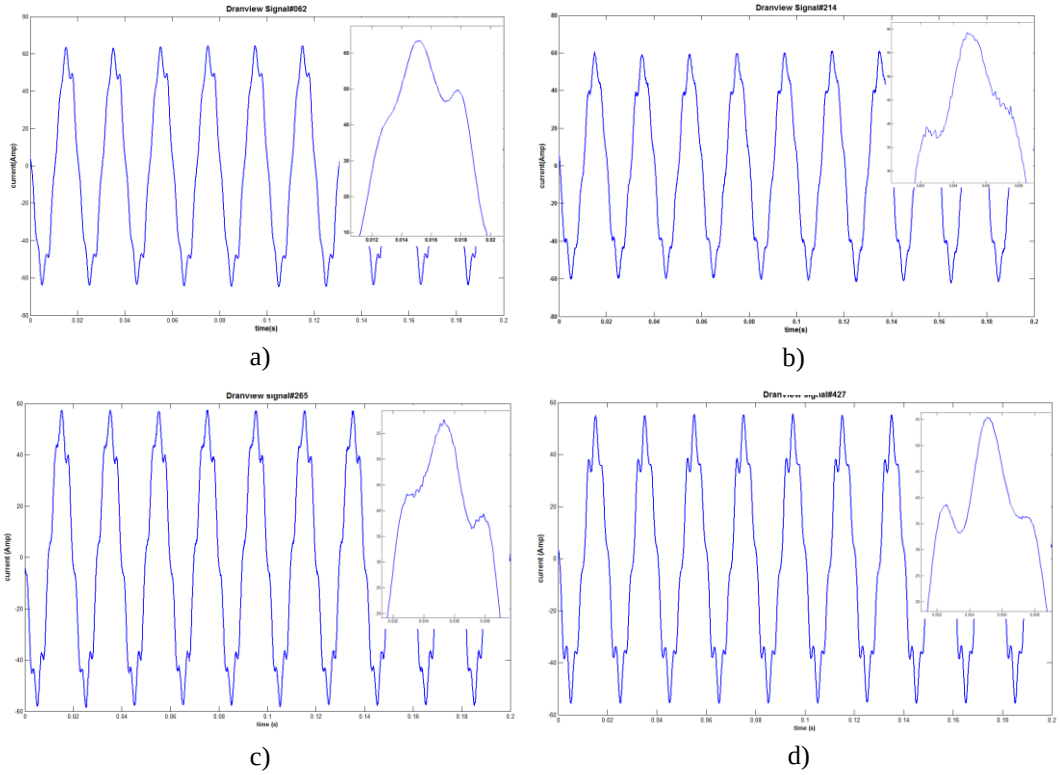

a) b)

c) d)

Figure 7.2.1.3 The measured signals at various measurement time

a). Dranview#062, b). Dranview#214, c). Dranview#265, d). Dranview#427

7.2.2. PQube Signal

The PQube PQ analyzer produced by Power Standards Lab is a tiny, user-friendly PQ recorder with built-in power and energy monitoring. All recorded data is written directly onto an SD memory card installed in the device in a number of ready-to-use formats and therefore, PQube doesn’t require any specific software to read the data. In addition, the recorded data can be sent to a cloud database of PQ events.

Table 7.1

The Measurement time of Various Dranview Signals

Event name	Measurement time	
	date	time
Event#024	7/08/2012	4:20:00 PM
Event#037	7/08/2012	5:50:00 PM
Event#052	7/08/2012	8:20:00 PM
Event#062	7/08/2012	10:10:00 PM
Event#214	8/08/2012	2:10:00 PM
Event#265	8/08/2012	10:40:00 PM
Event#273	9/08/2012	12:00:00 AM
Event#298	9/08/2012	3:50:00 AM
Event#387	9/08/2012	4:20:00 PM
Event#427	9/08/2012	10:40:00 PM

The instruments have been used in many countries to record and share PQ data for academic research. The recorded PQ data are regularly updated and available at http://map.pqube.com which can be accessed as free public sources of information [63]. Figure 7.2.2.1 shows PQube DRK-270-00, a variant of PQube power quality analyzer devices.

Figure 7.2.2.1 PQube DRK-270-00 PQ analyzer device

(source: jsdata [64])

A voltage signal recorded at 20 July 2014 by a Pqube PQ measuring device from single phase voltage measurement at Gossen Mettrawat (GMC-I) company in Massy Cedex, France is shown in Figure 7.2.2.2(a). Figure 7.2.2.2(b) shows a current signal recorded at 9 February 2011 by a Pqube device from phase ‘a’ of a 3 phase current measurement at IMH Technologies in UK. IMH Technologies LTD is a PQ instrumentation consultant in Rochford, United Kingdom that has carried out

consultancy for major utilites and customers in United Kingdom and offshore to solve PQ problems.

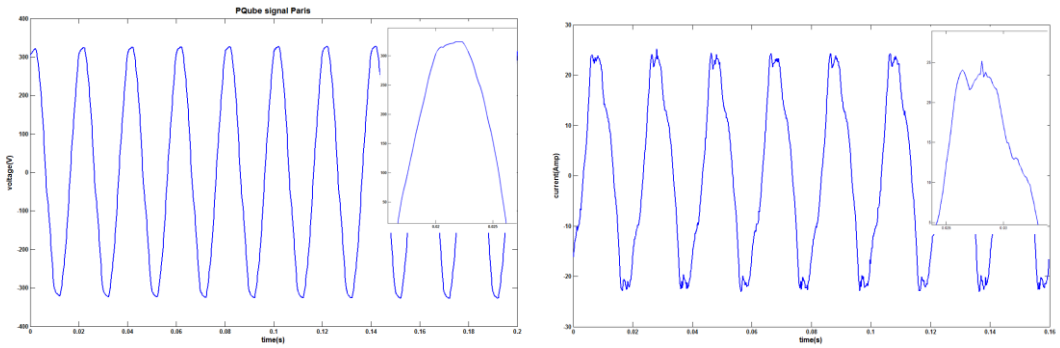

a) b)

Figure 7.2.2.2 Pqube signal a) GMC-I signal, b) IMH signal

As shown in Figure 7.2.2.2(a), the noise content in the signal is less than the other Pqube signal in Figure 7.2.2.2(b). Figure 7.2.2.2(b) shows a more noisy signal as indicated by the multiple peaks at the top of the signal and also as shown in the zoomed box. It will be demonstrated later that such signal will create problems for the traditional decomposition techniques.

7.3. The analysis of the stationary measured signals.

In this section the less noisy PQ signal Dranview Event#062 shown in Figure 7.2.1.3(a) will be analysed by using the standard HHT. The iterative HHT is then applied to improve the accuracy of the decomposition result. Another signal Dranview Event#214 which is more noisy will then be used to demonstrate how the standard HHT produces the intermittent mixed IMF from the decomposition process in which the Iterative HHT is not able to resolve. The EEMD and Iterative EEMD is then used to demonstrate the ability of the method to resolve the mode mixing issue in the decomposition process of more noisy signal Dranview Event#214. A noisy signal from the Pqube cloud storage is then used to further test the performance of the decomposition methods to identify the components of the signal.

7.3.1. Dranview Signals

The phase ‘a’ current signal (Dranview Event#062) measured by Dranetz PowerXplorer PX5 shown in Figure 7.2.1.3(a) in Section 7.2.1 is first analyzed using the standard HHT. The signal is first decomposed into IMFs using the EMD method. Figure 7.3.1.1 shows the IMFs obtained from the EMD process.

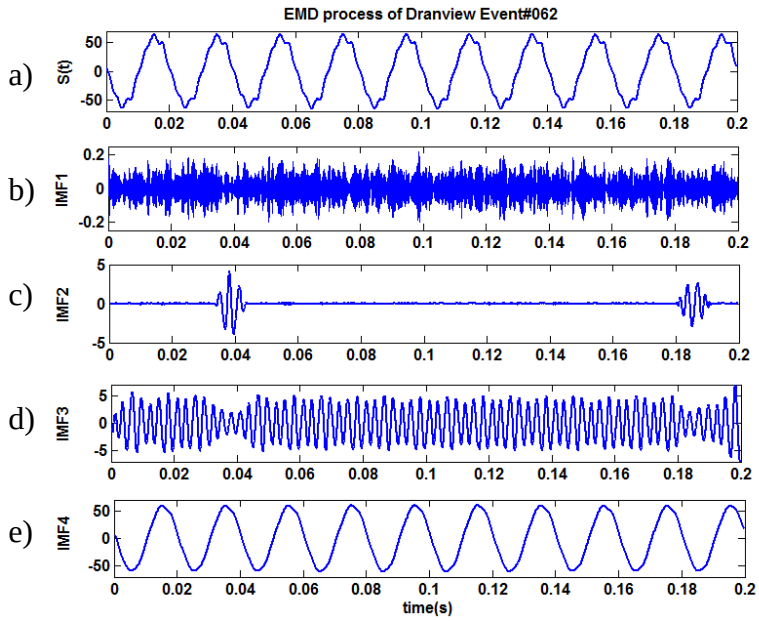

Figure 7.3.1.1 The IMFs obtained from the EMD process of Dranview Event#062

Figure 7.3.1.1 shows that the EMD process has decomposed the noise content in IMF_1 and IMF_2. In IMF_2, the noise is mixed with a small portion of the lower frequency component which should be contained in IMF_3. Therefore, the associated portion of IMF_3 waveform is lower due to the mixing issue.

When the IMFs are passed through the Hilbert Transform, the results are shown in Table 7.2 which shows that the mean frequency of IMF_1 and IMF_2 are around 4632 and 2711 Hz respectively, suggesting that IMF_1 and IMF_2 are related to noise frequency. However the mean frequency of IMF_3 is exactly 350 Hz which is related to the 7^{th} harmonic of the 50Hz fundamental frequency signal in Australia. Therefore, it can be concluded that the identified mean value of the instantaneous frequency of IMF_3 is quite accurate, which is 350 Hz. Table 7.2 suggesting that the signal only contains the 50 Hz signal and the 7th harmonics. Figure 7.3.1.2 shows the reconstructed signal from the identified 50Hz and 350Hz components compared with the original signal. The residue (the difference between the reconstructed signal and the original signal) is also shown in Figure 7.3.1.2. It can be observed that the reconstructed signal is quite close to the measured signal. However, the residue of the decomposition process indicates that some components of the signal are not identified since the component was mixed with the high frequency (noise) content in IMF_2. Therefore, the iterative HHT should be used to obtain a better decomposition result.

Table 7.2

The Hilbert Transform results of IMFs

from EMD process of Dranview Event#062

IMF	Amp (p.u)	Freq (Hz)	Phase (deg)
1	0.118	4632	-0.51
2	0.076	2711	0.60
3	4.417	350	-114.80
4	59.528	50	80.99

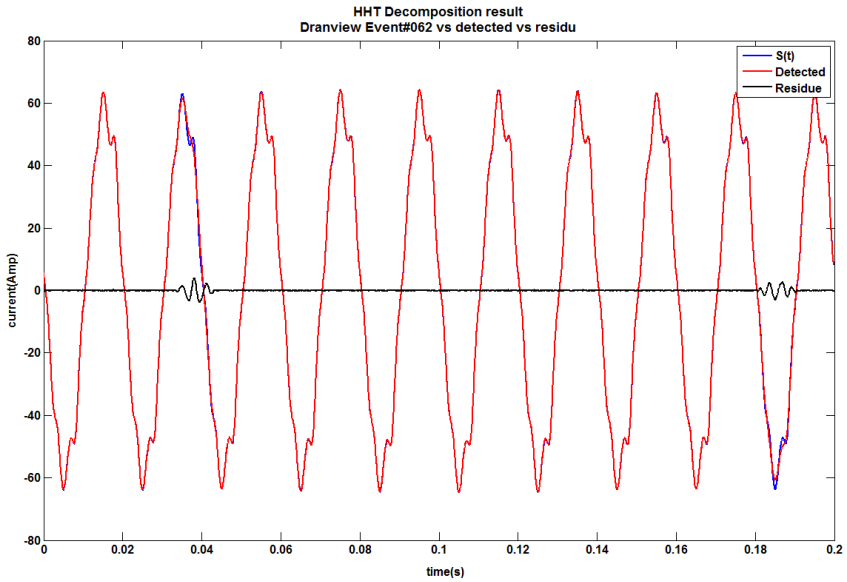

Figure 7.3.1.2 Final result of HHT process of Dranview Event#062; the original signal, the reconstructed signal and the residue

To obtain more accurate decomposition result of the measured signals using the Iterative HHT process, a modification of the algorithm is necessary since the first IMF from the EMD process of the measured signal always related to the noise content which should be disregarded as part of the signal components. Therefore, a technique to identify the significant IMFs which will be processed further (similar to the Iterative EEMD algorithm described in section 6.3) is also used by the Iterative HHT to process the measured signals. The sinusoidal representations of all the significant IMFs (not from the first significant IMF only) are then subtracted from the signal being analyzed.

By applying the modified Iterative HHT algorithm, the high frequency IMF_1 and IMF_2 shown in Table 7.2 are considered insignificant and will be ignored since they are related to the noise content. The sinusoidal representations of IMF_3 and

IMF_4 are created according to Table 7.2 and they are then subtracted from the original signal to obtain the first residue shown in Figure 7.3.1.3(a). The residue is taken as the new signal to be processed by applying the EMD again to the residue to obtain the IMFs of the second iteration, which are shown in Figure 7.3.1.3(b) –(f).

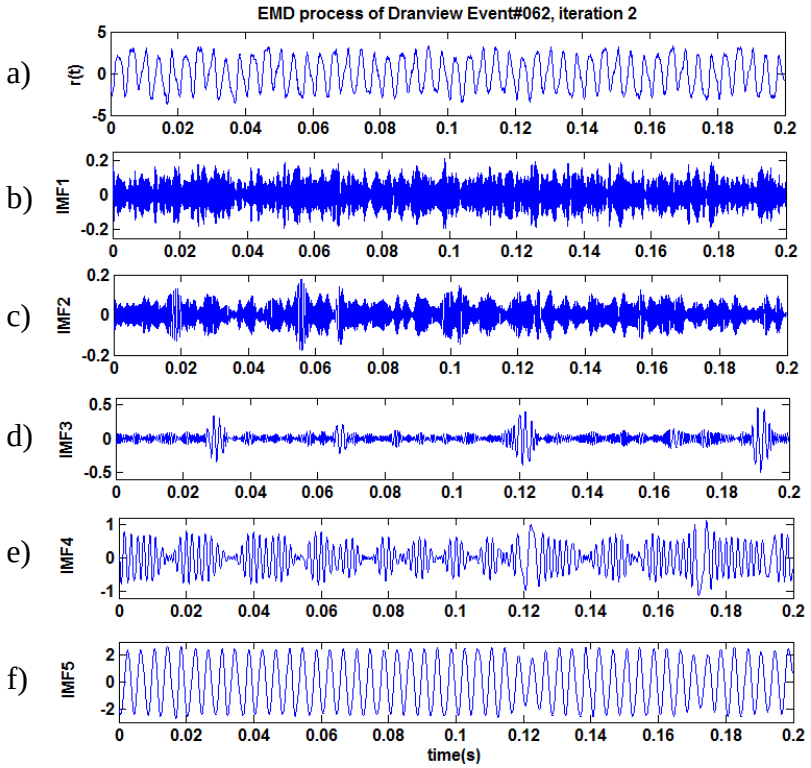

Figure 7.3.1.3 The IMFs obtained from the EMD process of Dranview Event#062 iteration 2

When these IMFs shown in Figure 7.3.1.3 are processed using the Hilbert Transform, the results are shown in Table 7.3. The mean frequencies of the first 3 IMFs are relatively large and therefore they should be considered as noise which are insignificant. IMF_4 has lower frequency than 1000 Hz and therefore it is not associated with the noise content. However, IMF_4 waveform in Figure 7.3.1.3(e) clearly show mixed frequencies issue which can also be identified by a high standard deviation of the instantaneous phase angle 102.4 as shown in Figure 7.3.1.4. Hence IMF_4 will also be considered insignificant and will be ignored as described in section 6.3.

Table 7.3

The HT results of IMFs from IHHT process

of Dranview Event#062 iteration 2

IMF	Amp (p.u)	Freq (Hz)	Phase (deg)
1	0.119	4612	-1.71
2	0.075	2719	2.41
3	0.079	1643	7.5
4	0.447	660	6.59
5	2.436	250	143.81

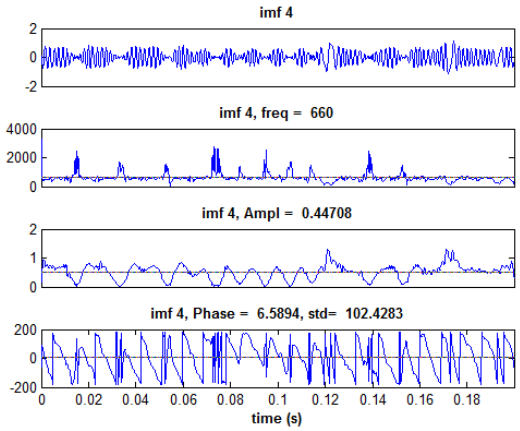

Figure 7.3.1.4 The HT of IMF_4 shown in Figure 7.3.1.3(e)

As shown in Table 7.3, the only signal that can be obtained from the second iteration is the additional 250Hz component obtained from IMF_5. The sinusoid representation of IMF_5 is then created and subtracted from the signal being analyzed to obtain the next residue. When the residue is processed, there is no more significant frequency component obtained and therefore the process is terminated. The reconstructed signal built from the detected components of 50Hz, 250Hz and 350 Hz given in Table 7.2 and Table 7.3 is shown in Figure 7.3.1.5(a) when compared to the original signal.

Figure 7.3.1.5 shows that 3 sinusoidal representations of IMFs have been detected by using the proposed Iterative HHT. There is no mixed IMF and the reconstructed signal is quite close to the original. The Hilbert Transform of the final result of the Iterative HHT process is shown in Table 7.4.

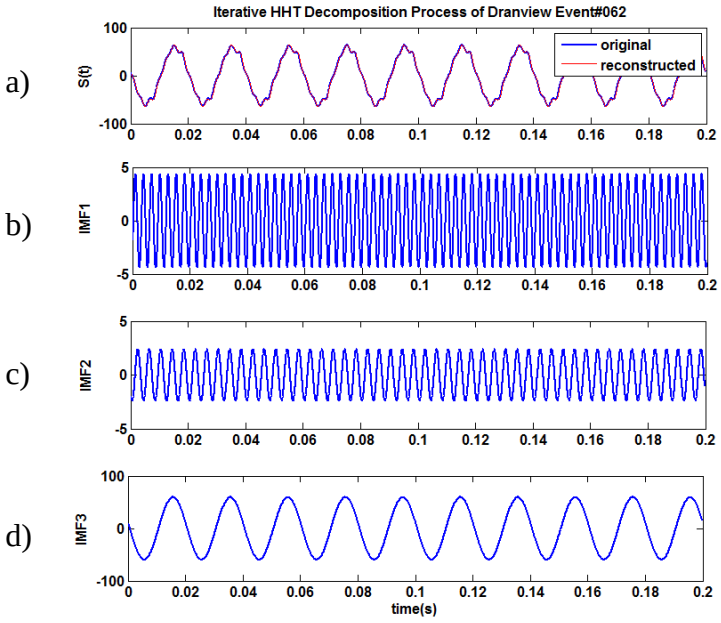

Figure 7.3.1.5 The Final Result of Iterative HHT process of Dranview Event#062

Table 7.4

Final Result of IHHT process on Dranview Event#062 signal

Amp (p.u)	Freq (Hz)	Phase (deg)
4.42	350	-114. 8
59.53	50	81.0
2.44	250	143.8

Table 7.4 demonstrates that the IHHT process has been able to extract 250 Hz frequency components which were unidentified by using the traditional HHT.

The standard HHT is then tested to decompose the more noisy signal Dranview Event#214 shown in Figure 7.2.1.3(b). The resulting IMFs are shown in Figure 7.3.1.6.

Figure 7.3.1.6 shows that the EMD process has decomposed the noise content in IMF_1 and IMF_2. The rest of the IMFs are all mixed even the one with the lower frequency components such as IMF_4 and IMF_5. When The Hilbert transform is applied to these IMFs, the results are shown in Table 7.5.

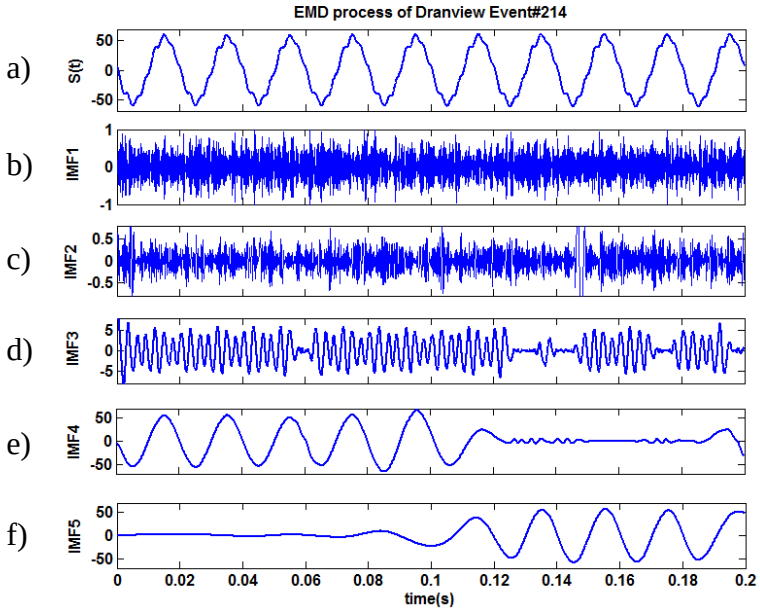

Figure 7.3.1.6 The result of EMD on Dranview#214

Table 7.5

The HT of the IMFs from EMD process on Dranview#214

IMF	Amp (p.u)	Freq (Hz)	Phase (deg)
1	0.52	4191	-0.29
2	0.34	2130	8.72
3	3.72	480	3.36
4	38.96	108	4.67
5	26.92	39	-38.91

Table 7.5 shows that no multiple of 50Hz frequecy is obtained from all the IMFs suggesting the failure of the decomposition process using the standard HHT when analysing more noisy signal such as Dranview Event#214.

The instantaneous frequency, amplitude and phase of IMF_3, IMF_4 and IMF_5 obtained from the Hilbert Transform are shown in Figure 7.3.1.7.

The standard deviation of the the instantaneous phase angle of IMF_3, IMF_4 and IMF_5 also indicate that the IMFs are mixed as shown in Figure 7.3.1.7. The mixing issue causes the calculated mean value of instantaneous frequencies are incorrect and therefore, applying the Iterative HHT for this case will not help to obtain more accurate result.

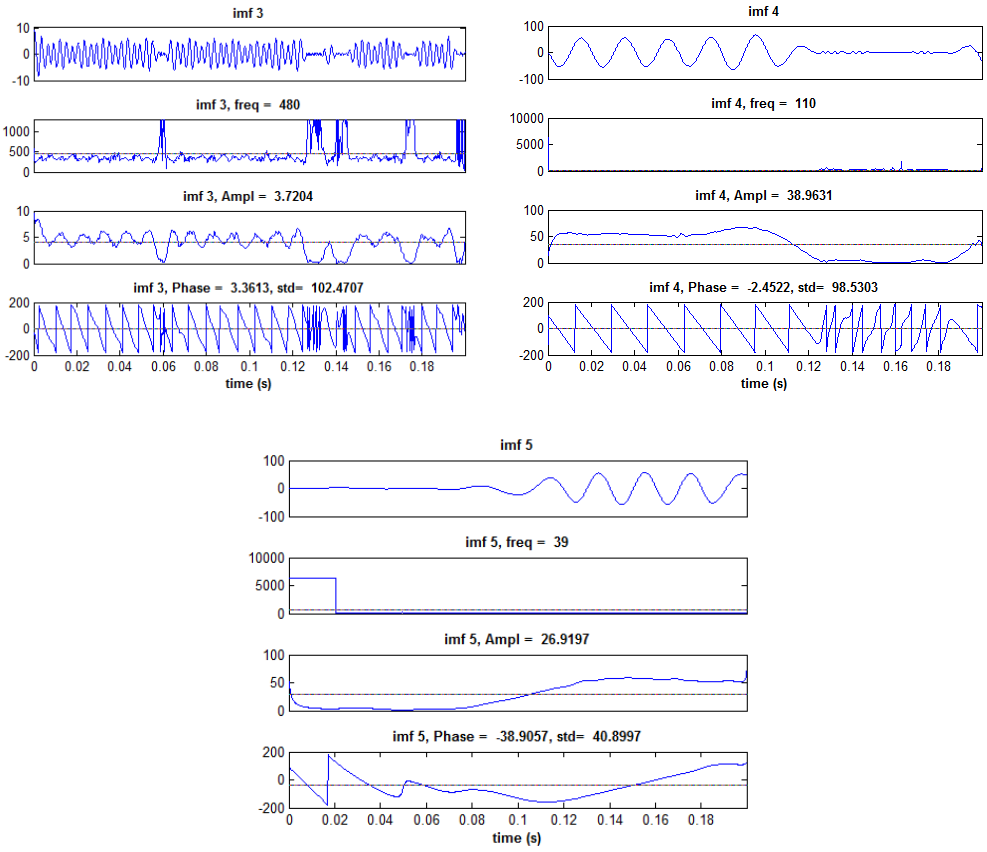

Figure 7.3.1.7 The Hilbert Transform of the IMFs from EMD process of Dranview#214

As suggested in Section 6.1, a potential method to resolve the problem of intermittently mixed IMFs, is by using the EEMD method, where an ensemble of white noise-added signal is created from the original data. The EMD is applied to each of these signals to produce an ensemble of IMFs which are then averaged to obtain the final IMF which is considered as the true result [9].

The averaged IMFs obtained from the EEMD method when applied to the Dranview#214 signal, are shown in Figure 7.3.1.8. Figure 7.3.1.8 shows that the intermittently mixing issue has been reduced significantly. While IMF_4 appears to still have frequency mixing, IMF_5-IMF_7 appear to be relatively good

.

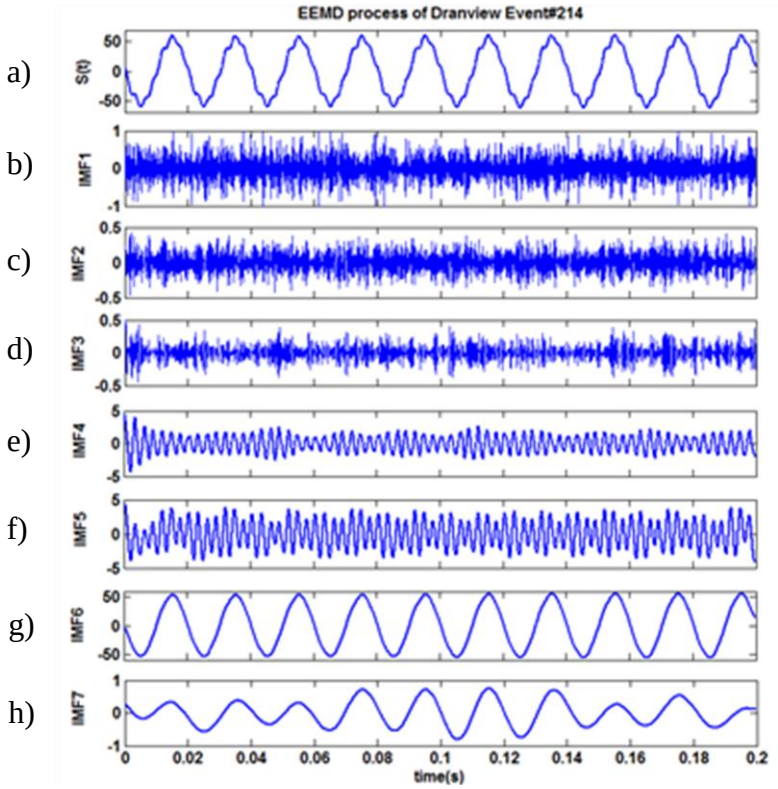

Figure 7.3.1.8 The resulting IMFs from the EEMD process of Dranview#214 signal.

Figure 7.3.1.8 demonstrates that the averaging process of the ensemble of IMFs has recovered the IMFs from the mixing issue. The Hilbert Transform is then applied to these averaged IMFs and the results are shown in Table 7.6.

Table 7.6

The HT of the IMFs from the EEMD process

of Dranview#214 signal.

IMF	Amp (p.u)	Freq (Hz)	Phase (deg)
1	0.427	4101	-0.38
2	0.183	2675	2.75
3	0.148	1640	1.18
4	1.644	355	-0.78
5	2.764	350	-76.13
6	54.328	50	86.71
7	0.634	50	118.39

MSE = 6.5948%

Table 7.6 shows that three components are identified, 350 Hz, 50 and 50 Hz. The instantaneous frequency, amplitude and phase of IMF_5, IMF_6 and IMF_7 obtained from the Hilbert Transform are shown in Figure 7.3.1.9.

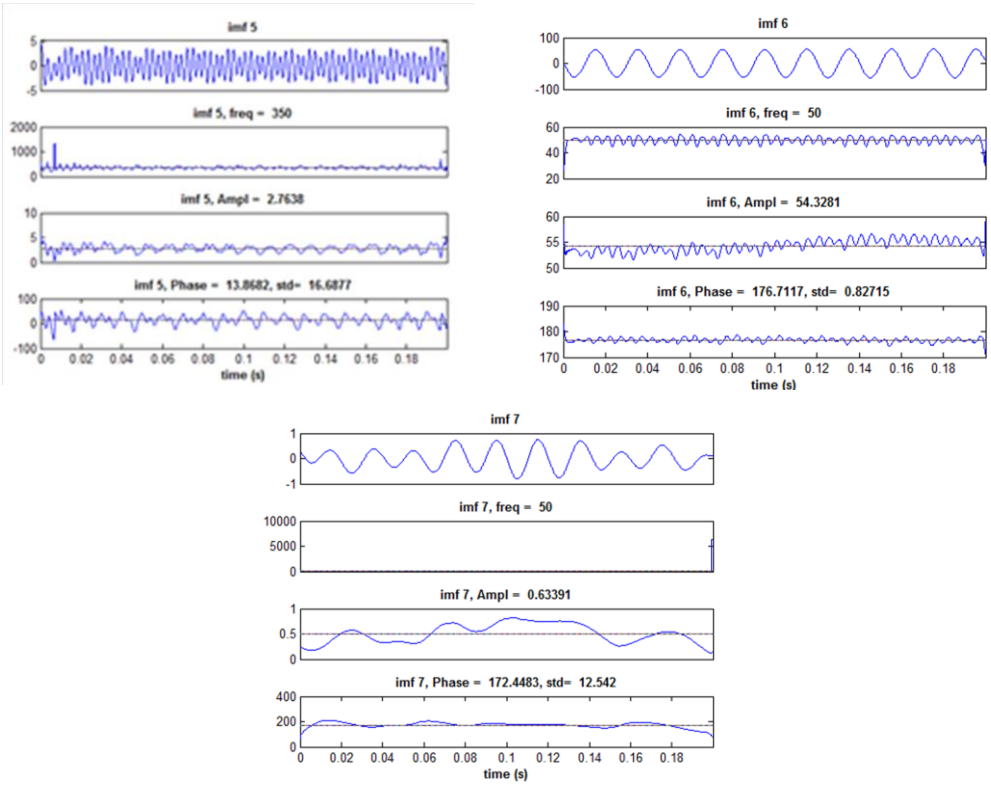

Figure 7.3.1.9 The Hilbert Transform of the IMFs from EEMD process of Dranview#214

Figure 7.3.1.9 shows that the standard deviation of the instantaneous phase angle of IMF_5, IMF_6 and IMF_7 are quite low which indicate that the IMFs are not mixed. The results demonstrate the superiority of the EEMD process to resolve the intermittently mixed IMF issue.

However, the calculated MSE (Mean Square Error) between the reconstructed signal and the original signal 6.59% is relatively high, suggesting that there are still part of the signal that have not been identified from the decomposition process using EEMD, therefore, as discussed in Section 6.2, the proposed Iterative EEMD needs to be applied to the signal to obtain a better decomposition result. For the iterative EEMD method, the result in Table 7.6 is considered as the outcome of the first iteration and then more iterations will be applied to the residue of the first iteration.

The iteration process is applied until the stopping criterion is met, i.e the amplitude of the significant IMFs reaches a low threshold value (3% of the maximum amplitude of the original signal) or no more significant IMF is obtained. The result of the IEEMD process is shown in Table 7.7.

Table 7.7

The HT of the IMFs from IEEMD process of Dranview#214

Amp (p.u)	Freq (Hz)	Phase (deg)
2.764	350	-76.13
54.328	50	86.71
0.634	50	118.39
1.343	250	28.15
1.167	350	-108.60

Table 7.7 shows that 2 more components are identified in the next iterations. The components with similar frequencies are then accumulated to obtain the final result. Table 7.8 shows the final result of the IEEMD process.

Table 7.8

Final Result of IEEMD process of Dranview#214

Amp (p.u)	Freq (Hz)	Phase (deg)
3.916	350	-165.12
1.343	250	-61.86
54.952	50	-3.34

Table 7.8 shows that more accurate result is obtained. The MSE between the constructed signal and the original signal is 2.21%., which is within the accepted tolerance and therefore the iteration is terminated.

Figure 7.3.1.10 shows the final result of IEEMD process of DranviewEvent#214.

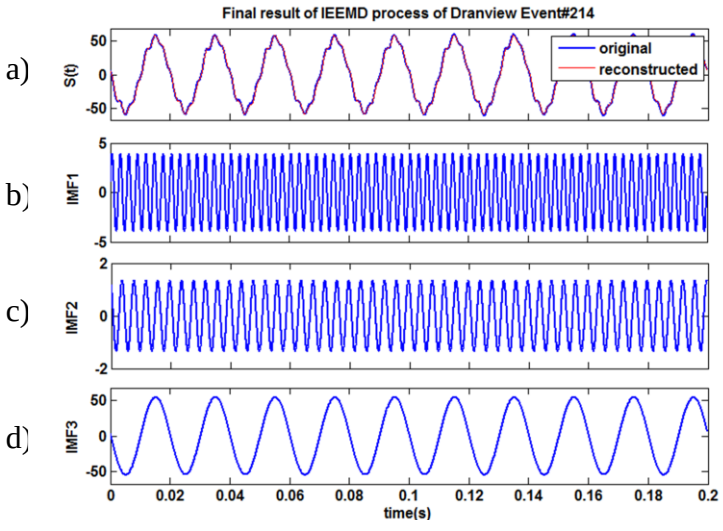

Figure 7.3.1.10 Final result of IEEMD process of DranviewEvent#214

Figure 7.3.1.10 shows that the sinusoidal representations of the IMFs do not have any mixing issue, in addition the calculated MSE between the reconstructed signal shown in Figure 7.3.1.10 (a) and the original signal 2.21% is more accurate than the result of the standard EEMD with the MSE 6.59%.

7.3.2. PQube Signal

The phase 'a' measured current signal from Pqube cloud storage shown in Figure 7.2.2.2 is first analysed using the standard HHT. The signal is decomposed by using the EMD process to obtain the IMFs as shown in Figure 7.3.2.1.

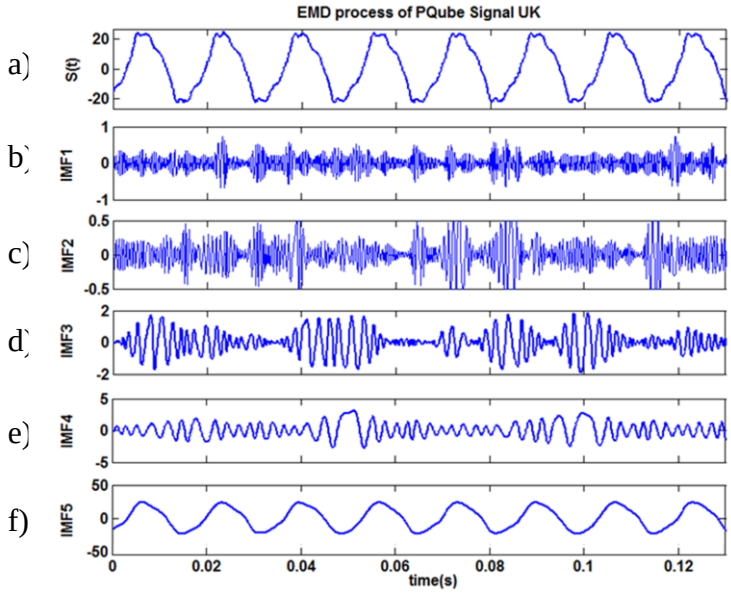

Figure 7.3.2.1 The IMFs obtained from EMD process of Pqube signal

Figure 7.3.2.1 shows that the EMD process has extracted the noise content in IMF_1 and IMF_2. In IMF_2, the noise is intermittently mixed with lower frequency component. Similarly, IMF_3 and IMF_4 appear to also be mixed with another lower frequency components, while IMF_5 is the only IMF which does not look mixed. When the Hilbert Transform is applied to the IMFs to obtain the intantaneous amplitude, frequency and phase waveforms, the results are shown in Table 7.9.

Table 7.9 shows that the mean frequency of IMF_1 and IMF_2 are 2154 Hz and 1267 Hz respectively, suggesting that IMF_1 and IMF_2 are related to noise frequency. The frequency of the rest of the IMFs are lower than a typical noise frequency (1000 Hz), however it is necessary to check which IMF is significant by evaluating the standard deviation of the instantaneous phase angle of the IMFs.

Table 7.9

The HT of the IMFs from EMD process of Pqube signal

IMF	Amp (p.u)	Freq (Hz)	Phase (deg)
1	0.29	2154	-11.00
2	0.26	1267	0.93
3	0.92	540	5.21
4	1.62	280	1.73
5	23.02	50	-148.29

To identify which IMF is mixed, the instantaneous phase angles of the IMFs obtained from the Hilbert Transform are processed to identify their standard deviations. The standard deviation of the instantaneous phase angle of the IMFs are shown in Figure 7.3.2.2.

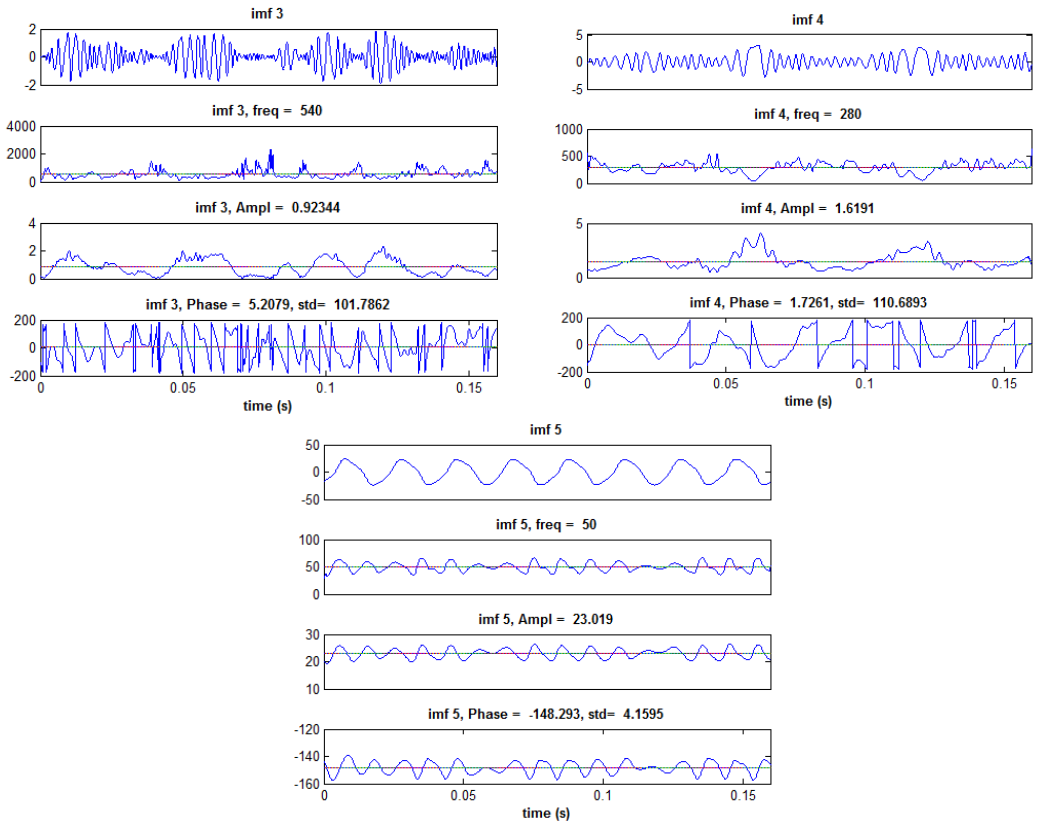

Figure 7.3.2.2 The Hilbert Transform of the IMFs from EMD process of Pqube signal

Figure 7.3.2.2 shows that the mean frequency of IMF_3 is 540 Hz which is lower then a typical noise frequency (1000 Hz), however, it is mixed with other frequency which is indicated by the unstability of the instantaneous phase angle with very high standard deviation around 101 and therefore the IMF can not be used as a

correct representation of the signal component. Similarly, the standard deviation of instantaneous phase angle plot of IMF_4 is 110 which is higher than the threshold, indicating that it is mixed with other frequency and therefore, the result can be considered erroneous. The only non-mixed IMF obtained by the standard HHT is IMF_5 which is the fundamental frequency component in the UK, 50 Hz. Since most of the IMFs obtained are mixed, the result of the decomposition process using the standard HHT is inaccurate which is indicated by the calculated MSE between the reconstructed signal and the original signal equals 22.22%.

To obtain more accurate result, the Iterative HHT process is then used to decompose the signal. In the Iterative HHT process, IMF_1 and IMF_2 shown in Table 7.9 are considered insignificant since they are related with noise. IMF_3 and IMF_4 are also considered as insignificant since they are mixed with other frequencies. IMF_5 is the only significant IMF which is processed further by creating its sinusoidal representation according to Table 7.9. The sinusoidal representation is then subtracted from the signal to obtain the first residue. The EMD process is again applied to the residue to obtain the IMFs as shown in Figure 7.3.2.3.

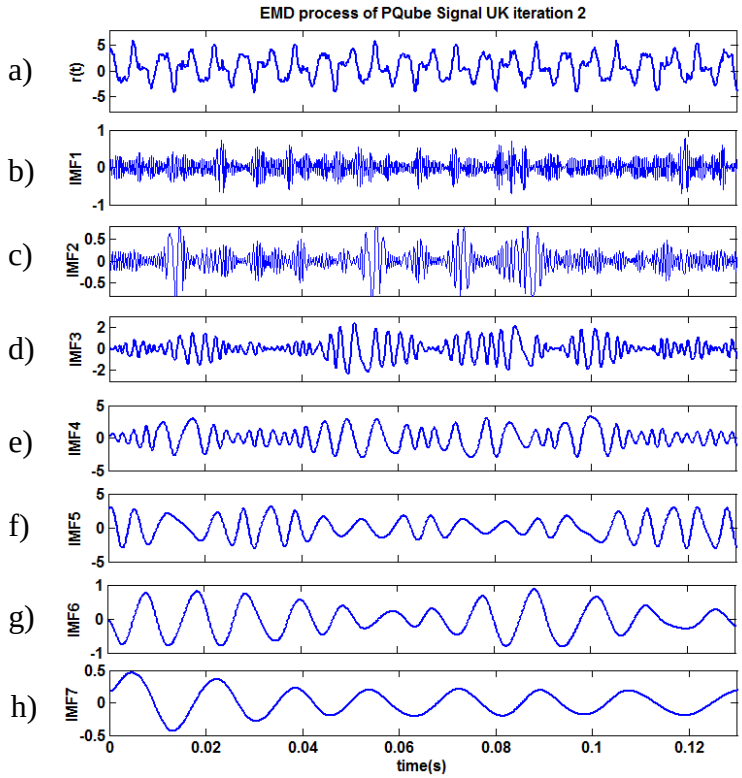

Figure 7.3.2.3 The IMFs obtained from EMD process of Pqube signal Iteration 2

The mean value of the instantaneous frequency, amplitude and phase obtained from the Hilbert Transform of the IMFs is shown in Table 7.10.

Table 7.10

The Hilbert Transform of IMFs

from IHHT process of Pqube signal iteration 2

IMF	Amp (p.u)	Freq (Hz)	Phase (deg)	IMF	Amp (p.u)	Freq (Hz)	Phase (deg)
1	0.30	2104	3.39	5	1.57	120	32.46
2	0.34	1093	15.87	6	0.54	80	37.20
3	1.24	430	3.57	7	0.20	50	-74.52
4	2.28	200	10.67				

Table 7.10 indicates that IMF_1 and IMF_2 are related to the noise frequency, while the rest of IMFs are lower than the noise frequency. To identify which IMF is mixed, the Hilbert Transform is used to calculate the instantaneous frequency, amplitude and phase of IMF_3, IMF_4 and IMF_5. The standard deviation of the instantaneous phase angle of the IMFs are then calculated as shown in Figure 7.3.2.4.

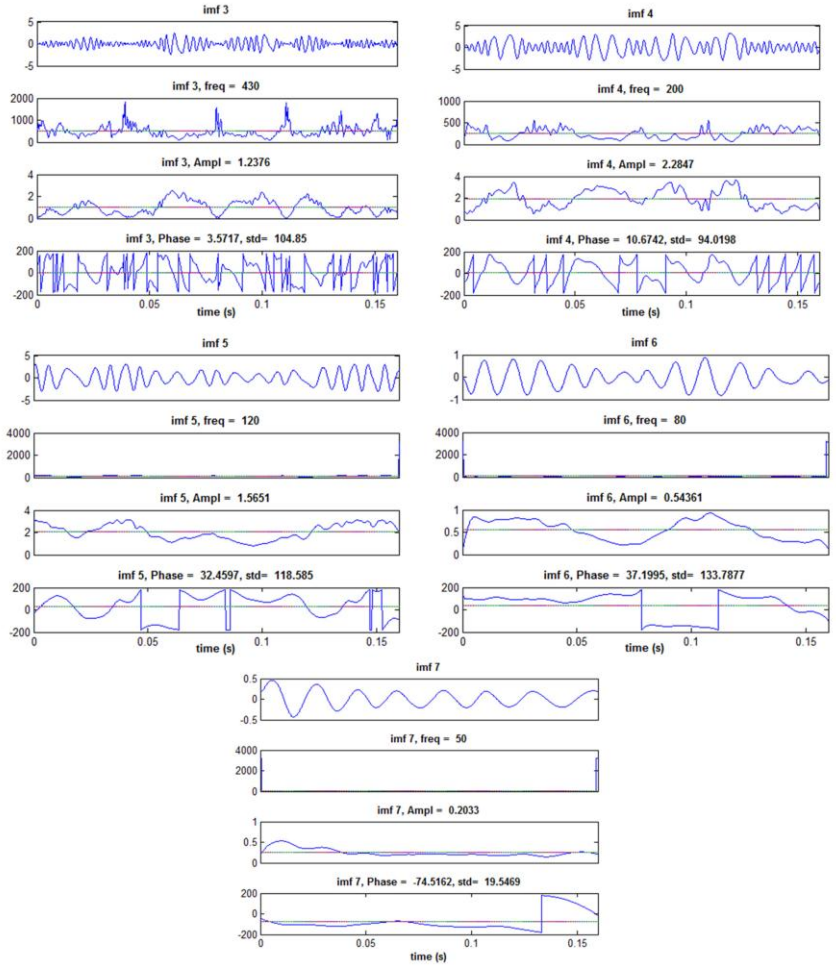

Figure 7.3.2.4 The Hilbert Transform of IMF_3, IMF_4, IMF_5, IMF_6 and IMF_7 from Iterative HHT process of Pqube signal at iteration 2

As shown in Figure 7.3.2.4, IMF_3 to IMF_6 are lower frequency IMFs but they are mixed with other frequency as indicated by the standard deviation of the phase angle plot. The standard deviation of the phase angle plot of IMF_3 to IMF_7 are 104.85, 94.02, 118.6, 133.8 and 19.55 respectively. Therefore, the only IMF that is not mixed is IMF_7 and the sinusoidal representation of the IMF is then created from the mean value of instantaneous amplitude, frequency and phase as shown in Table 7.10. The sinusoids is subtracted from the waveform being analyzed to obtain the next residue. However, when the residue is processed by EMD, no more significant IMF is obtained and therefore the process is terminated. The MSE (Mean Square Error) between the reconstructed signal and the original signal is calculated as 22.3% which shows that the Iterative HHT does not help much to decompose the signal.

The standard EEMD technique is then applied to the Pqube signal. The signal is decomposed by using 500 ensemble member (*nE*=500) and the standard deviation of the added noise of 0.032 (*a*=0.032). Figure 7.3.2.5 shows the IMFs obtained from the EEMD process.

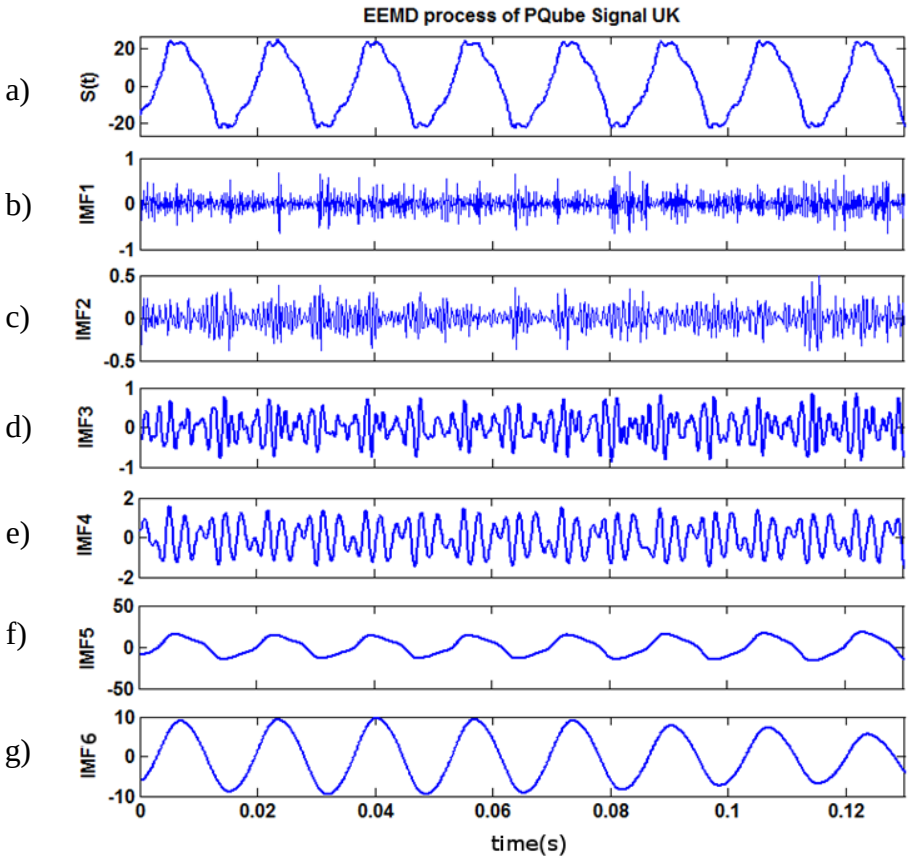

Figure 7.3.2.5 EEMD process of Pqube signal

Figure 7.3.2.5 shows the IMFs obtained from the EEMD process of Pqube signal. The EEMD process has extracted the noise content in IMF_1 and IMF_2. IMF_3 to IMF_6 show less mixed frequency waveforms. It is obvious that the averaging process of the ensemble of IMFs has reduced the mode mixing issues that appeared in the result of HHT process shown in Figure 7.3.2.1. The mean value of the instantaneous frequency, amplitude and phase obtained from the Hilbert Transform of the IMFs is shown in Table 7.11.

Table 7.11

The HT of IMFs from EEMD process of Pqube signal

IMF	Amp (p.u)	Freq (Hz)	Phase (deg)	IMF	Amp (p.u)	Freq (Hz)	Phase (deg)
1	0.242	2539	-3.19	4	1.047	360	-1.405
2	0.145	1450	-6.65	5	13.838	50	-147.455
3	0.437	510	0.455	6	8.905	50	-149.406

Table 7.11 shows that the mean value of instantaneous frequency of IMF_1 and IMF_2 are greater than 1000 Hz which indicates that they are related to the noise content of the signal. While the mean value of instantaneous frequency of IMF_3 to IMF_6 are lower than 1000 Hz. To identify which IMF is mixed, the standard deviation of the instantaneous phase angle obtained from HT of the IMFs are then calculated as shown in Figure 7.3.2.6.

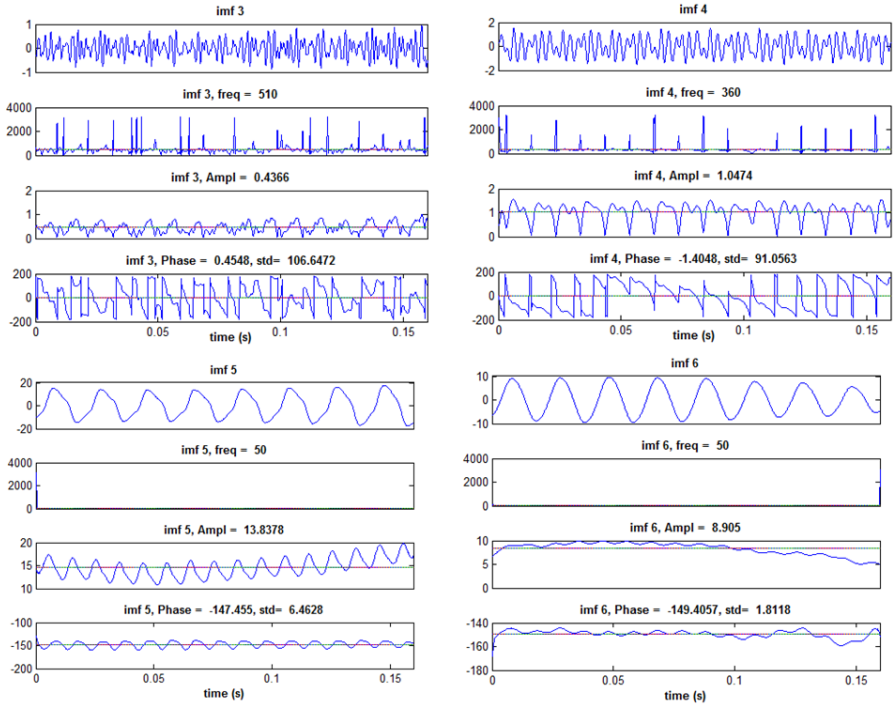

Figure 7.3.2.6 The Hilbert Transform of the IMFs in Figure 7.3.2.5

Figure 7.3.2.6 shows the instantaneous frequency, amplitude and phase from the Hilbert Transform of the IMFs. The standard deviation of the instantaneous phase angle of IMF_3 and IMF_4 are 106.7 and 91.1 respectively, which are greater than 30. Therefore, IMF_3 and IMF_4 are considered as mixed IMFs and can not be used as correct representations of the signal components. The standard deviation of the instantaneous phase angle of IMF_5 and IMF_6 are 6.5 and 1.8 respectively which are below the threshold of 30 and therefore IMF_5 and IMF_6 are considered part of the signal components since they are not mixed. The calculated MSE between the reconstructed signal and the original signal is 21.96%, which is still high.

To identify the components of the signal more accurately, the proposed iterative EEMD is then applied to the Pqube signal. The results shown in Table 7.11 is considered as the first iteration result. Since the significance check identifies that only IMF_5 and IMF_6 are considered as significant, these IMFs are represented as sinusoidals which are then subtracted from the original signal to obtain the first residue. The second iteration of the Iterative EEMD is then applied to the residue to obtain the IMFs as shown in Figure 7.3.2.7 .

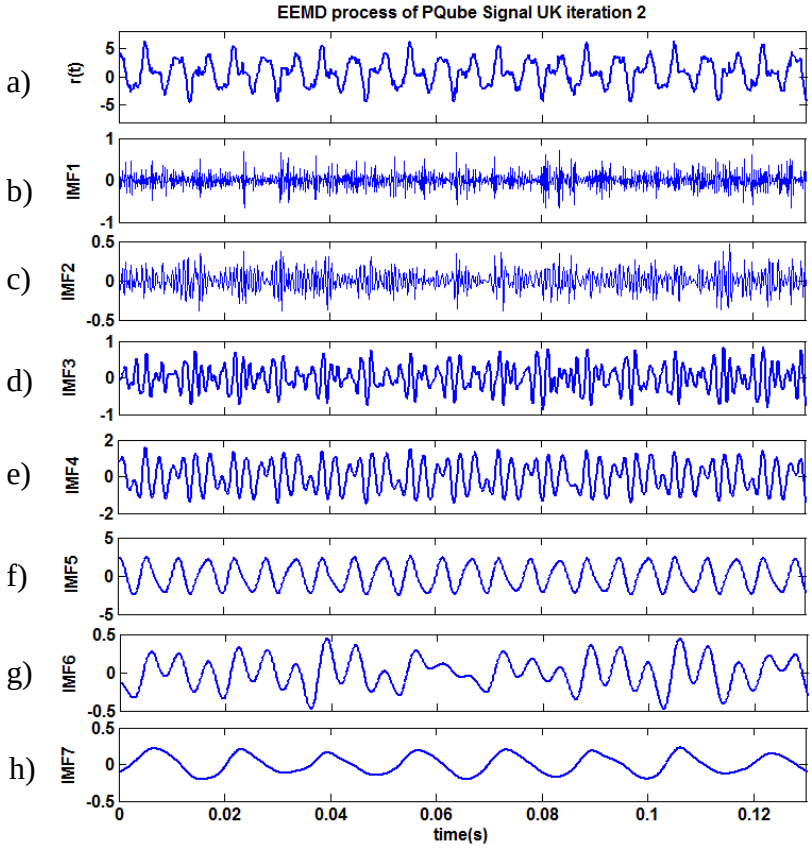

Figure 7.3.2.7 The IMFs from IEEMD process of Pqube signal iteration 2

Figure 7.3.2.7 shows the IMFs obtained from iteration 2 of the EEMD process of Pqube signal. The mean value of the Hilbert Transform of the IMFs are shown in Table 7.12.

Table 7.12

The HT of the IMFs in Figure 7.3.2.7

IMF	Amp (p.u)	Freq (Hz)	Phase (deg)
1	0.243	2098	-2.87
2	0.147	1215	-9.86
3	0.424	530	-6.44
4	1.061	400	-5.88
5	2.219	150	9.94
6	0.238	260	-3.89
7	0.172	50	-147.04
8	0.098	50	-76.55

Table 7.12 shows that the EEMD process has extracted the noise content in IMF_1 and IMF_2. While the mean value of instantaneous frequency of IMF_3 to IMF_7 are lower than noise frequency. To identify which IMF is mixed, the Hilbert Transform is used to calculate the instantaneous frequency, amplitude and phase of IMF_3 to IMF_8. The standard deviation of the instantaneous phase angle the IMFs are then calculated as shown in Figure 7.3.2.8.

Figure 7.3.2.8 shows that the mean frequency of IMF_3 to IMF_8 are lower then a typical noise frequency (1000 Hz). However, IMF_3, IMF_4, IMF_6 and IMF_8 are mixed with other frequency which are indicated by the unstability of the instantaneous phase angle with standard deviation greater than 30 and therefore the IMFs can not be considered as the significant results of the process. The standard deviation of the instantaneous phase angle of IMF_5 and IMF_7 are 16.178 and 8.49 respectively and therefore they are considered as significant IMFs and will be processed further. The sinusoidal representation of these IMFs are then created and subtracted from the waveform being analyzed to obtain the second residue. The calculated MSE between the cumulative identified components to the original signal is 8.84%.

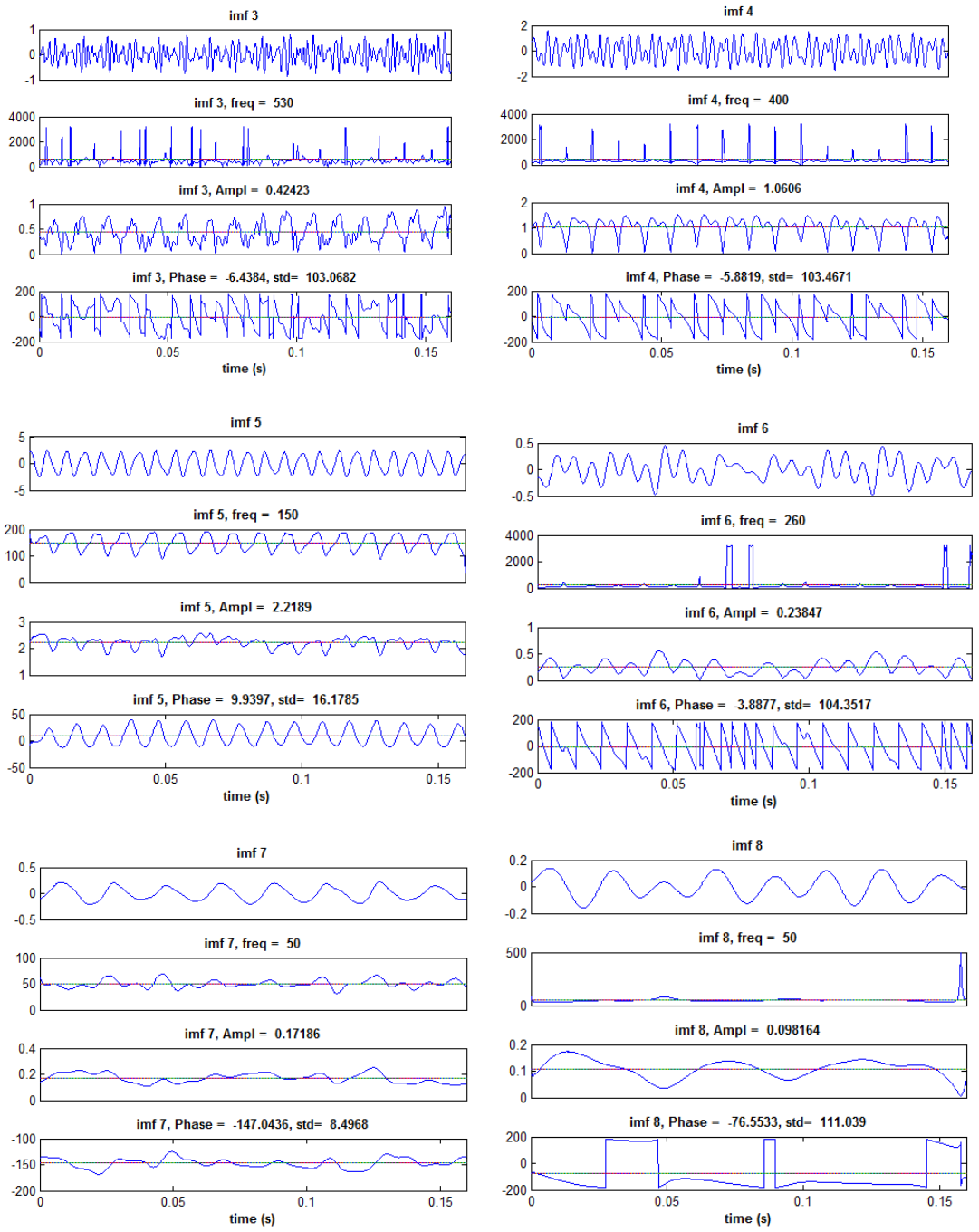

Figure 7.3.2.8 The Hilbert Transform of the IMFs in Figure 7.3.2.7

The decomposition process is then applied in the iterative fashion until the stopping criteria of the process is met according to the IEEMD algorithm in Section 6.3. The final result of the Iterative EEMD process is shown in Figure 7.3.2.9 and Table 7.13.

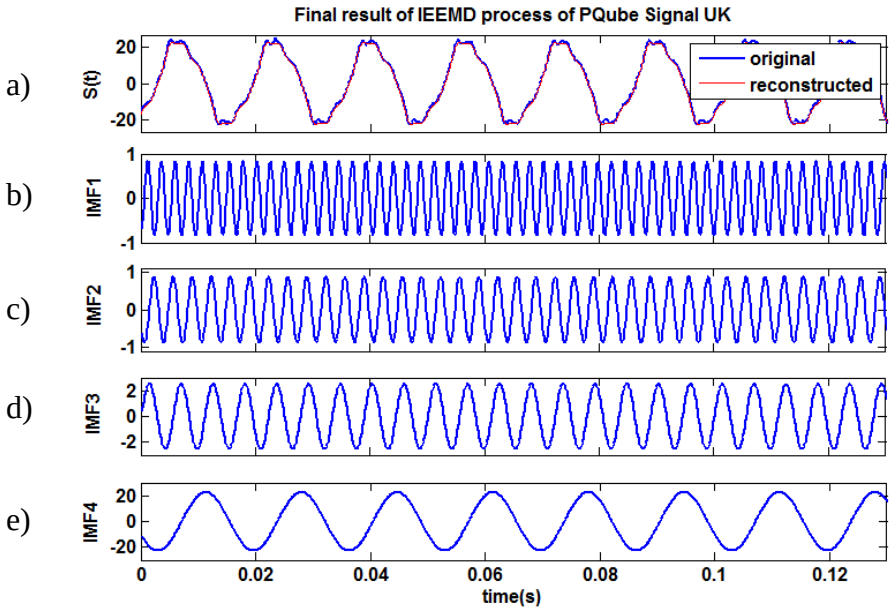

Figure 7.3.2.9 The Final result of Iterative EEMD process of Pqube signal

Table 7.13.
The result of the HT of the IMFs from Pqube signal

Amp (p.u)	Freq (Hz)	Phase (deg)
13.838	50	-147.45
8.905	50	-149.41
2.219	150	9.94
0.172	50	-147.04
0.546	250	-136.51
0.327	150	-0.44
0.118	50	7.10
0.832	350	-58.25
0.329	250	-130.92
0.053	50	25.61

Table 7.13 shows the result of the Iterative EEMD of the Pqube signal until 4 iterations (the next iteration does not give significant IMF any more and therefore the process is terminated at iteration 4). The IMFs with similar frequency are then combined to obtain the final result shown in Table 7.14.

Table 7.14.

The final result of the IEEMD process of Pqube signal

IMF	Amp (p.u)	Freq (Hz)	Phase (deg)	IMF	Amp (p.u)	Freq (Hz)	Phase (deg)
1	0.832	350	-58.25	3	2.541	150	8.61
2	0.873	250	-134.41	4	22.753	50	-148.07

Table 7.14 shows the final result of the Iterative EEMD process of the Pqube signal. The calculated MSE between the reconstructed signal shown in Figure 7.3.2.8(a) and the original signal is 3.70% which indicates that the result of IEEMD process is more accurate than the result of the standard EEMD process with the MSE 21.96%.

7.4. Non-stationary signals

The decomposition methods proposed in the research are then tested to analyze non-stationary measured PQ signals from Dranetz PQ Analyzer as well as from Pqube cloud storage of PQ events.

The SAX based boundary detector is first employed to identify the instant of changes of the non-stationary signal which are then used to segment the non-stationary signal. Subsequently, the decomposition methods are applied to each signal segment to identify the components of the (stationary) signal.

7.4.1. Dranview signal

By using window size w = 16 and alphabet size a = 50, a SAX representation of the non-stationary Dranview signal is obtained as shown in Figure 7.4.1.1

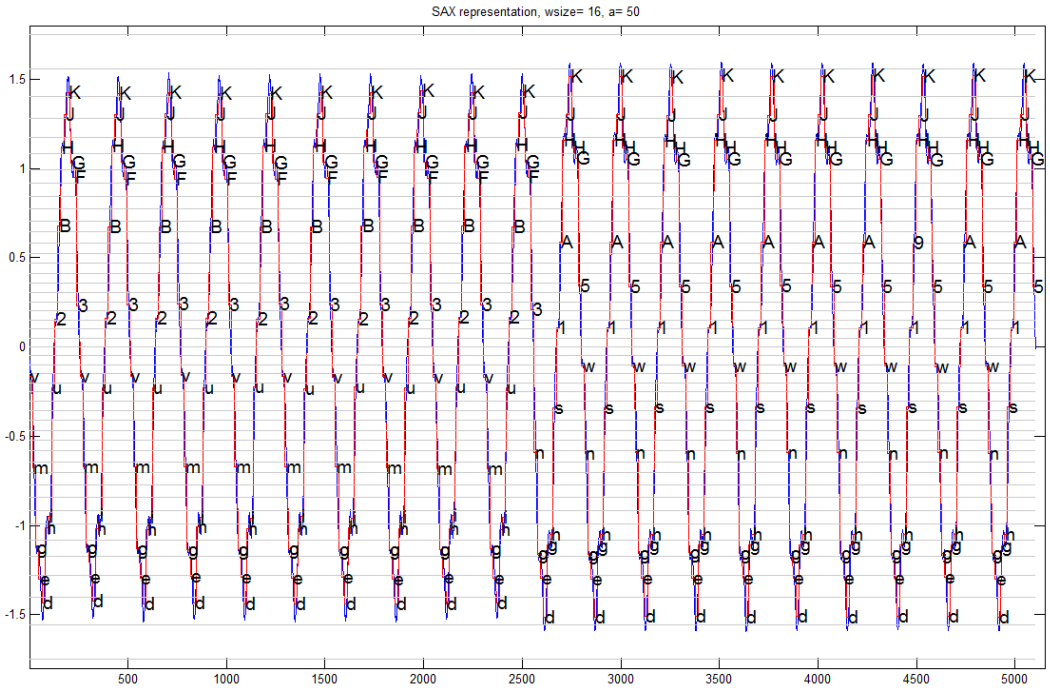

Figure 7.4.1.1 A SAX representation of non-stationary Dranview signal

Figure 7.4.1.1 shows the symbolic representation of the non-stationary signal which illustrates the repetitive patterns of the signal. It can be seen that the pattern in the first 10 cycles are different to the pattern of the next cycles, which demonstrates the ability of SAX algorithm to tanslate the original signal to a more simple representation that can be used for a boundary identification process. The boundary detector algorithm is then applied to the symbolic representation to identify instant of changes as shown in Table 7.15

Table 7.15

The SAX word for two consecutive cycles of non-stationary Dranview signal

$S_1(n_1)$			$S_2(n_2)$			Euclidean Dist Sum
n_1	symbol l_1	value	n_2	symbol l_2	value	
157	'K'	47	141	'K'	47	0
158	'G'	43	142	'G'	43	0
159	'F'	42	143	'F'	42	0
160	'3'	30	144	'3'	30	0
161	'n'	14	145	'v'	22	8

As shown in Table 7.15, the instant of change is detected at point no 161 which coincides with t = 0.2 sec. Using this point of change, the non-stationary signal is then divided into 2 segments which are then analyzed using the decomposition methods.

The decomposition of these 2 segments will be performed by the EEMD and Iterative EEMD techniques since these methods have shown higher accuracy than the standard HHT and Iterative HHT for measured signal decomposition. The result of decomposition process using the standard EEMD and the Iterative EEMD are shown in Table 7.16 and Table 7.17 respectively

Table 7.16

Result of EEMD decomposition of non-stationary Dranview signal

IMF	segment 1			segment 2		
	Amp (p.u)	Freq (Hz)	Phase (deg)	Amp (p.u)	Freq (Hz)	Phase (deg)
1	0.3	4263	1.01	0.32	4276	-1.06
2	0.15	2594	-8.92	0.15	2624	-2.09
3	0.12	1650	-8.39	0.12	1499	6.23
4	4.45	350	-134.04	5.05	350	-139.55
5	4.34	1250	-1.67	4.16	1385	0.74
6	44.83	50	87.46	46.8	50	85.41

Table 7.17

Result of IEEMD decomposition of non-stationary Dranview signal

IMF	segment 1			segment 2		
	Amp (p.u)	Freq (Hz)	Phase (deg)	Amp (p.u)	Freq (Hz)	Phase (deg)
1	4.45	350	135.95	5.33	350	130.44
2	0.27	150	-145.21	0.11	150	-135.28
3	49.16	50	85.8	51.2	50	83.7

Table 7.16 and Table 7.17 show the detected components of the non-stationary signal using EEMD and IEEMD. The reconstructed signal is then created from the detected components which is then compared to the original signal to estimate their difference. The calculated MSE between the original signal and the reconstructed signal using EEMD and IEEMD methods are 21.96% and 6.06% respectively which demonstrates the accuracy of the IEEMD process over the standard EEMD method.

Figure 7.4.1.2 shows the final result of the Iterative EEMD process of the non-stationary signal.

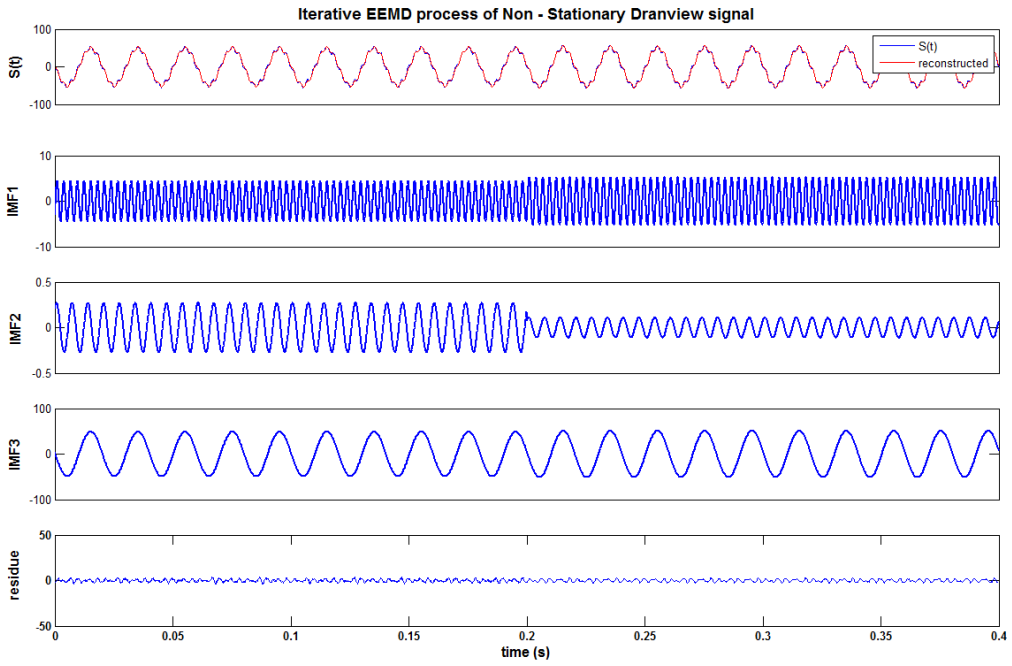

Figure 7.4.1.2 Final result of the Iterative EEMD process on non-stationary Dranview signal

Figure 7.4.1.2 shows that the proposed Iterative EEMD has decomposed the non-stationary Dranview signal accurately.

7.4.2. PQube signal

The proposed method is also applied to decompose a 3-phase signal available from a UK voltage sag snapshot event from the PQube cloud storage of PQ events [65], as shown in Figure 7.4.2.1. The occurrence of the event is 6.95 sec, the detected voltage swell level is 173% with rated frequency 50 Hz and rated voltage 240 / 415 V.

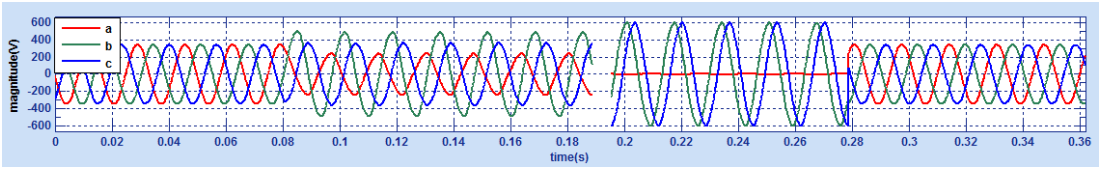

Figure 7.4.2.1 The PQube voltage sag signal

The snapshot shows some missing point in the top plot representing some time lapse during the transition. For the purposes of this study, the signal is assumed to be continuous and connected as shown in Figure 7.4.2.2 (a). The SAX boundary detector is then used to identify the boundaries of the signal as shown in Table 7.18.

Table 7.18 The detected boundaries of PQube signal

Segment 1	Segment 2	Segment 3	Segment 4
0 - 0.083 sec	0.0831 - 0.188 sec	0.01881 - 0.272 sec	0.2721 -0.3555 sec

The IEEMD using 500 ensemble member (nE=500) and the standard deviation of the added noise 0.032 (a=0.032) is then applied to the signal, which produces the results shown in Figures 7.4.2.2 (b) – (e). Two main frequencies were identified; 50 Hz and 150 Hz denoted as IMF_1 and IMF_2 in Figures 7.4.2.2(b) - (c). The residue of the decomposition process is shown in Figure 7.4.2.2(d) which is relatively small (around 4% of the original signal).

The three instantaneous phases in each segment of the 50 Hz three phase signal are shown in Figure 7.4.2.2 (e) in a phasor form. It is interesting to note that the three phases are, as expected, phase shifted by 120 degrees during normal operation in segments 1 and 4, but when voltage sag occurs in phase ‘a’ (60% in segment 2 and 1% in segment 3), the three phases are now unbalanced, with phase ‘b’ and phase ‘c’ being larger and the three phases are no longer phase shifted by 120 degrees as shown in Figure 7.4.2.2 (e) for segments 2 and 3.

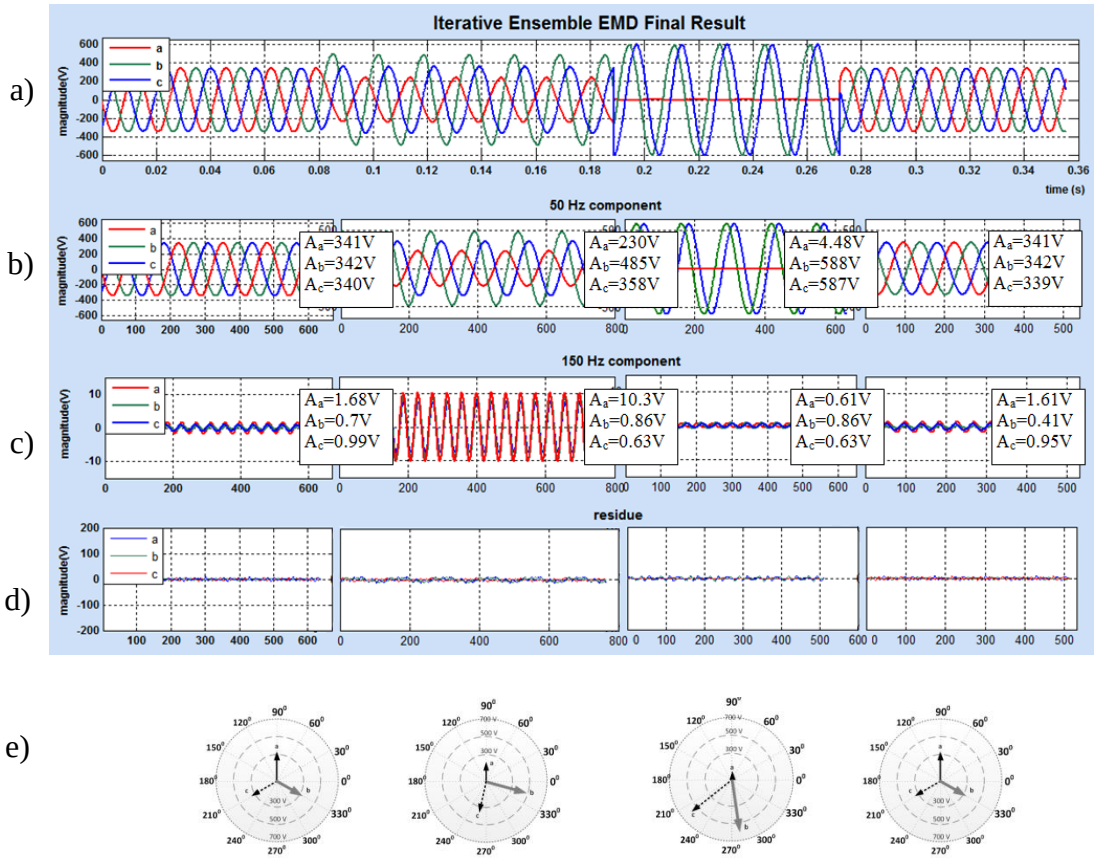

Figure 7.4.2.2: Final Result of IEEMD of the connected PQube signal: (a) The original signal (b) IMF_1 (c) IMF_2, (d) Residue (e) Phasor Diagram of 50 Hz IMF shown in (b)

7.5. Chapter summary

In this chapter, measured signals obtained from Dranetz PQ analyzer and PQube cloud storage of PQ events are introduced. These are more realistic signals compared to the simulated waveforms used in the previous chapters. Some of the Dranetz and Pqube signals are found to have more noise than others.

Initially the measured data from the Dranetz PQ analyzer with less noise is used to test the traditional HHT analysis. For such signal, the standard HHT can be used to decompose the signal. However, the residue of the decomposition process indicates that some of the signal components are not decomposed properly, suggesting that the decomposition process is not quite accurate.

Therefore, to improve the accuracy, the proposed Iterative HHT is used by taking the sinusoidal representations of the IMFs obtained by EMD process as the result of the first iteration. The sinusoids are then subtracted from the original signal to obtain the first residue. The EMD is then applied to the residue in the iterative

fashion. The result of the Iterative HHT is found to be more accurate than the standard HHT method.

However, when the Dranetz waveform with a higher level of noise such as Dranview#214 was used, the HHT produces intermittently mixed frequencies in the IMFs which causes the Hilbert Transform to produce incorrect mean frequencies calculation. Therefore, some frequency components are missed out resulting in inaccurate decomposition.

When the Dranetz waveform is processed using the Iterative HHT, the first IMF (after ignoring IMFs that appear as noise) also contains intermittently mixed frequency, which causes the calculated mean of the instantaneous frequency from the Hilbert Transform is inaccurate. Therefore, using sinusoidal representation of the IMFs and subtracting them from the original signal will not help to identify actual frequency components of the signal.

To resolve the problem, the standard EEMD technique is used where an ensemble of white noise-added signals is created from the original data. The EMD is applied to each of these signals to produce an ensemble of IMFs which are then averaged to obtain the final IMF which is considered as the true result [9]. The averaged IMFs obtained by EEMD is far less mixed than the IMFs obtained by EMD process, and therefore, more accurate results of the mean value of the instantaneous amplitudes, frequencies and phases of each decomposed component can be obtained using the Hilbert Transform. However, as discussed in Chapter 6 and shown in the calculation result of this chapter, EEMD process usually produce smaller values of the mean amplitudes. When the MSE between the reconstructed signal and the original signal is calculated, the value is still higher than the accepted tolerance confirming this potential issue.

To improve the decomposition process, the proposed IEEMD is used to decompose the signal components remaining in the residue. The result from the Iterative EEMD is found to be more accurate than the standard EEMD and the calculated MSE between the reconstructed signal and the original signal is now within the accepted tolerance.

Finally, the non-stationary signals from Dranetz and Pqube are used to test the decomposition method. As discussed in Chapter 3, while EMD method can obtain automatically the instantaneous amplitude, frequency and phase in the non-stationary

signal, inaccuracies occur on the instantaneous amplitude, frequency and phase due to overshoot and ambiguity around the area of a transition/discontinuity. Therefore, the SAX based boundary detector is applied to the symbolic representation of the signal, to identify the instants of changes in the non-stationary signal. After obtaining the boundaries of the signal by using SAX algorithm, the signals are segmented according to the identified boundaries and the decomposition methods are then applied to each segment. The results show that the Iterative EEMD method can decompose the signal more accurately than the standard EEMD.

This chapter shows that the developed methods in Chapter 4 to Chapter 6 can provide accurate decompositions of both stationary and non stationary signals, particularly with the help of the iterative EMD methods and the SAX-based boundary detector.

CHAPTER 8 CONCLUSION

8.1. Discussions and Conclusions of the Research Work

This final chapter presents a summary of the thesis and the conclusion it draws. The thesis presents the outcome of a Ph.D research program that focused on investigating the effectiveness of the recently developed methods for decomposing both stationary and non-stationary PQ signals such as Hilbert Huang Transform (HHT) and the Ensemble Empirical Mode Decomposition (EEMD) technique, and methods to improve their accuracy.

PQ issue has become a major concern since poor PQ can cause failure or malfunction of sensitive electrical equipment. The electric utilities need to ensure that they provide the customers with a good PQ level to obtain the customers satisfaction. PQ monitoring and PQ troubleshooting are becoming more important to the electric utilities to provide a high level of service.

In Chapter 2, the issue of PQ disturbances on power systems has been discussed, followed by a discussion of their effects to the equipment. A PQ disturbance classification based on the IEEE 1159-1995 and IEC 61000 classification method shows that there are several PQ disturbances that need to be considered. To help identify PQ problems, PQ meters are required. Many utilities are now considering to carry out PQ monitoring study of their system and therefore more PQ meters will be installed to monitor the PQ of their system. The analysis of the PQ data collected by the instruments is needed to identify the type of PQ disturbance, in particular the amount of harmonic components, swell, sags, flickers etc.

Several methods to decompose PQ waveforms into their components have also been described. FFT is reported to have difficulties to analyze non - stationary signal, and therefore STFT is developed to enable the FFT algorithm work for non-stationary waveforms. However, STFT has a fixed resolution which depends on the fixed window size which is chosen before the analysis. The wavelet transform is designed to do the signal analysis using windowing technique with variable-sized regions and therefore the resolution is better than the STFT. However, the method has difficulty in the adaptivity since the mother function has to be chosen prior to the analysis.

Prony, ESPRIT and MUSIC algorithms are parametric methods which model the signal to several oscillations which require the number of sinusoids known prior

to the analysis and hence, these methods cannot be used to decompose unknown signals. The HHT technique is well suited for analysing stationary and non-stationary signals and requires no initial assumption of the signal and hence is adaptive to any unknown signals. The methods is most suitable for decomposing non-stationary signals often found in PQ waveforms and therefore it is chosen to be investigated in this thesis.

In Chapter 3, the explanation of the basic steps in performimg HHT has been provided. The HHT has also been tested by using stationary and non-stationary PQ signals. The results have demonstrated that HHT can be effective to decompose such signals, particularly when the signals are simulated, with insignificant noise content, and does not have components with close frequency.

Several issues in implementing HHT have also been discussed. The problem of mode mixing is the primary difficulty in using HHT for stationary PQ signals particularly those containing close frequency and noise. For non-stationary signals, the HHT has been found to produce inaccuracy on the instantaneous amplitude, frequency and phase due to overshoot and ambiguity around the area of transitions / discontinuities.

In Chapter 4, several techniques from the literature to improve the HHT method in resolving the problems of signals having close frequency components have been described. The disadvantages of the techniques have also been discussed, such as some assumptions have to be made prior to the analysis (EMD using Masking Signal method) and the need to perform FFT to obtain the frequency components prior to HHT decomposition (EMD with Masking Signal and FFT method).

A new method using an iterative process has been proposed to improve the HHT when dealing with signals containing close frequency components, which does not require any assumption or the use of FFT prior to the analysis [47]. The proposed method has been applied to decompose several test signals each containing close frequency components and the results show that it is effective in resolving the problems.

In Chapter 5, the SAX based boundary detector algorithm to identify the instant of changes (boundaries) of the PQ non-stationary signals is described. Firstly, a window size and alphabet size are chosen to transform the original signal to a

symbolic representation. The SAX representation of the signal is then passed through a pattern detector to check the cumulative sum of the Euclidean distances of two corresponding sub-sequences of two consecutive cycles. When the cumulative sum exceeds a predefined threshold, the first point of change is then marked as the boundary.

The detected boundaries have been used to segment several simulated non-stationary signals to a sequence of stationary signal segments. Once segmented, the HHT and iterative HHT methods are then applied to decompose the segments of the non-stationary signals. The results from the simulation show that the proposed approach can accurately decompose non-stationary signals.

In Chapter 6, the recently published Ensemble Empirical Mode Decomposition (EEMD) to resolve the mixed IMF issues produced by the traditional EMD process of noisy signal is described. EEMD algorithm works by creating an ensemble of white noise-added signal from the original data. The EMD is applied to each of these signals to produce an ensemble of IMFs which are then averaged to obtain the final IMF which is considered as the final answer.

The EEMD is then tested with noisy signals which produces mixed IMF when processed by using the traditional EMD. The EEMD has been found to be effective in resolving the mode mixing issues of the noisy signals. However, the EEMD method can produce inaccuracy of the identified amplitudes of the detected components, resulting in inaccurate decomposition and relatively high Mean Square Error (MSE) between the reconstructed signal and the original signal.

To overcome this issue, an Iterative EEMD has been proposed, where the significant IMFs are selected from each EEMD process. The sinusoidal representation of the significant IMFs are then subtracted from the signal to obtain the residue which is then considered as the new signal to be processed in the next iteration.

The proposed iterative EEMD has been tested by using several simulated noisy signals and the results show that the amplitudes of the components are now closer to the specified amplitudes and the MSE has been reduced considerably.

In Chapter 7, the decomposition methods described in Chapter 3 to Chapter 6 are applied to decompose measured signals obtained from Dranetz PQ analyzer measurement and from Pqube cloud storage. The traditional HHT method described

in Chapter 3 has been found to be able to decompose less noisy signal (obtained from Dranview), however, some signal components remain unidentified. When the Iterative HHT described in Chapter 4 is used to decompose the signal, more frequency components of the signal are found, confirming the effectiveness of the proposed iterative method.

For signal with higher level of noise (such as the more noisy Dranview signal and signal obtained from Pqube cloud database), the standard HHT and the Iterative HHT cannot resolve the mode mixing issue introduced by the EMD process of such signals. Therefore, the standard EEMD technique described in Chapter 6 is used to resolve the issue. Although the method works for the measured signals, as described in Chapter 6, the amplitude of the detected components are found to be smaller than the actual amplitude which means that part of the signal components remain unidentified in the residue of the process. To obtain more accurate result, the proposed IEEMD is used to decompose the residue of the EEMD results. The result from the Iterative EEMD is found to be more accurate than the standard EEMD, as indicated by the MSE between the original and reconstructed signal smaller than that obtained from EEMD.

For more noisy non-stationary signal, the SAX based boundary detector described in Chapter 5 can be used to segment the signals and the iterative EEMD method is used to decompose the segments individually. The results show that the proposed approach can decompose more noisy non-stationary signals quite accurately.

In conclusion, the research has described several new methods to improve the standard HHT method to decompose both stationary and non-stationary PQ signals and the newly developed EEMD to decompose more noisy signals. Results for both simulated and measured signals have been presented and they confirm the effectiveness of the proposed method.

8.2. **Major contributions**

The following methods are the major contributions of the research.

a. The development of the Iterative Hilbert Huang Transform.

b. The development of the Iterative Ensemble Empirical Mode Decomposition.

c. The development of SAX-based boundary detector to identify the instant of changes of the non-stationary signal.

8.3. Future Work

A number of significant issues related to the decomposition of PQ signals have been addressed and several new methods have been proposed, such as the Iterative EMD methods and the SAX-based method to determine the boundaries of non-stationary signals.

Further research that can be developed further in this area are as follows:

- Improvement to the cubic spline method in the Empirical Decomposition process to reduce the end effect problem.
- Optimisation of the determination of ensemble number and noise standard deviation in the EEMD process
- Further investigation into the decomposition of interharmonics, which has not been investigated in this thesis. Since interhamonics represents a signal with frequency components which are non-multiple of the fundamental frequency, mode mixing issue can be expected.
- Further investigation into the effectiveness of the Iterative HHT on decomposing PQ signal with many harmonic components particularly with high frequencies.
- Optimisation of the iterative EEMD algorithm to speed up the process, particularly when large number of ensembles are used. Parallel processing may be used to help speed up the calculation.

LIST OF REFERENCES

[1] J. Dixit and A. Yadav, *Electrical power quality*: Laxmi Publications, Ltd., 2010.

[2] N. E. Huang, Z. Shen, S. R. Long, M. C. Wu, H. H. Shih, Q. Zheng, N. C. Yen, C. C. Tung, and H. H. Liu, "The empirical mode decomposition and the hilbert spectrum for nonlinear and non-stationary time series analysis," *Proceedings of the Royal Society A: Mathematical, Physical and Engineering Sciences*, vol. 454, pp. 903-995, 1998.

[3] F. J. Harris, "On the use of windows for harmonic analysis with the discrete fourier transform," *Proceedings of the IEEE*, vol. 66, pp. 51-83, 1978.

[4] M. H. J. Bollen and I. Y.-H. Gu. (2006). *Signal Processing Of Power Quality Disturbances*.

[5] G. Rilling, P. Flandrin, and P. Gonçalves, "On Empirical Mode Decomposition and its algorithms," *IEEE-EURASIP Workshop on Nonlinear Signal and Image Processing, NSIP-03, Grado (I)*, 2003.

[6] R. Deering and J. Kaiser, "The use of a masking signal to improve empirical mode decomposition," in *IEEE International Conference on Acoustics, Speech, and Signal Processing, 2005 Proceedings.*, 2005, pp. 485-488.

[7] N. Senroy and S. Suryanarayanan, "Two Techniques to Enhance Empirical Mode Decomposition for Power Quality Applications," *Power Engineering Society General Meeting, 2007, IEEE*, pp. 1-6, 2007.

[8] M. J. Afroni, D. Soetanto, and D. Stirling, "The Analysis Of Noisy Non-Stationary Power Quality Events By Using Sax Algorithm And Iterative Ensemble Empirical Mode Decomposition (IEEMD) (Submitted)," *Advances in Adaptive Data Analysis*, 2014.

[9] Z. Wu and N. E. Huang, "Ensemble Empirical Mode Decomposition: A Noise-Assisted Data Analysis Method," *Advances in Adaptive Data Analysis*, vol. 1, pp. 1-41, 2009.

[10] M. H. J. Bollen. (1999). *Understanding Power Quality Problems: Voltage Sags and Interruptions*. *5*.

[11] V. Gosbell, S. Perera, and V. Smith. (1998) APQRC Technical Note No. 1, Understanding Power Quality.

[12] T. D. Nguyen, "Exploring Novel Methods For Power Quality Disturbance And Fault Type Classification," Ph.D, The Graduate School, University of Kentucky, Lexington, Kentucky, 2008.

[13] C. Sankaran, *Power quality*: CRC press, 2001.

[14] R. C. Dugan, M. F. McGranaghan, and H. W. Beaty, "Electrical power systems quality," *New York, NY: McGraw-Hill,| c1996*, vol. 1, 1996.

[15] B. H. Chowdhury, "Power quality," *Potentials, IEEE*, vol. 20, pp. 5-11, 2001.

[16] A. Baggini, Ed., *Handbook of power quality*. Wiley, 2008.

[17] AS 61000.3.100, "Limits - Steady State voltage limits in public electricity systems," ed.

[18] AS/NZS, "Electromagnetic Compatibility (EMC), Part 4.7 Testing and Measurement techniques – General guide on harmonics and interharmonics measurements and instrumentation, for power supply systems and equipment connected thereto, AS/NZS 61000.4.7:2012, 2012," ed, 2012.

[19] Emerson Industrial Automation. (2011, October 14, 2014). *Power Quality Guidebook*. Available: http://www.mc-mc.com/Portals/1/articles/SolaPowerQualityGuide.pdf
[20] IEEE, "1159-1995, Recommended practice for monitoring electric power quality, 1995," vol. 1159-1995, ed, 1995.
[21] M. Misiti, "Wavelet Toolbox User's Guide, Version 1: For Use with MATLAB," ed: Math Works, 1996.
[22] M. Weeks, *Digital Signal Processing Using MATLAB & Wavelets*: Jones & Bartlett Learning, 2010.
[23] Wikipedia. (2015, 1 September 2015). *Fast Fourier Transform*. Available: https://en.wikipedia.org/wiki/Fast_Fourier_transform
[24] J. Allen, "Short-term spectral analysis, and modification by discrete Fourier Transform," *IEEE Transactions on Acoustics Speech and Signal Processing,* vol. 25, pp. 235-238, 1977.
[25] E. Jacobsen and R. Lyons, "The sliding DFT," *Signal Processing Magazine, IEEE,* vol. 20, pp. 74-80, 2003.
[26] N. El-Sheimy, A. Osman, S. Nassar, and A. Noureldin, "Innovation-Wavelet Multiresolution Analysis-A New Way to Integrate GPS and INS-Applying wavelet multiresolution analysis, in place of Kalman filter estimation, to integrated inertial and DGPS," *GPS World,* vol. 14, pp. 42-49, 2003.
[27] R. Flores, "Signal processing tools for power quality event classification," Lic.Eng. thesis, School Elect. Eng, Chalmers University of Technology, Gothenburg, Sweden, 2003.
[28] P. K. Dash, B. K. Panigrahi, and B. K. Panigrahi, "Power quality analysis using S-transform " *IEEE Transactions on Power Delivery,* vol. 18, pp. 406-411, 2003.
[29] S. Santoso, E. J. Powers, and W. M. Grady, "Power quality disturbance data compression using wavelet transform methods," *IEEE Transactions on Power Delivery*, vol. 12, pp. 1250-1257, 1997.
[30] V. Pham and K. Wong, "Wavelet-transform-based algorithm for harmonic analysis of power system waveforms," in *Generation, Transmission and Distribution, IEE Proceedings*-, 1999, pp. 249-254.
[31] The MathWorks Inc. (2014, October 16, 2014). *Continuous Wavelet Transform*. Available: http://www.mathworks.com/help/wavelet/gs/continuous-wavelet-transform.html
[32] W. G. Morsi and M. E. El-Hawary, "Suitable Mother Wavelet for Harmonics and Interharmonics Measurements Using Wavelet Packet Transform," *Electrical and Computer Engineering, 2007. CCECE 2007.Canadian Conference on*, pp. 748 – 752, 2007.
[33] J. Barros and R. I. Diego, "Application of the wavelet packet transform to the estimation of harmonic groups in current and voltage waveforms," *IEEE Transactions on Power Delivery*, vol. 21, pp. 533-535, 2006.
[34] A. Domijan, A. Hari, and T. Lin, "On the selection of appropriate wavelet filter bank for power quality monitoring," *Int. J. Power Energy Syst*, vol. 24, pp. 46-50, 2004.
[35] S. Singh, "Application of Prony analysis to characterize pulsed corona reactor measurements," Master of Science, Department of Electrical and Computer Engineering, The University of Wyoming, Wyoming, 2003.

[36] J. F. Hauer, C. Demeure, and L. Scharf, "Initial results in Prony analysis of power system response signals," *Power Systems, IEEE Transactions on*, vol. 5, pp. 80-89, 1990.
[37] Wikipedia. (2015, 19 January). *Prony's Method*. Available: http://en.wikipedia.org/wiki/Prony%27s_method
[38] C. F. Drummond and D. Sutanto, "Classification of Power Quality Disturbances using the Iterative Hilbert Huang Transform," *Harmonics and Quality of Power (ICHQP), 2010 14th International Conference on* pp. 1-7, 2010.
[39] E. C. Titchmarsh. (1948). *Introduction to the theory of Fourier integrals*.
[40] P. Flandrin, G. Rilling, and M. E. Torres. (2014, October 17, 2014). *Empirical Mode Decomposition*. Available: http://perso.ens-lyon.fr/patrick.flandrin/emd.html
[41] R. Deering, "Fine-Scale Analysis Of Speech Using Empirical Mode Decomposition: Insight And Applications," Ph.D, Department of Mathematics, Duke University, 2006.
[42] S. L. Hahn, Ed., *Hilbert Transforms in Signal Processing*. London: Artech House, Boston, 1996.
[43] The MathWorks Inc. (2014, October 17, 2014). *hilbert*. Available: http://www.mathworks.com/help/signal/ref/hilbert.html
[44] G. Rilling and P. Flandrin, "One or two frequencies? The empirical mode decomposition answers," *Signal Processing, IEEE Transactions on*, vol. 56, pp. 85-95, 2008.
[45] P. C. Chu, C. Fan, and N. Huang, "Compact Empirical Mode Decomposition: An Algorithm to reduce mode mixing, end effect, and detrend uncertainty," *Advances in Adaptive Data Analysis*, vol. 4, 2012.
[46] N. Senroy, S. Suryanarayanan, and P. F. Ribeiro, "An Improved Hilbert-Huang Method for Analysis of Time-Varying Waveforms in Power Quality," *IEEE Transactions on Power Systems*, vol. 22, pp. 1843-1850, 2007.
[47] M. J. Afroni, D. Sutanto, and D. Stirling, "Analysis of Non-Stationary Power Quality Waveforms Using Iterative Hilbert Huang Transform and SAX Algorithm " *IEEE Transactions on Power Delivery* vol. 28, pp. 2134 - 2144, 2013
[48] E. Keogh, J. Lin, and A. Fu, "HOT SAX: Efficiently Finding the Most Unusual Time Series Subsequence," *Proceedings of the Fifth IEEE International Conference on Data Mining (ICDM'05),* pp. 226-233, 2005.
[49] P. Patel, E. Keogh, J. Lin, and S. Lonardi, "Mining Motifs in Massive Time Series Databases, In proceedings of the 2002 IEEE International Conference on Data Mining," *Maebashi City, Japan. Dec*, pp. 9-12, 2002.
[50] J. Lin, E. Keogh, S. Lonardi, and B. Chiu, "A Symbolic Representation of Time Series, with Implications for Streaming Algorithms," *8th ACM SIGMOD Workshop on Research Issues in Data Mining and Knowledge Discovery Proceeding of*, pp. 1-11, 2003.
[51] J. Lin, E. Keogh, L. Wei, and S. Lonardi, "Experiencing SAX: a novel symbolic representation of time series," *Data Mining and Knowledge Discovery*, vol. 15, pp. 107-144, 2007.
[52] P. Karvelis, I. P. Tsoumas, G. Georgoulas, C. D. Stylios, J. A. Antonino-Daviu, and V. Climente-Alarcon, "An intelligent icons approach for rotor bar

fault detection," in *Industrial Electronics Society, IECON 2013-39th Annual Conference of the IEEE*, 2013, pp. 5526-5531.
[53] J. A. Antonino-Daviu, M. Riera-Guasp, M. Pineda-Sanchez, and R. B. Perez, "A critical comparison between DWT and Hilbert–Huang-based methods for the diagnosis of rotor bar failures in induction machines," *Industry Applications, IEEE Transactions on*, vol. 45, pp. 1794-1803, 2009.
[54] A. Notaristefano, G. Chicco, and F. Piglione, "Data size reduction with symbolic aggregate approximation for electrical load pattern grouping," *Generation, Transmission & Distribution, IET*, vol. 7, 2013.
[55] M. Alam, K. Muttaqi, and D. Sutanto, "A SAX-based advanced computational tool for assessment of clustered rooftop solar PV impacts on LV and MV networks in smart grid," *Smart Grid, IEEE Transactions on*, vol. 4, pp. 577-585, 2013.
[56] E. Keogh, "Mining Shape and Time Series Databases with Symbolic Representations," in *Proceedings of the 13th ACM SIGKDD International Conference on Knowledge Discovery and Data Mining*, 2007, p. 7.
[57] C.-S. Chen, C.-C. Liu, H.-T. Wu, and A.-B. Liu, "Ensemble Empirical Mode Decomposition for atherosclerosis in high-risk subjects," in *Information, Communications and Signal Processing (ICICS) 2011 8th International Conference on*, 2011, pp. 1-4.
[58] H. Li, Y. Wang, and Y. Ma, "Ensemble empirical mode decomposition and Hilbert-Huang transform applied to bearing fault diagnosis," in *Image and Signal Processing (CISP), 2010 3rd International Congress on*, 2010, pp. 3413-3417.
[59] X. Jia, Y. Fan, and M. Fenghai, "Research on Nonstationary Signal Denoising Based on EEMD Filter," in *Multimedia Technology (ICMT), 2010 International Conference on*, 2010, pp. 1-3.
[60] A. Papoulis and S. U. Pillai, *Probability, random variables, and stochastic processes*: Tata McGraw-Hill Education, 2002.
[61] Wikipedia. (2015, 2 September 2015). *Mean Squared Error*. Available: https://en.wikipedia.org/wiki/Mean_squared_error
[62] Davis Instruments. (2014, November 29, 2014). *Dranetz BMI Power Quality Analyzers*. Available: http://www.inotek.com/catalog/dranetz1et.html
[63] Wikipedia. (2014, November 29, 2014). *PQube*. Available: http://en.wikipedia.org/wiki/PQube
[64] Jsdata. (2014, November 29, 2014). *PQube (AC & DC Power Monitor)*. Available: http://jsdata.co.kr/product/product1_4.php
[65] http://map.pqube.com/. *Power Standards Lab, PQube Live World Map of Power Quality*.